Development of modular microfluidic devices for bio-analytical sensors

Zur Erlangung des akademischen Grades eines

Doktors der Ingenieurwissenschaften

an der Fakultät für Maschinenbau der

Universität Karlsruhe

(genehmigte)

Dissertation

von Dipl. Chem. – Ing. Ivan Stoyanov Stoyanov

aus Gorna Oryahovica, Bulgarien

Tag der mündlichen Prüfung: 26.06.2006

Hauptreferent: Prof. Dr. V. Saile

Korreferent: PD Dr. E. Quandt

Kurzfassung

Diese Arbeit beschäftigt sich mit der Entwicklung mikrofluidischer Komponenten basierend auf thermoplastischen Elastomeren für ein bioanalytisches Oberflächenwellensensorsystem.
Die Verwendung von kommerziell erhältlichen Elastomerfolien und die Nutzung von Heißprägeverfahren ermöglichte eine kostengünstige und produktnahe Herstellung der mikrofluidischen Komponenten, auch als Einwegprodukte.
Die thermoplastischen Polyurethanfolien zeichnen sich durch eine hohe chemische Widerstandsfähigkeit gegen die im Biosensorssystem verwendeten Substanzen und durch eine sehr gute Dichtungsfähigkeit aus. Die Entwicklung geschlossener Mikrofluidikstrukturen und die Integration aktiver Ventilstrukturen ermöglichte eine deutliche Erhöhung der Temperaturstabilität und die getrennte Immobilisierung biologischer Rezeptormoleküle auf der Sensoroberfläche.
Im Anschluss an die Einleitung im Kapitel 1 wird im Kapitel 2 der Stand der Technik der Biosensorsysteme und das physikalische Sensorprinzip und die Wechselwirkung der Sensoroberfläche mit Flüssigkeiten detailliert beschrieben. Die mikrofluidischen Eigenschaften und die Herstellungstechnologie wird im Kapitel 3 dargestellt. Kapitel 4 gibt einen Überblick über die Funktionsweise des verwendeten Biosensorsystems und der Heißprägeanlage. Im Kapitel 5 werden die erzielten Resultate zur Herstellung und Optimierung von 1- und 2-seitig geprägten Flusszellen sowie die Entwicklung der geschlossenen Mikrofluidikstrukturen präsentiert. Beispielhafte Messungen und Analysen werden zur Bewertung der erzielten Strukturen herangezogen. Die Weiterentwicklung der fluidischen Komponenten wird im Rahmen der Integration aktiver Ventilstrukturen im Kapitel 6 dargestellt. Verschiedene biologische Echtzeit-Messungen zeigen die Funktionsfähigkeit der entwickelten Strukturen im Biosensorsystem.
Die Arbeit endet mit einer kurzen Zusammenfassung und einem Ausblick im Kapitel 7.

Summary

In this work, novel microfluidic devices based on thermoplastic elastomers for SAW based bio-analytical system have been developed.
Commercially available foils of thermoplastic polyurethanes and hot embossing fabrication technology allowed inexpensive batch production of the microfluidic devices and their use as disposables. The thermoplastic polyurethanes showed high chemical resistance against the substances used in the bio-analytical system. Moreover, they showed excellent sealing properties. The microfluidic devices have been optimised for maximal temperature stability of the sensor signal. Integration of active valve structures into the microfluidic devices allowed immobilization of different receptor molecules on the same bio-chip for detection of different analyts.
Section 1 presents a short introduction and the aim of this work. The state of the art of the bio-analytical systems, the physical working principle of the SAW sensor and the influence of the parameters of the liquids are explained and discussed in **Section 2**. The properties of the fluid flow in the microliter range and the fabrication technologies for microfluidic devices are discussed in **Section 3**. A description of the used technical equipment, including the hot embossing system and the bio-analytical system used for characterization of the microfluidic devices is given in **Section 4**.
In Section 5, the technology for the fabrication of one-side and double-side embossed devices is described. The double-side embossed structures have been used for fabrication of closed fluidic devices, which gave the possibility for integration of active fluidic valves. The experiments aimed the development and optimization of suitable fabrication technology. The influence of the parameters of the fluidic devices on the temperature stabilization and on the fluid flow have been determined and discussed. The successful integration of active pneumatic valves, described in **Section 6**, gave the possibility to guide the fluid through different fluidic chambers over the sensor chip, allowing immobilization of different receptor molecules. The proper function of the microfluidic devices with integrated valves have been assured by a number of real-time bio-analytical measurements.
In Section 7 the results of all experiments have been briefly summarized. Future aims of the development of the microfluidic devices and possibility to integrate them into a disposable module with the bio-chip have been presented.

TABLE OF CONTENT:

1 INTRODUCTION AND AIM OF THE WORK

Bio-analytical sensor systems have become important instruments for a vast variety of applications (such as medical diagnostics, e.g. [SAN00], bio-chemical research and biomedical research [WEI03], environmental and food analysis [PAT02]. There is a need for convenient and reliable methods for highly sensitive and highly specific detection of small amounts of bio-molecules (proteins, DNA, RNA), viruses, bacteria etc.
The development of the bio-analytical methods led to the need of reliable handling of sample volumes in the micro- and nanoliter range. The state of the art micro-mechanical technologies allow fabrication of miniaturized microfluidic devices with integrated active components such as valves, pumps, flow sensors etc. Moreover, many standard analytical separation methods have been steadily miniaturized. The integration of such analytical methods with the microfluidic components aims to accomplish the whole analysis within miniaturized systems called micro-total analysis systems (μTAS) [MAN90].

Starting with the thesis of M. Schlensog [SCH03] a complete bio-analytical system "S-sens" has been developed within the last years at the *center of advanced european studies and research (caesar)*, Bonn, Germany. It is designed for detection of real-time macromolecular interactions. The system is based on surface acoustic wave (SAW) sensors, fabricated on a quartz substrate. The surface waves are propagating in an additional amorphous SiO_2 guiding layer at the sensor surface (Love waves). The velocity of the Love waves depends on the mass-loading on the sensor surface. The mass changes result from binding of an analyte to receptor molecules immobilized on the sensor surface.
For the commercialization of the "S-sens" system, the development of reliable, modular and cost-efficient microfluidic handling system was of great importance.

Therefore, the aim of this work was to develop novel microfluidic devices for the bio-sensor system. They had to be integrated in a modular approach, assuring an easy separation with the sensor chip. The material for the microfluidic devices had to possess a high chemical resistance against the standard substances used for bio-analytical measurements, as well as excellent elastic properties for achieving a good sealing to the chip. Moreover, the material had to be inexpensive and allow the use of the microfluidic devices as disposables. The fabrication technology had to allow a batch fabrication process.

The volumes of the fluidic devices had to assure short fluidic exchange times (less then 10 s) for accomplishment of real-time analysis. The fluidic design had to assure repeatable and reliable measurements and had to be optimized for minimization of the influence of sensitivity factors (such as temperature shifts, change of the liquid parameters, shape of the devices) on the sensor signal.

In order to reduce the fluidic exchange times, as well as for reduction of the sample volume, active valves had to be integrated into the fluidic channels. The integrated valves had to allow immobilization of different receptor molecules on the same bio-chip. Thus, one bio-chip can be used for detection of different analytes. The fabrication technology of the integrated valves had to be cost-efficient and allow the use of the microfluidic devices as disposables.

2 BIO-SENSOR SYSTEMS

In this section, the existing concepts of the bio-sensor systems and the working principles of the bio-sensors will be briefly discussed.

2.1 Concept of the bio-sensor systems

There are two main detection approaches in building a bio-sensor system: sensor method and separation method [BEC99]:

The *sensor method* makes use of some chemical or bio-chemical reactions, which are correlated with the concentration of a certain substance in the sample. The sensor output is an electronic signal proportional to the concentration of the substance. The advantages of the sensor method are the relatively simple fabrication technologies and the high-speed analysis, which allow a real time monitoring. The disadvantages are: necessity of preliminary preparation of the sensor for the detection of a certain component in the sample; lack of possibility to detect a completely unknown component in the sample; cross-sensitivities (sensitivity of the sensor to chemically (biologically) similar components) and to changes in the environmental parameters. The sensitivity of the sensor based detection system is closely correlated with reduction of the sensor dimensions and the proper handling of sample solutions in the microliter or nanoliter range.

The conventional *separation methods* (gas-chromatography (GC), high performance liquid chromatography (HPLC), capillary elecrophoresis (CE)) use different detection approach. Here, the sample is first separated into components that can be detected. The separation methods do not need preliminary preparation in order to detect a certain component in the sample and can be used for analysis of samples with unknown content. A disadvantage of this approach is the slow speed (in the range of hours). It is not suitable for bio-chemical reactions, where the components are not stable or highly reactive. What is more, all separation methods are complicated, consume lots of materials and need trained operators.
The disadvantages of the separation methods may be overcome by reduction of the characteristic dimensions of the analytical systems in the micro- (or nano-) meter range. Smaller sample volumes lead to shorter transport and diffusion times and to an increase of the surface to volume ratio as well. That in turn leads to shorter analysis times with higher sensitivity. The reduction of the dimensions of the analytical devices leads to reduced sample consumption, shorter analysis times, higher sensitivity and possibility to build portable analytical systems [BAS04].

In the last years, the incorporation of the separation methods into a single micro-chip has become an important issue. The *micro-total analysis systems (μTAS)* or *Laboratory on chip (Lab-on-chip, LOC)* concepts combine the advantages of the sensor and the separation methods: in addition to their possibility to detect a diversity of substances contained in the sample, the separation systems are miniaturized and can be fabricated in a cost-effective way by using micro-electromechanical systems (MEMS) technology [REY02], [AUR02]. The μTAS systems are going to found a number of applications in the areas of cell culture and handling, medical diagnosis, polymerase chain reaction (PCR), DNA separation and analysis, for immunoassays, etc.
One of the most important aspects of the LOC concept is the proper sample handling in order to allow reliable analysis. This requirement is assured by using microfluidic devices or systems. There are two main approaches for the development of fluidic devices for μTAS purposes [AND03]: the first one is focused on the combination and integration of fluidic components (valves, pumps, flow sensors) into whole system. The second one is the miniaturization of the analytical chemical methods, especially the separation processes. The later one is of a special importance for DNA and protein analysis, as well as for cellomics.

The combination of the micro- and nanotechnology with the biomedical science led to the development of miniaturized systems for handling and analysis of biological and chemical species called *BioMEMS* [BAS04]. The BioMEMS systems developed for diagnostic applications are called *"BioChips"*. They are used for detection of nucleic acids, DNA, proteins, viruses, cells or small molecules. Important feature of the BioChips is the use of receptor molecules as a part of the sensor element. The receptor molecules have dimensions comparable to that of the target species, providing a high sensitivity.

In the most cases, the analysis should give information not only about the presence of a certain component in the sample, but also about its concentration. Furthermore, for observation of many bio- (chemical) processes it is important to get information not only about the final result, but also about the binding process itself. The most molecular interactions represent a dynamic equilibrium between association and dissociation events. For measurement of the association and dissociation constants the sensor system should detect the changes in real-time (in-situ measurements).

2.2 Biosensor principles – review

Biosensors combine a biologically sensitive element with a physical or chemical transducer to selectively and quantitatively detect specific target molecules [LUP01], [BAS04]. The sensitivity and the performance of the biological sensors have been substantially improved with the use of nanostructured materials [VOD01], [JIA04]. The nanotechnology allowed an introduction of new transduction technologies in

biosensors by using self-assembly techniques and nano-electromechanical systems (NEMS).

The biosensors have the following main detection principles: ***optical, mechanical, electrical*** **and** ***magnetic.***

Examples of an ***optical detection*** technique are different luminescence methods [KUL03]. Here, a variety of luminescent phenomena such as photoluminescence (PL), chemiluminescence (CL), electrochemiluminescence (ECL) are used for indication of a bio- chemical reaction.
Most analytes does not exhibit a natural luminescence. However, luminescent molecules can be synthesized and used as marker (labels) bound to the analyte and can be accurately determined quantitatively at very low concentrations by an optical system. Solid luminescent nanoparticles also have been used as labels [SEY05].

PL is divided in two sub-classes: fluorescence and phosphorescence. The fluorescence methods are based on the use of fluorescent tags that are optically detected [LAK95], [BAR97]. Single molecule fluorescence detection on chip has already been reported [FIS98].

The CL is a process of generation and release of electromagnetic radiation (light) by chemical reaction. Time resolved measurements are very difficult to be achieved by CL methodology, because the molecule excitation process is a single shot event that destroys the molecule. However, the CL is a very sensitive technique and allows outstanding selectivity and sensitivity if coupled with a suitable separation technique (capillary electrophoresis, CE). The CL does not need a light source, which significantly lowers the noise levels [KUL03]. The CL is based either on a chemiluminescence labels that bind to the analytes, or on chemilumonogenic compounds that react with the analytes generating CL. A multichannel immunosensor for biodetection using chemiluminescence has been reported by Yacob-George et. al. [GEO02].
The ECL can be considered as a type of chemiluminescence, taking place due to electron transfer between an electrode and species present in the contacting solution or bound to the electrode surface. A fully integrated probe for on-chip generation and detection by ECL has been reported [FIA97]. The CL and ECL have the advantage of lower cost, because of the lack of expensive lasers or accurate excitation optics [KUL03].

The high sensitivity is typical for all luminescence methods. The limit of detection (LOD) for some of them is in the sub-picomolar range.

In addition to the luminescence methods, the optical detection methods comprise absorption, refractive index and transmittance measurements. An essential advantage of the "interfacial optical biosensors" is that no labeling of any kind is necessary [WOO99]. Such methods are: Total Internal Reflectance Fluorescence

(TIRF), Surface Plasmon Resonance (SPR), Resonant Mirror (RM) and Optical Grating Coupler Sensor (CGS). Versatile optical detection systems use organic or inorganic nanoparticles as labels for optical detection [SEY05].

Real-time detection of bio-molecular binding events has been already carried through with the SPR method [JOE93][BIA06]. SPR is a collective resonance vibration of the electrons in a metal layer caused by polarized light. SPR appears when light is reflected by a conducting film at the interface between two media with different refractive indexes. SPR causes reduction of the light intensity at a certain angle of reflection. In the Biacore system [BIA06] gold is used as a conducting film, the sample and the glass sensor chip are the media with different refractive indices. Binding of molecules on the sensor surface leads to change of the refractive index at the surface. The change in the refractive index causes a change of the angle of reflection in which SPR occurs. The angle at which the resonance appears is very sensitive to the refractive index at the metal-dielectric interface. This process is continuously monitored and the change of the SPR position is plotted against time. The SPR method is marker-free and allows quantitative measurements with a limit of detection of 1-10 pg/mm^2. Since the way of detection is indirect and relies on the dependence of the angle of reflection of light on the surface bound molecules, calibration measurements are needed. A disadvantage of the system is the difficult on-chip integration of the optical parts.

An example for ***mechanical detection*** method is the bending e.g. [WIL00], [RAI01],[HAN01],[HAN05],[CAL05] or change of the resonance frequency e.g. [ILI00] of a cantilever, whose surface was preliminary functionalized for detection of specific target molecules. Cantilever arrays have also been used for detection of analyte in a gas phase e.g. [GIM94], [BAL00], [LAN02].
Quartz Crystal Micro-balances (QCM) are piezo-electric devices that change their resonance frequency by mass changes at the surface [SAU59]. QCM with typical working frequencies between 5 and 20 MHz have been widely used for in-situ thickness measurements for mass changes down to 1 ng/cm^2 [MAR93]. The biosensors based on excitement and detection of acoustic waves in a piezo-electrical material are described in more detail in Section 2.2.1.

The ***electrical detection*** methods comprise Potentiometric, Amperometric and Conductometric detection.
Potentiometric methods – employ the change of the potential of a receptor covered measurement electrode in comparison with a reference electrode. An example for such detection is the measurement of cellular respiration and acidification by using ion-sensitivive field effect transistors (ISFETs) [LEH01].
Amperometric methods – here, the measured electron current is proportional to the product of a redox reaction e.g. [HIN91], [HIN95].
Conductometric methods – utilize changes of the electrical impedance between two electrodes. The changes arise due to a bio-molecular reaction or excretion of cellular

metabolic products that lead to interface or bulk changes between the electrodes e.g. [BAS04], [GOM02], [STE97].
The bio-analytical system "S-Sens" developed at caesar has an additional possibility to work with impedance biosensors. The working principle of the impedance sensor is based on the change of the capacitance between two electrodes when the buffer solution between them with a dielectric constant ε is partly replaced by molecules with different dielectric constant (ε_{bio}), leading to an effective dielectric constant ε_{eff} [LÖH05],[MAL05]. Here, the change of ε depends on the number of the molecules presented in the space between the electrodes.

The ***magnetic detection*** uses magnetic particles as labeling for bio-molecular recognition [BAS98][FER03]. The potential advantages of the magnetic labels over other labels are the stable magnetic properties, not affected by photo-bleaching or reagent chemistry, the possibility to manipulate the magnetic particles by applying of external magnetic fields etc. [RIF03].

The choice of suitable detection principle should be met considering the parameters of the corresponding biosensors. The most important of them are:

sensitivity - this is the change in the output signal of the sensor in comparison with the change of the value of measurement.

selectivity - the possibility of the sensor to distinguish the analyte from all the other similar molecules presented in the sample. It depends on the quality of the receptor immobilization process and on the selectivity of the receptor itself.

resolution – the smallest change of the measured value that causes a sensor response.

limit of detection - the smallest value of the measured value that can be detected by the sensor.

saturation limit – the upper value of measurement that can be detected.

cross-sensitivity – the reaction of the sensor to environmental changes such as temperature, humidity, etc. not connected with the specific detection process. For most bio-sensors one of the most important factors is the temperature.

response time – the interval of time between the change of the measured value and the sensor reaction to it.

reversibility – the possibility of the sensor to be regenerated after the measurement and to be prepared for the next one.

stability – in order to avoid changes of the biological samples under the influence of the environmental parameters, buffer solutions (delivering constant pH) are used.

2.2.1 Acoustic wave sensors

The acoustic waves propagate in solid medium due to the interaction between the atoms and their propagation speed depends on the properties of the solid medium. Depending on the mutual position of the propagation direction of the wave and the axis of oscillation of the atoms, there are two types of waves: shear (transverse) and longitudinal. In case of shear waves the wave propagation direction is perpendicular to the oscillation axis. If all atoms oscillate in one plane, the wave is called linear polarized. In the case of longitudinal waves the propagation direction coincides with the oscillation axis. Depending on the position of the oscillating atoms in the medium, the waves are divided in volume waves (the wave propagates through the whole volume of the medium) and surface waves (the wave propagates on the surface of the medium).
The acoustic wave sensors are based on propagation of acoustic waves in a piezo-electric material. The velocity of the waves depends on the mass-loading on the sensor surface and the phase shift between the input and the output signal is correlated with the additional mass bound at the sensor surface.

The mass-sensitivity of the sensors based on volume waves decreases with an increase of the sensor thickness. This leads to low mechanical stability of the sensors. For this reason, sensors based on surface acoustic waves (SAW) are preferred. Their sensitivity depends on the wave decay into the substrate, but not on the substrate thickness itself.

There are different types of SAW sensors: Rayleigh SAW, Lamb Wave and Love-Wave sensors. If Rayleigh SAW sensors contact a liquid, excitation of an acoustic wave normal to the surface leads to energy loss (damping) and decreased sensitivity. The Lamb waves propagate in a thin membrane (several micrometers thick). Since the sensitivity of the Lamb wave sensors increases with the decrease of the membrane thickness, the mechanical stability is an essential disadvantage of the Lamb wave sensors.

Horizontally polarized shear waves are preferred for sensor purposes in liquids, because they do not couple elastically with an ideal fluid [DUJ96] and the energy remains concentrated at the sensor surface. This provides the high sensitivity of the SAW sensors. The Love sensors use shear waves that propagate in an additional guiding layer on the surface. They are called “Love” waves. If the propagation speed of the waves in the material of the guiding layer is lower than their propagation speed in the substrate medium, the waves are reflected at the layer-substrate

interface. The SAW sensors based on "Love" waves are described in more detail in Section 2.3.

2.3 SAW sensor

2.3.1 Principle of the SAW sensor

The SAW sensors based on "Love" waves possess higher sensitivity than sensors based on volume waves, because the energy of the wave is concentrated at the sensor surface [BAL97]. Here, horizontally polarized shear acoustic waves are generated and detected by interdigitated transducers (IDTs) situated on either side of the active sensor area. The acoustic waves are excited by alternating electrical field. Because of the piezo-electrical effect, the alternating electrical input signal is transformed into acoustic waves. The adsorption of bio-molecules on the top of the guiding layer changes the velocity of the shear waves propagating along the sensor surface. The propagating waves are received and transformed by the output IDTs into an electrical signal again. The differences in the phases and the changes of the amplitudes between the input and the output signal are proportional to the loading on the sensor surface. Typical working frequencies of the SAW devices are between 30-300 MHz [MAR94].
In order to reduce damping of the wave, which is caused by energy dissipation into the substrate, the substrate and the guiding material must be chosen in a way that the wave propagation speed in the crystal substrate (v_Q= 4952 m.s^{-1} in quartz) is much higher then the propagation speed in the guiding layer (v_{SiO2}= 3764 m.s^{-1}). In this case the waves are reflected at the silicon dioxide /quartz interface and remain in the guiding layer. Polymer materials have also been used as guiding layers e.g. [GIZ96],[NEW03]. They possess lower acoustic wave velocity in comparison with the SiO_2, but have higher acoustic losses.
The type of the excited acoustic waves depends on the parameters of the IDTs and the media of propagation. Fig. 2.1 shows schematically the position and the parameters of the IDTs.

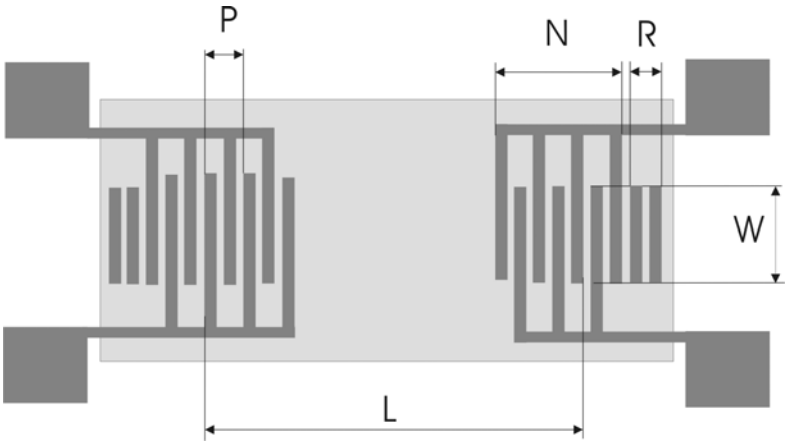

Fig. 2.1 Scheme of the guiding layer and the position of the input and output IDTs of the SAW sensor. N and R are the numbers of the fingers of the IDTs and the reflector electrodes, respectively, P is the periodicity of the fingers, W is the acoustic aperture, L is the distance between the centers of the IDTs.

The optimal frequency for the excitation of the acoustic wave (F_{op}) depends on the periodicity of the finger structures (P) and the propagation speed of the wave (V) as follows:

$$F_{op} = \frac{V}{P} \qquad (1)$$

The energy transfer from the electrical signal into an acoustic signal is mainly dependant on the acoustic aperture (W) of the input IDTs. The acoustic aperture is the length of overlapping of the IDTs fingers (see Fig. 2.1).
Every finger pair of the IDTs forms a capacitor. With increasing aperture the capacity increases and the electrical conductivity of the IDTs can cause a short circuit. In this case the acoustic wave generation in the crystal is terminated. That is why the acoustic aperture is optimized for the specific SAW sensor, taking into account the parameters of the signal generation and read-out electronics. The number of fingers influences the bandwidth of the sensor [MAI73]**.** For high sensitivity of the SAW sensor, the active sensor area between the IDTs, which is in fact the surface contacting the sample, must be as large as possible. On the other hand, the increase of the distance between the IDTs means increase of the wave damping as well. Thus, the distance between the IDTs should be optimized.
The thickness of the guiding layer has to be optimized with respect to the mass sensitivity of the sensor. The sensitivity of the Love-wave sensors is strongly dependant on the length of the acoustic wave and the thickness of the guiding layer.
The acoustic waves generated by the input IDTs propagate not only toward the output IDTs, but also in the opposite direction. In order to reduce the energy loses, reflection electrodes behind the input IDTs can be designed that reflect the wave towards the output IDTs.

If ΔV is the change of the wave velocity (V) and $\Delta\varphi$ is the change of the phase (φ) in an oscillating crystal for mass loading Δm and S_m is the mass sensitivity, then [SCH03]:

$$S_m = \frac{\frac{\Delta V}{V}}{\Delta m} = \frac{\frac{\Delta \varphi}{\varphi}}{\Delta m} \qquad (2)$$

The bio-chemical sensitivity of the SAW sensor strongly depends on the immobilization method of the receptors [BAR01]. The packaging density of the receptor molecules on the sensor surface influences the total sensor sensitivity as well. In this work, a gold layer deposited on the SiO_2 guiding layer was used as a surface for the bio-molecular binding processes. The coupling chemistries are described in Section 2.3.2

The limit of detection of the bio-analytical system depends on the sensitivity of the sensor and the electronic signal to noise ratio, as well as on the quality of the bio-chemistry used for the sensor surface preparation.

SAW have been used for mass loading detection and measurement of fluid properties [KAN85]. Real-time detection of biological molecules e.g. [TES97], [GIZ03] and binding events e.g. [SAH03],[SCH04] have already been reported.

2.3.2 Bio-chemical binding processes

The SAW bio-sensors used in this work have been developed for detection of macromolecules (DNA, RNA, proteins, as well as cells, viruses etc.). In all cases the molecules that are to be detected (analytes), should be reliably bound to the sensor surface.
The binding takes place by using special receptor molecules that are pre-immobilized on the active sensor area. The receptor molecules must possess a high affinity to the analyte and must not bind similar biological molecules. The choice of suitable receptor depends on the molecules that are to be detected. Receptor/analyte coupling represents specific binding between different organic macromolecules (or cells): proteins, enzymes, antibodies and aptamers can be used.

Enzymes are proteins that catalyze bio-chemical processes in living organisms [ABU94]. Their active side consists of 5-10 nucleic acids and is usually located in the middle of the enzyme in order to assure reactions only with specific molecules. The enzymes lose part of their specificity in vitro. The binding properties and selectivity of the enzymes are sensible to change of environmental parameters (temperature,

pH, irradiation, etc.). Enzymes have typically molecular weights between 13 kD and 50 kD.

Antibodies. They are a part of the immune system. They represent proteins produced by the blood plasma cells for neutralization of foreign substances (antigens). The antibodies are highly specific and hardly take part in chemical reactions with bio-molecules similar to their cognate. They cannot be in vitro synthesized and are extracted from the living organisms. Their molecular weights are typically between 140 kD and 200 kD. In comparison with the enzymes their binding properties are less dependant on environmental parameters.

Cells. They are the smallest independent viable unit. They possess a wide range of binding possibilities. However, the cells need special environmental conditions in order to be kept alive outside the human body. Cell-based biosensors have been developed by different research groups [BOU96], [PIZ97],[PAN98], [GRA01],[GIL01].

Aptamers. The aptamers are in vitro selected nucleic acids. The selection is fulfilled by a SELEX process [LAN99] within a pool containing more then 10^{15} different sequences by iterative cycles. They can be selected for different targets such as proteins, peptides, or low molecular weight ligands. The process represents a flow-through of a broad range of nucleic acids (DNA, RNA) through a column with immobilized analyte molecules for which receptor molecules are sought. The nucleid acids that bind on the analyte molecules in the column are further concentrated. Afterwards, their sequence is determined in order to be produced in vitro. The aptamers have weaker specific binding properties compared with that of the antibodies. However, the aptamers are smaller, easier to regenerate and less expensive.
A review of the receptor-ligand binding technologies has been published by de Jong et al. [JON05].

For reliable bio-analytical analysis the immobilization of the receptors to the sensor surface must be stable and should not be influenced by small changes of the temperature, pH or the flow parameters. Moreover, the receptor immobilization process must be reproducible. It must not change the binding affinity of the receptors to the analyte.

There are different ways for immobilization of the receptor molecules [SCO95].
The adsorption on insoluble matrices due to surface forces like van-der Waal´s forces, ion binding forces etc. is not stable enough. The binding is very sensitive to the solvent parameters, pH, temperature etc.
The commonly used method for receptors immobilization is a covalent binding to an intermediate layer. It represents a binding of the receptor molecules to gold surface via an intermediate self-assembled monolayer (SAM). In this work, SAM of alkanethiols was used (Fig. 2.2). The alkanethiols spacer molecules have two active parts – with the first one (thiol group) they covalently bind to the gold surface

arranging a close-packed single molecular layer. The second active part contains Amino (NH_2)-, Phosphate (PO_4)- or Cyano (CN)- groups that bind the receptor molecules.
The receptors should be immobilized at moderate concentrations. At higher concentrations, there are reduced spaces between the receptor molecules that hampers the access of the analyte.

A scheme for immobilization of receptors via alkanethiols SAM on gold surface is shown in Fig. 2.2.

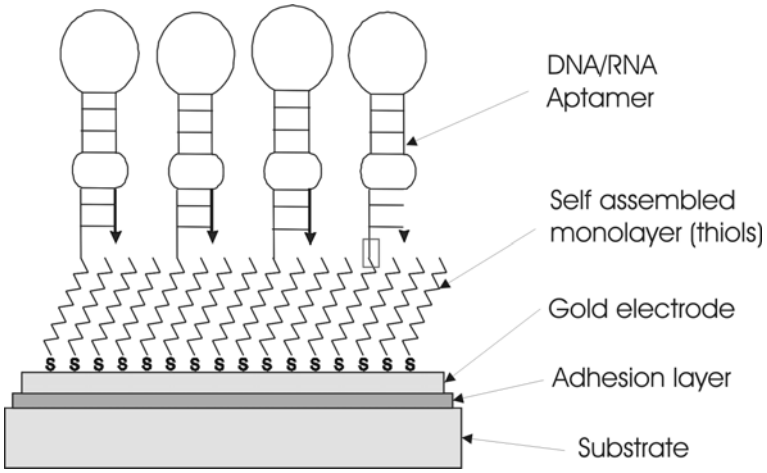

Fig. 2.2 Structure of the SAW sensor surface with the immobilized alkanethiols monolayer and coupled DNA/RNA aptamer.

The covalent binding of the receptors is stable and is preferred to the other immobilization methods. For achieving a 3-dimensional layer, the receptor molecules can be embedded into a dextran matrix e.g. [BAR01].
An alternative immobilization technique is the use of 100 nm thick carboxylmethyldextran (CMD) [WOO99]. The molecules of interest can be either adsorbed or covalently bound to the CMD.

In some cases, the immobilization process can alter the biological activity of the receptors [WOO99]. One possible reason for the loss of protein activity can be their attachment to the substrate with several different amino-acid residues that causes a random orientation of the attached protein. Furthermore, the covalent binding can alter the functional groups of the receptors and change their binding activity to the analyte by either inactivation or loss of specificity. The binding possibility of the analyte is also affected on the density of the bound receptors. On the other side, a

non-covalent adsorption of the receptors to the activated surface can take place. All these factors lead to loss of specificity or unspecific binding events that always should be considered by the interpretation of the results.
A disadvantage of the binding approach is that the immobilization process can be non-uniform that influences the sensitivity of the system.
The covalent binding is a well-established immobilization method e.g. [GIZ97], [JOS01], [SCH04].

2.3.3 Physical effects at the SAW sensor/fluid interface

In this work, the SAW sensors are used in liquid environment, therefore the physical effects at the interface between an oscillating solid material and liquid medium will be discussed in more detail.

The SAW sensors detect not only mass loading on the sensor surface. An additional damping of the wave occurs when the sensor surface contacts a liquid medium. Because of the adhesion forces between the sensor surface and the liquid, evanescent waves are generated in the liquid, causing energy loss of the wave propagating in the crystal. Furthermore, changes of the environmental parameters influence the liquid properties, which leads to phase and/or amplitude shifts of the acoustic signal. For minimization of this effect the design of the sensor system must be optimized.

2.3.3.1 Loading of a rigid layer

The effects at the interface between the oscillating crystal and liquid medium have been investigated for QCMs [KAN85]. The change in resonance frequency of QCM is proportional to the mass of a thin film loaded on the surface [SAU59]:

$$\Delta f = -\frac{2 f_0^{\,2} \Delta m}{A\sqrt{\mu_q \rho_q}} \qquad (3)$$

where f_0 is the resonance frequency of the quartz substrate without mass loading on the surface, ρ_q is the specific density of quartz, μ_q is the shear modulus of quartz, A is the active surface area, Δm is the mass bound at the surface.
If the deposited layer is homogeneous, rigid and has a constant density, in vacuum conditions the shift of the resonance frequency Δf is proportional to the thickness of the layer, respectively to the mass Δm bound at the surface [KAN85]:

$$\frac{\Delta f}{f_0} = \frac{\Delta m}{m} \qquad (4)$$

where f_0 is the resonant frequency and m is the mass of an unloaded resonator. At the same time, the amplitude of the signal does not depend on the layer thickness and no phase shift is observed. Such layers are called acoustically thin layers (films). In case of acoustically thin layers, the entire film moves synchronously with the oscillating substrate surface. In contrast, the oscillation of the upper part of an acoustically thick film delays the wave in comparison to the film-substrate interface [MAR94].
For acoustically thin layer the sensitivity of the SAW sensor does not depend on the thickness of the layer.

2.3.3.2 Loading of a Newtonian liquid

When the QCM contacts a Newtonian liquid [KAN85], its surface transmits the oscillation via the adhesion forces into the liquid. A plane-parallel laminar flow U_x (Y) is generated in the liquid, which can be described with the following equation [WHI74]:

$$U_x(Y) = U_{x0} e^{-[((1+i)/\delta)y]} \qquad (5)$$

where U_{x0} is the surface particle velocity, $i = \sqrt{-1}$, δ is the decay length (also called penetration depth) of the wave into the liquid, y is the axis perpendicular to the surface.
The penetration depth of the wave into the liquid δ is shown in Fig. 2.3. It depends on the viscosity and density of the liquid and on the operation frequency. It is given by:

$$\delta = \sqrt{\frac{2\eta_l}{\omega\rho_l}} \qquad (6)$$

where ω is the angular frequency (ω=2πf), η_l and ρ_l are the shear viscosity and the density of the liquid.
If the height of the liquid is much larger than the penetration depth δ, the liquid acts as "semi-infinite liquid". The exponential decay of the amplitude of the acoustic vibrations in the liquid with an increase of the distance to the sensor surface leads to a decrease of the sensor sensitivity to liquid changes. Only changes of the liquid properties near to the solid/liquid interface influence the sensor signal. By increasing the working frequencies in the MHz range, the decay length of the acoustic wave into the liquid decreases.

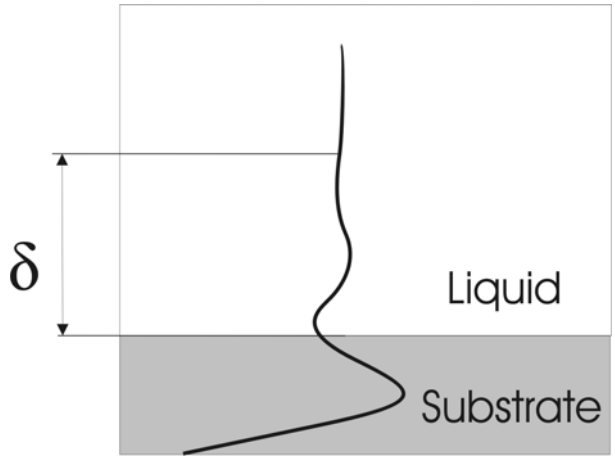

Fig. 2.3 Excitation of a viscous shear wave in liquid in contact with an oscillating QCM. δ is the penetration depth of the wave into the liquid.

According to Kanzawa [KAN85] if the QCM contacts a Newtonian fluid, the phase shift is accompanied by damping of the acoustic wave, which depends on the density-viscosity product of the liquid. The liquid loading increases the mechanical impedance on the oscillating surface according to Martin et. al. [MAR93] leading to a decrease of the resonance frequency and an increased damping of the propagating wave proportional to $\sqrt{\eta_l \rho_l}$ [KAN85]:

$$\Delta f = -fo^{\frac{3}{2}} \sqrt{\frac{\eta_l \rho_l}{\pi \mu_q \rho_q}} \qquad (7)$$

As can be seen from (3) and (7) the mass loading and the liquid medium have different contributions to the SAW sensor signal.
The surface acoustic wave is propagating into the guiding layer as a polarized shear wave. That is why, considering the properties of the Newtonian fluids (see Section 3), no compressional waves are excited in the liquid. The lack of energy losses for excitation of compressional waves is an essential advantage of the Love-waves for mass – sensing applications.

2.3.3.3 Simultaneous thin film and liquid loading

If QCM is loaded with an acoustically thin layer that contacts a Newtonian liquid, the phase and amplitude changes of the sensor signal are the sum of the changes caused by the thin film and the liquid.
If the loading on the surface is not an acoustically thin layer, the mass of the liquid will be also measured and the sensor signal does not correspond to the real mass-

loading on the surface. If the binding at the sensor surface is accompanied by significant amplitude changes that are not due to the fluid properties, this is a proof for a non-rigid loading. In the case of metal layers bound to the sensor surface, the increase of the layers thickness leads to phase shifts, as well as to energy losses of the acoustic wave.

The equations of Sauerbrey, Kanazawa and Martin describe the ideal cases of acoustically thin layers contacting Newtonian fluids. In the real case, the SAW sensor surface is covered with multiple protein layers, long DNA chains or polymer layers. Their behavior can not be completely described neither by acoustically thin layer nor by Newtonian fluid theories. For immunosensing purposes, the pure mass effect is dominant when dealing with one or two protein layers [WEI98] and the mass loading could be considered as an acoustically thin film. This type of mass loading causes only phase changes of the acoustic signal propagating within the guiding layer.
The damping of the wave into the liquid must be considered if binding analytes are larger then the penetration depth of the wave in the liquid. In this case the sensor does not accept the analyte as a rigid mass bound to the surface, but as a new liquid loading with its own density-viscosity product [TES97].

2.3.3.4 Additional sensitivity parameters of the SAW sensors

The interaction between the surface acoustic wave and the liquid medium leads to changes of the velocity and the amplitude of the wave. Except mass coupling on the surface, the SAW sensors are sensitive to changes in the temperature, conductivity, dielectricity, static pressure, viscosity and density of the liquid. The acoustic signal is also influenced by the mechanical stress built in the substrate and in the surface layer, roughness of the surface [MAR93], temperature changes in the guiding layer or substrate. However, if the SAW sensor is properly optimized, the major contribution to the change of the sensor signal is the change in mass [BAR01].
Fig. 2.4 shows schematically the factors influencing the surface acoustic waves propagation when the sensor surface contacts a liquid.

The *roughness* of the surface R_a can be neglected if it is much less then the wave decay length in the liquid $R_a < 0.15\delta$, as has been reported by Martin et. al. for thickness-shear mode resonators [MAR93]. Such surfaces are called hydro-dynamically smooth surfaces. Here, the surface wetting properties do not influence the sensor signal.
As the surface roughness becomes comparable with the wave decay length $Ra > 0.15\ \delta$, effects such as liquid trapping and compressional wave generation become more important. In this case, the resonance frequency is affected [ROD96]. The low contact angles (hydrophilic surfaces) lead to maximum liquid penetration into the microcavities, while hydrophobic surfaces limit the liquid trapping.

According to [MAR94A], the shift in the QCM resonance frequency Δf can be described by:

$$\Delta f = \Delta f_v + \Delta f_t = -\frac{\sqrt{f}}{2t_q\rho_q}\sqrt{\frac{\rho_f \eta_f}{\pi}} - \frac{f}{t_q\rho_q} t_f \rho_f \qquad (8)$$

where Δf_v is the induced frequency shift due to the liquids viscosity and density, Δf_t is the frequency shift due to the trapped liquid with an average thickness t_f. ρ_f and η_f are the density and the viscosity of the fluid respectively, t_q and ρ_q are the thickness of the quartz substrate and its density respectively, f is the resonance frequency of the unloaded quartz.
Since the roughness of the sensor surface does not change during the measurements, it has a constant contribution to the sensor signal and can be neglected.

Thickness of the metal layer providing the binding surface. In the ideal case the gold electrode is considered as an acoustically thin layer. In reality, it has also visco-elastic contribution that increases with increasing of the layer thickness. In this work, the 300 nm thick gold layer was considered as acoustically thin. As in the case with the surface roughness, the layer thickness is constant during the measurements and causes no cross-sensitivity effects.

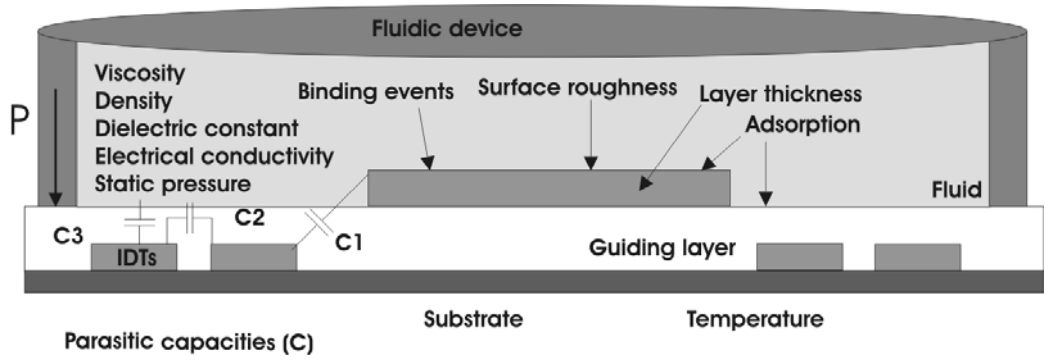

Fig. 2.4 Factors influencing the signal of the SAW sensor in contact with a liquid. C1, C2, C3 are parasitic capacities. The seal exerts pressure P on the sensor surface.

The *temperature* influences the velocity of the acoustic wave in the piezo-electrical substrate e.g. [ROY00],[GAU02]. In order to minimize the influence of the temperature on the quartz substrate, the quartz crystal should be cut through a

crystallographic plane that assures minimal temperature dependence of the frequency of the acoustic waves.
Therefore, the used SAW sensors were fabricated on ST-cut quartz substrates. Here, temperature deviations near the room temperature cause mutual compensating effects caused by the wave velocity shifts and the thermal expansion. In this way, the temperature deviation of the acoustic properties of the crystal is minimized. In the case of "Love" waves, the temperature properties of the guiding layer should also be considered.
In addition, most of the liquid parameters that influence the sensor signal such as density, viscosity, dielectricity are temperature dependant as well. This leads to a complex temperature dependence of the acoustic wave sensor response.
For reliable measurements, it is important to achieve a stable signal "base line", without phase and amplitude drifts. The only way to achieve this is to keep the temperature constant during the measurements. In this work, additional temperature stabilization for the chip-carrier was realized by using a Peltier element. The fluidic design was optimized (see Section 5) in order to reduce the temperature effects by minimization of temperature difference between the liquid and the sensor surface.

Density (ρ_l) and *viscosity* (η_l) of the liquid. The density and viscosity of the liquid influence the phase shift of the acoustic signal. The density influences to a large extent the phase shift, while the viscosity leads to damping of the wave amplitude. At higher operation frequencies the liquid loses its pure viscous properties, typical for a Newtonian fluid, and the elastic behavior component increases.
The density and viscosity of the liquid can change during the measurements, because of temperature fluctuations. During the measurement, the density/viscosity product of the liquid could be changed also due to mixing of the sample and buffer solutions. This effect can be reduced by proper liquid handling, which is described in Section 5.

The *electrical conductivity* and the *dielectric constant* of the liquid also affect the sensor signal. The vibration of the atoms of the piezo-electric material causes creation of an evanescent electric field. If the liquid is conductive or polarized, the electrical field of the crystal is transmitted into the liquid. With the increase of the electrical conductance of the liquid, the damping of the wave in the crystal increases. Higher conductivity increases the electrical losses of the IDTs, their capacity increases and influences their coupling factor (input admittance).
The buffer and sample solutions are usually weak electrolytes, containing polar molecules or ions. At the working frequencies (in the range of 140 MHz) the ions (or polar molecules) are still mobile and can follow the changes of the alternating electrical field. Thus, the electrical conductive liquids lead to an appearance of additional parasitic capacities at the substrate / liquid interface (see Fig. 2.4).

The influence of the liquid conductivity can be substantially reduced by using higher working frequencies. However, according to equation (1) the periodicity P of the IDTs must be reduced. The fabrication of IDTs beyond those fabricated by optical lithography is more expensive.

Some authors [BAR01] have reported use of shielding layer on the sensor surface to prevent the electrical interaction between the liquid and the IDTs. The shielding layer must be conductive and connected to the ground. It was observed with the "S-sens" system, that shielding layers led to an increase of the cross-talk between the IDTs, which varies with the change of the operation frequencies.
The active surface area between the IDTs is a metal layer and serves as a shielding layer as well.
In Section 5 another approach for preventing the contact between the IDTs and the liquid was tested. The seal of the fluidic cell contacted the chip between the IDTs on the active sensor area. However, the seal can cause an additional damping of the acoustic wave.
In the case of "Love" waves, the electric fields in the piezoelectric material are partly separated from the liquid by the non-piezoelectric guiding layer e.g. [JAK98].

Adsorption at the surface (unspecific binding). The surface of the SAW sensor is covered with immobilized receptor molecules that specifically bind the analyte molecules present in the sample. In some cases, it is possible for some biological species different from the analyte, but with similar biological affinity, to bind to the surface. This leads to unspecific binding events and subsequently to false interpretation of the results. Furthermore, some species from the sample could be deposited on the surface by simple adsorption. This effect is also not specific and does not depend on the type of the receptor molecules.

Static pressure. The static pressure of the liquid can be neglected, concerning the fact that it does not change during the measurement.
The sealing between the microfluidic device and the sensor chip is assured by applying of a spring-loaded force on the top of the fluidic device. The pressure is transmitted through the sealing onto the sensor surface. The pressure exerted by the fluidic device on the surface of the sensor chip is constant during the measurement. However, rash changes of the flow rate or switching of the integrated valves can cause a slip of the sealing on the sensor surface, which is detected from the sensor.

2.3.3.5 Methods for reduction of the influence of the cross-sensitivity parameters

Reference Sensor

In order to correct for the effect of the unspecific binding, as well as to correct for the influence of the fluid parameters, a reference sensor is used. The reference sensor is covered with biological species acting as blocking agents. They bind on the active sites on the sensor surface and prohibit the analyte binding. Assuming that the unspecific binding events and the fluctuations of the fluid parameters should be equal to all sensors, the signal due to specific binding events (desired signal) could be

plotted by simple subtracting of the reference sensor signal from the total signal of the active (measuring) sensor [GLA03].

Two-frequency mode measurements

The above mentioned assumption is only valid, if the parameters of the measuring and the reference sensors are equal for the chosen frequency band. However, the different SAW sensors on the same bio-chip have certain fabrication tolerances, which lead to discrepancies in the absolute values of the phase of the acoustic signal. This results in different interference between the signals and cross-talk between the capacities. For measurements of different glycerol concentrations, carried through at a specific frequency, the deviation of the signals obtained from all five SAW sensors on the same biochip was up to 30 % [GLA04]. This deviation increases when the analyte and the buffer are salts with different concentrations or have different pH.
In order to compensate for the contributions of the fabrication tolerances on the sensor parameters, the measurements can be carried out at two different frequencies. In this way, the sensitivity deviations between the sensors on a single SAW chip were reduced to 5%. Thus, in a two-frequency mode the sensitivity deviation between the sensors can be practically eliminated.

Reference Liquid

The liquid parameters are measured parallel to the mass-loading on the surface. The changes due to the fluid medium should be considered in order to separate the real signal (due to mass loading on the surface) from the total sensor signal.
It is known [SAU59], [KAN85] that the mass loading on the sensor surface causes only phase shift, while changes in the fluid parameters cause phase as well as amplitude variations. One possible way to separate the mass-loading and the fluid effects from the sensor signal is the injection of a reference fluid that possess a higher viscosity in comparison with the used buffer solution.
The phase and the amplitude of the acoustic signal are proportional to $\sqrt{\rho_l \eta_l}$. If φ_L and A_L are shifts in the phase signal and in the amplitude correspondingly, the ratio R_L (equation 9) is a constant for every sensor.

$$R_L = \frac{\varphi_L}{A_L} \qquad (9)$$

During the following sample injection, the total phase signal φ_t contains phase change due to mass loading φ_m and phase (φ_s) and amplitude changes (A_s) due to the sample solution. Then:

$$R_L = \frac{\varphi_s}{A_s} \qquad (10)$$

and the phase signal due to the mass–loading is calculated as follows:

$$\varphi_m = \varphi_t - R_L A_s \qquad (11)$$

3 MICROFLUIDICS

Microfluidic devices have already found limited, but important applications for transport and handling of small amounts of gases and liquids. The first micro-fluidic handling was accomplished by Lord Rayleigh in 1878, who managed to break liquid jets into individual droplets. This principle was the base for the first developed technology for operation with liquid droplets - the continuous ink-jet printing technology in the 1970s.

In the following years a variety of fluidic devices such as active and passive valves, micromachined pumps, flowsensors, chemical microreactors, micromixers, chemical and bio-chemical sensors have been developed. The technologies for fabrication of such devices are nowadays still not mature enough and in most cases can not meet all the requirements needed. However, there is a huge application potential in the future, especially in the area of life sciences and medicine. Some of the promising fields of application are the drug development, micro-dispensing and delivery of drugs, genotyping and gene expression, diagnostics and toxicology screening. Microfluidic devices are needed also for environmental and food analysis, chemical microanalysis systems, etc.

As it was described in Section 2, the ultimate goal of the microfluidic development is fabrication and operation of an analytic system onto a single chip, called micro-total analysis system (μ-TAS). All the necessary processes for analysis (sample preparation, chemical (physical) reaction, data transformation into an output signal proportional to the concentration of the component) should take place on a single chip.

The main reason for the emerging and the fast development of the microfluidic technology was the need of fluid handling in the micro- and nanoliter range for genomic and proteomic analysis. The first Lab-on-chip device that has been fabricated was a gas-chromatographic analyzer [MAN90], [MAN90A]. It was made by silicone micromachining and consisted of an injection valve and 1.5 m long separation column.

In the early 90s the μTAS concept gained popularity. New approaches for pumping of liquids in small channels have been developed (electroosmosis, electrophoresis). In 1992 the electroosmotic pumping was demonstrated for achievement of injection, separation and detection on the same chip by Harrison et. al. [HAR92]. The same group reported on chip separation of fluorescein isothiocyanate-labeled amino acids by using laser-induced fluorescence [SEI93]. In the following years micro-fluidic devices for DNA amplification (Polymerase Chain Reaction, PCR), cellular methabolism and flow cytometry appeared. By using electrical fields on chip separation of DNA, amino acids, oligonucleotides as well as cell manipulation have been reported [REY02].

3.1 Theoretical basis of fluidic mechanics in the microliter range

The aim of the development of microfluidic devices is to utilize the scaling laws in order to improve the device performance. With reduction of the dimensions in the micro-range the surface effects prevail over the volume effects and the capillary forces dominate over the gravity force.

Capillarity is observed as rising or decrease of the liquid in narrow channels due to the surface tension. The surface tension is an effect taking place at the interface between two phases and is defined as a force F_σ exerted over length l:

$$\sigma = \frac{F_\sigma}{l} \qquad (12)$$

The molecules of the liquid that contact the solid surface interact with other molecules from the liquid, with gas molecules, as well as with the solid molecules [NGU02]. Fig. 3.1 presents the surface tensions at the gas/liquid/solid interface:

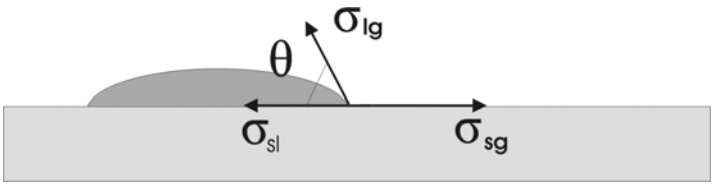

Fig. 3.1 Solid/liquid/gas interface. σ_{lg}, σ_{sg}, σ_{sl} are the surface tensions at the liquid/gas, solid/gas and solid/liquid interfaces correspondingly. θ is the contact angle of the liquid on the solid surface.

From the balance of the forces applied:

$$\sigma_{sg} = \sigma_{sl} + \sigma_{lg} \cos\theta \qquad (13)$$

where σ is the corresponding surface tension at the solid/gas, solid/liquid and liquid/gas interface, θ is the contact angle. If the contact angle θ is smaller then 90°, the surface is wetted by the liquid and is called hydrophilic. For θ>90, the surface is hydrophobic and the liquid is called non-wetting.

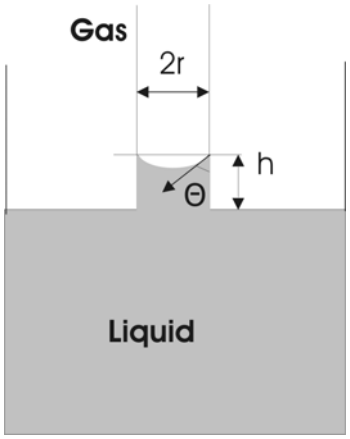

Fig. 3.2 Capillarity of liquids in a narrow hydrophilic tube. r is the radius of the tube, θ is the wetting angle, h is the height of the liquid in the tube.

Fig. 3.2 shows the liquid behavior of fluid when contacting a narrow hydrophilic tube. Because of the surface tension, the liquid wets the walls of the tube and has higher level as the liquid in the big vessel. The form of the meniscus depends on the surface tension of the liquid. The height h of the liquid in the tube is given by:

$$h = \frac{2\sigma_{lg}\cos\theta}{\rho g r} \qquad (14)$$

The liquid behavior at the solid/liquid interface is an important issue in microfluidics, because the liquid contacts the surface of the vessel during the liquid transport. The relative increase of the surface to volume ratio increases the influence of the surface tension on the liquid flow. It is difficult to fill hydrophobic tubes with liquid, as well as to empty filled with liquid hydrophobic channels, because of the capillary effects.

The increase of the surface to volume ratio causes relatively more interface surface available for mass or heat transfer. With the reduction of the system size the homogenization or temperature gradients need less time to reach the equilibrium state. Thus, considering the rapid decrease of the diffusion times, as well as the reduced sample volumes, the equilibrium states are often established within seconds or sub-seconds [MAD97].

Let us consider a fluid placed between two parallel plates [NGU02]. If the upper plate is subjected to shear force and is removed to position 2 (Fig. 3.3), the fluid will deform. When the force is removed, the fluid will remain in its position, because it does not exhibit an elastic behavior. When the shear stress (shear force/area fluid contact) is directly proportional to the strain within the fluid, the fluid is called

Newtonian. The Newtonian fluid is not compressible and has uniform viscosity throughout the volume.

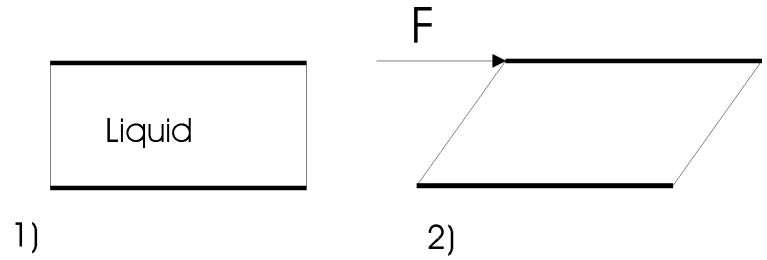

Fig. 3.3 Fluid between two parallel plates (1). Position (2) shows the upper plate displaced by shear force F.

The *Reynolds number*, [GER60], [GRA93], [KOC00], [NGU02], [ATE05] is an important characteristic of every liquid flow. It is a measure of the ratio between the inertial forces and the viscous forces in a particular flow.
The Reynolds number is given by:

$$\mathrm{Re} = \frac{\rho u D_H}{\eta} = \frac{u D_H}{\nu} \qquad (15)$$

where u is the velocity of the flow, D_H is a hydraulic diameter, η and ν are the dynamic and the kinematic viscosities respectively, ρ is the density of the fluid. The hydraulic diameter is given by:

$$D_H = \frac{4A}{P} \qquad (16)$$

where A is the cross-section area and P is the wetted perimeter.

Depending on the Reynolds number, there are three types of liquid flow:

Laminar flow takes place when Re of the flow is lower than the transitional Reynolds number Re_t. For short channels with length L ($L/D_H < 50$) the transitional Reynolds number $Re_t \sim 30L/D_H$. For longer channels ($L/D_H > 50$) $Re_t = 2300$. The laminar flow is dominated completely by the viscous forces and this allows the realization of purely diffusive, convection free transport. The pressure drop in a capillary with radius r for a laminar flow over distance Δx is given by:

$$\frac{\Delta p}{\Delta x} = -\frac{8\eta u}{r^2} \qquad (17)$$

The laminar flow permits streams containing not only different substances, but also different concentrations of the same substance, to flow side by side [ATE05]. The width of the diffusive layer represents the effective membrane thickness and can be adjusted by varying the flow rate.

Transitional flow – it is valid for systems with $Re \sim Re_t$. Some authors consider the transition Re number to be between 2100 and 4000 [MAD97].

Turbulent flow – The turbulent flow takes place in fluidic channels where $Re > Re_t$. Here, the velocity vectors of the particles are varying unpredictably in time. In case of turbulent flow, the inertial forces, which describe the tendency of body in motion to retain its initial motion, prevail over the viscous forces.

3.2 Fabrication technologies for micro-fluidic devices

The micro-fabrication technologies have already found applications in the area of biotechnology and bio-chemical processing [CHO02]. Here, a short description of the main fabrication approaches will be given and the choice of suitable technology for fabrication of micro-fluidic devices will be discussed.

3.2.1 Silicon-based technologies

Most of the micro-fluidic devices nowadays are fabricated either by the micro-electro-mechanical systems (MEMS) technology or by a combination of microstructuring and molding processes.

MEMS technology allows miniaturization and batch processing of mechanical systems not accessible by the conventional machining techniques [MAD97]. It enables definition and control of small geometries, repeatability, reliability and low cost production. Furthermore, the MEMS technology provides an opportunity for integration of mechanical systems with electronics for the closed-loop-controlled MEMS.

Many fabrication methods that had been developed for the microelectronic industry have been adopted by the MEMS technology. The mechanical properties of silicon, silicon oxide (SiO_2) and silicon nitride (Si_3N_4), polycrystalline silicon, are well suited for fabrication of robust and reliable micromechanical devices. Manufacturing techniques such as photolithography, deposition (physical sputtering, low pressure chemical vapor deposition (LPCVD), plasma enhanced chemical vapor deposition (PECVD), oxidation) and etching techniques (ion-beam etching (IBE), reactive ion etching (RIE)) are used for structuring of thin layers (surface micromachining). In addition, new technological processes have been developed for achieving 3-dimensional structures. Wet and dry etching techniques have been used for

orientation-dependant (anisotropic) or orientation independent (isotropic) etching. The process of etching of most of the substrate material to form micromechanical elements is known as bulk micromachining.

Surface micromachining does not suit the microfluidic needs because of the insufficient structure depth and the adjacent sticking problems. However, the bulk micromachining has found vast applications for production of micro-mixers, valves and pumps. Substantial disadvantages are the high cost of the silicon and the expensive techniques for its structuring. In addition, the mechanical properties of silicon (Young's modulus, thermal expansion coefficient) are not always favorable when dealing with fluids.

One of the most popular technologies for fabrication of micro-fluidic devices is based on fabrication of fluidic channels and reservoirs in the silicon by dry or wet etching, followed by bonding a cover of glass on the top for sealing of the cavities. There are different bonding techniques such as anodic bonding (silicon bonded to glass) or fusion bonding (silicon to silicon).

Silicon is still the most preferred material for production of microfluidic devices that have to fulfill complicated tasks (micropumps, most of the microvalves). Additional advantage of the silicon is the possibility to work at higher temperatures (from –80°C to + 1000°C) and high pressures (up to 300 atm.), chemical compatibility, possibility to integrate optical and electrical sensors etc. [JEN06].

Combinations of etching and bonding techniques have been used in the microfluidics for the fabrication of sealed channels and reservoirs, nozzles, mixing chambers, active and passive valve structures and micropumps.

Silicon micromachining is comparatively expensive – many processes are involved for the structuring of micro-fluidic configurations. In order to be profitable, the silicon based technology must fabricate large number of pieces. Moreover, the sealing is accomplished with additional bonding process, more often with glass, that provides stable and inseparable connection between the fluidic components. For these reasons, the silicon micromachining is not compatible with the production of cheap microfluidic disposables.

3.2.2 Polymer-based technologies

Parallel to the further development of the MEMS technologies, polymer materials became increasingly interesting [BEC02], [GUB04]. Polymers are usually less expensive and can be formed easily by using injection molding, thermoforming and hot embossing processes [HEC04]. The fabrication of fluidic devices from polymer materials is based on a combination of a master stamp fabrication (also called mold insert or mold) and subsequent molding process of the polymer. The cost of the raw

polymer material is in most cases comparatively low and the fabrication costs of these techniques are set by the costs of the equipment and the technology for production of the mold inserts.

The choice of suitable technology for production of the master stamps depends on the complexity of the design and the necessary spatial resolution that has to be achieved. Several thousand molding processes can be accomplished with a single molding insert [HEC04]. As a result, even very complex polymer structures can be produced in an inexpensive way that allows their use as disposables. Another advantage of the use of polymers for micro-fluidic applications is their biocompatibility, the possibility for implantation and in-vivo experiments.

A very popular technology for fabrication of mold inserts is LIGA (abbreviation from German lithography, electroplating, molding) [BEC82], [MEN97], [SCH94], [SCH95]. Here, a thick resist layer (from several microns up to centimeters) is exposed with highly parallel X-ray radiation from a synchrotron source. The developed patterns are subsequently filled with a metal by electroplating. After resist removal, the metal forms are used as molds for different molding techniques (injection molding, hot embossing) with polymer materials. Typical parameters of the LIGA patterns are: structural height 20-500 µm, smallest patterns 1-2 µm, resolution 0.25-0.5 µm [MAD97]. The synchrotron radiation lithography allows achieving of high-aspect ratio structures.

Similar techniques can also be used with UV-light lithography in case of smaller aspect ratios, less stringent requirements to the parallelism of the resist walls and resist thickness up to 100 µm. Suitable UV – sensitive resists for such applications are SU 8, AZ 4000 and polyimide resists. Some authors have reported the use of SU-8 as a functional material for the fabrication of fluidic channels e.g. [HOS00], [JAC01]. After the photolithographical structuring of a double SU-8 resist layer the channels are sealed by a glass wafer with a thin unexposed SU-8 layer spun on it [JAC01].

Concerning the fabrication of microfluidic devices, LIGA has the advantage (in comparison with the standard silicon micromachining techniques) for producing of high aspect ratio structures. LIGA has been successfully used for production of active valves and pumps [SCH93]. Alternatively, mold inserts can be also fabricated by mechanical milling, electro- discharge or laser ablation processes. A compromise must be found between the desired resolution, quality of the structures and the production costs.

Most of the expenses for production of polymer microfluidic devices are for the fabrication of the molds. As though one mold can be used for a large number of embossing processes and the polymer materials are comparatively cheap, the whole technology is economically effective.

Some polymers possess very good elastic properties that can be used for fluidic sealing. This allows the usage of fluidic modules with separable connections to the chip and the macrofluidic components.

These advantages are beneficial for fabrication of microfluidic disposables. That is why here, polymer microfabrication process for the microfluidic devices has been chosen. However, by using microfluidic devices on polymer base, some significant factors, such as the chemical resistance of the polymer, must be taken into account. This topic is discussed in detail in Section 3.3.

3.3 Materials for production of microfluidic devices

A number of materials have already been used for microfluidic applications [ZHA06], [KEN06].
These materials have to meet strict requirements in order to assure reliable bio-analytical measurements. Considering the modular design of the bio-analytical system used, its construction and the used substances, the following are the most important requirements on the material for the microfluidic devices:

Chemical resistance. The material should be resistant against the used buffer and sample solutions. Resistance against weak acids and bases is necessary, because the measurements are performed in different pH ranges. The material should not react or be resolved in ethanol, which is used for surface hydrophilization for easier removal of air bubbles in the microfluidic system.

Modular concept. The bio- analytical chips based on SAW sensors and the fluidic devices must be exchangable. Hence, the connection between the sensor chip and the fluidic device should allow their easy separation. The sensor chip is reusable and can be cleaned by oxygen plasma process. However, the fluidic devices should be suitable for disposable usage. This concept makes irreversible connections like bonding or gluing irrelevant. Moreover, the glue impurities could pollute the fluidic channels, which influences the reliability of the analysis.

Sealing properties. The material should possess certain elastic properties that assure reliable sealing on the quartz surface of the SAW chip.

Suitable for batch production. The material should be cheap and readily be formed by conventional molding methods allowing inexpensive batch production.

Optical transparency. This is only important for optical detection methods. For the bio-analytical system used in this work, it is not a necessity. Nevertheless, it is advantageous for detection of air bubbles in the fluidic channels or fluid leakages.

Some materials such as glass, PMMA or PDMS have found vast applications in the production of microfluidic devices.

For applications in the "S-sens" bio-analytical system glass is not suitable, because of the requirement for reversible sealing towards the glass chip. For reliable sealing the glass fluidic should be bonded to the chip, which does not allow their separation. Furthermore, glass (SiO_2) is used as guiding layer for the SAW sensors and additional glass cover structure will influence the acoustic signal in the sensor. Other important issues are the connection to the macro-fluidic system and the expensive glass fabrication technologies.

Considering the requirement for inexpensive batch production that allows the use of the microfluidic devices as disposables, as well as the possession of elastic properties, revealed polymers as a potential group of materials for microfluidic applications. Here, the properties of the most important polymer types will be briefly discussed by taking into account the requirements for the "S-sens" system.

3.3.1 Polymer materials

The polymers are a class of materials built from macromolecules, consisting of a set of regularly repeated chemical units. The units can be of the same type (homopolymers) or very limited number of different types (copolymers) [BOW02]. The units are joined end to end and form chain molecule (backbone). In many cases the units can be arranged in more sophisticated ways, forming branches or nets. According to their properties the polymers are classified in three main groups: thermoplastics, rubbers (elastomers) and thermosets.

3.3.1.1 Thermoplastics

They consist of linear or branch molecules (Fig. 3.4). They can be softened or melted at elevated temperatures. Hence, they can be molded by heating. After cooling below

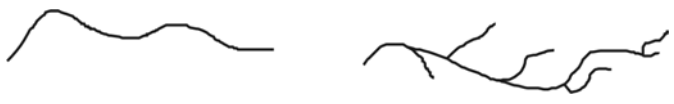

Fig. 3.4 Typical molecular chains of thermoplastic polymer.

a certain temperature, called glass transition temperature (T_g), they may form a glass state known as a "frozen liquid". This state is amorphous (non-crystalline). After cooling the thermoplastics retain the form of the mold without irreversible change of their physical or chemical properties. Due to this property the thermoplastics have found a wide range of applications. There are some types of thermoplastics that partially crystallize (liquid-crystal polymers). The thermoplastics include several groups of materials [DOM98]:

Polyolefines. The non-polar nature of the poleolefines contributes to their high chemical resistivity against a wide range of substances such as non-oxidizing acids, weak and strong bases, inorganic salt solutions, many organic solvents (including alcohols) etc. (see Appendix). Typical poleolefines are polyethylene (PE) and polypropylene (PP). Their chemical inertness and low surface tension lead to a poor adhesion to any other material. The polyolefines are difficult to be glued together, which additionally hampers their integration. Besides their poor adhesion properties, the polyolefines are not elastic (Young`s modulus of PP E_{pp}=1.4x10^9 Pa. For comparison, the rubbers have E_{rub}~ 10^6 Pa [BOW02]). Due to the weak elastic properties, devices made of polyolefines are not able to deliver proper sealing.

Vinylpolymers. They include polyvinylchlorid (PVC), as well as a variety of vinyl co-polymers. The soft PVC-P possesses poor chemical resistance against acids, bases and a number of organic substances. The harder PVC-U can be dissolved in organic acids. Both exhibit poor elastic properties.

Styrene polymers. Generally, they have moderate chemical resistance against organic substances. The mechanical properties of the styrenes are not favorable for sealing purposes.

Polyacrylates. These are polymers based on acryl- and methacryl- acids. Such polymers are the polymethylmethacrylate (PMMA), acrylimide (A/I)-copolymers etc. PMMA is a rigid material (E_{pmma} = 3,3x10^9 Pa) that is resistant against weak bases and acids at 25°C, as well as against non-polar organic solvents. The first generation fluidic devices used for the "S-Sens" system were made by PMMA with a Viton O-ring sealing [SCH03]. The limited resistance against alcohols and the lack of direct sealing properties hampered the further use of these fluidic devices. The construction with the O-ring sealing also sets limits for further miniaturization of the fluidic channels.

Polyvinylcarbazol. Regardless of its very good chemical resistance, the polyvinylcarbazol is rigid and stiff.

Polyacetal (POM) possesses high chemical resistance. It has remarkable mechanical properties among the polymer materials that have led to wide range of applications. However, its rigidness is not suitable for fabrication of sealing structures.

Fluorine-containing thermoplastic polymers. These are polymers in which some or all of the hydrogen atoms in the polyethylene backbone have been replaced by fluorine. Polytetrafluorethylene (PTFE) posseses excellent chemical resistance. It is not soluble in any known solvent at temperatures lower than 300°C. Unfortunately, PTFE has no adhesion properties. PTFE is difficult to be glued, except via special adhesion gluing procedure with preliminary surface treatment (sodium in liquid amoniac or naphtylsodium in tetrahydrofurane) [DOM98]. The PTFE and most of the fluorine-

containing thermoplastics (polytrifluorchlorethylene PCTFE, polyvinylfluoride PVF, polyvinylidene fluoride PVDF etc.) possess poor sealing properties. Because of the strong binding forces in their molecules, the fluorine-polymers have relative high T_g. They can be embossed at temperatures in the ranges of 205°C for PVDF and 370°C for Teflon AF2400. Co-polymers based on PTFE have reduced temperature stability and chemical resistance in comparison with PTFE. On the other hand they still possess comparatively high stiffness and poor adhesion properties.

Thermoplastic polycondensates. Typical representatives of this group are polyamide, PA (high stiffness, insufficient adhesion properties, poor chemical resistance against acids), polycarbonate, PC (poor resistance against bases and moderate against alcohols, high stiffness), polyethylene terephthalate, PET (stiff), polybutylene terephthalate, PBT (stiff). PET and PBT are prone to hydrolysis and prolonged contact with water at temperatures higher then 60°C influences their properties.

Table 3.1 List of the most important properties of the main polymer groups, concerning the requirements for microfluidic applications with the "S-sens" system (++ excellent, + good, 0 moderate, - bad, -- very bad, +/- varies for the different materials).

Material/ property	Chemical resistance	Technological processing	Sealing properties	Mechanical stability
Polyolefines (PE, PP)	+	++	-	++
Vynilpolymers (PVC)	-	++	-	++
Styrolpolymers (PS)	0	+	-	+
Polyacetate (PMMA)	-	++	-	++
Fluorpolymers	++	-	--	0
Thermoplastics (PSU, PEEK, PC, PA)	0	+	-	+
Duroplastic polymers (resins)	-	-	+/-	+
Silicones	+	+	++	-
TPU elastomers	+	++	++	+

Polysulfone, PSU (stiff, good chemical resistance), polyimide, PI (high temperature stability, used in the range from –240°C to 370°C, stiff, poor resistance against weak

bases), polyetherketone, PEEK (very high chemical resistance, weak adhesion properties). Some thermoplastic polycondensates have been used as housings in microfluidic devices fabricated by AMANDA technology [SCH99]. All of the thermoplastic polycondensates possess high rigidness and stiffness. They have high chemical resistance and very limited adhesion properties.
Table 3.1 shows a list of the most important properties of the main polymer groups, considering the requirements set by the "S-sens" bio-analytical system [STO05].

3.3.1.2 Thermosets and rubbers

They are cross-linked rigid polymers with a dense three-dimensional network [BOW02] (Fig. 3.5).

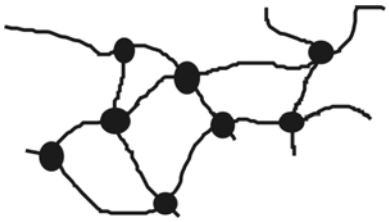

Fig. 3.5 Network structure of thermoset polymer.

The cross-linking process, also called "vulcanization" takes place by using heat, chemicals or radiation. The thermosets cannot be softened by heating and decompose at higher temperatures. Examples of thermosets are the epoxy resins, phenol resins, silicones, rubbers, polyesters, polyurethanes etc. They have limited chemical resistance (see appendix).

The rubber materials possess high elastic properties (Young's modulus typically of the order of 1 MPa for small strains, recoverable extensions up to 1000% often possible [BOW02]) that make them ideal for sealing purposes.

Silicones are inorganic polymers in which the silicon atoms join together with oxygen as chains or networks. The backbone consists of silicon and oxygen atoms (…-Si-O-Si-O-Si-O-…) with side groups connected to the silicon. The silicones are a wide range of materials that differ by their chain length, side groups and the extent of cross-linking. The silicones include silicone resins, -elastomers, -oils etc. The silicone elastomers are most suitable for sealing purposes. The most common silicone used for microfluidic applications is polydimethylsiloxane (PDMS). There, all side groups (two for every silicone atom) are methyl groups (CH_3).
Depending on the cross-linking reactions, also called vulcanizing or curing process, the silicones are separated in three main groups – with peroxide-initiated curing,

condensation curing and an addition curing [WEB01]. In Section 5 addition-cured silicone was used for fabrication of microfluidic devices.
The silicones have high gas permeability, which could lead in some cases to additional formation of air bubbles into the fluidic structures.

Polyurethanes include foamed materials, glues, varnishes, elastomers (networks and thermoplastic). The thermoplastic polyurethanes belong to the group of the thermoplastic elastomers – materials that combine the elastic properties of rubber with the properties of thermoplastics (see Section 3.3.2).

3.3.2 Thermoplastic elastomers

They are co-polymers that consist of two separated phases [HOL96],[HOL00]. Every phase has its own melting point (T_m) or glass transition temperature (T_g). The temperature range between the T_g of the soft (rubbery) phase and the T_m (T_g) of the hard phase indicates the area of the thermoplastic-elastomeric properties, also known as "rubbery plateau". At temperatures lower then T_g of the soft component both polymer components are hard and the material is rigid and brittle. For temperatures higher then T_m (T_g) of the hard component, both polymers are fluids and the elastomeric properties are lost.

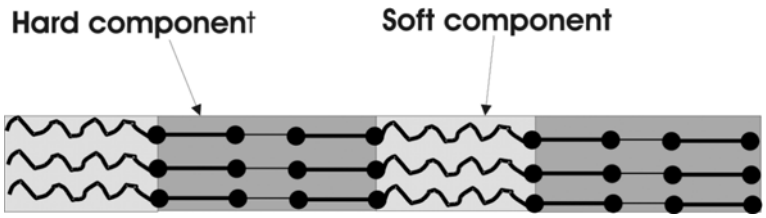

Fig. 3.6 Scheme of the macro-molecular structure of thermoplastic elastomer material. The hard and the soft components tend to build separate phases.

The common properties of the thermoplastic elastomers can be described as a function of their hardness: the elastomeric part reduces their stiffness, chemical resistance, as well as their T_g. The hard polymer contributes to the increase of the chemical resistance and the mechanical stiffness, but reduces the elastic properties of the copolymer. Most of the thermoplastic elastomers contain soft parts obtained from more then one monomer or from the same monomer arranged in different configurations. The structure of the soft parts is irregular. On the other side, the hard component is in most cases crystalline thermoplastic, which forms crystalline or semi-crystalline areas, either connected with elastomeric parts or among amorphous areas. The hard parts act at room temperature as physical cross-links that bind the elestomeric segments in a three dimensional network. The structure of the

thermoplastic elastomers is depicted in Fig. 3.6. By varying the ratio between the hard and the soft component, the properties of the thermoplastic elastomers can be adjusted within wide limits.

The *thermoplastic polyurethane elastomers* consist of hard segments thermoplastic polyurethanes, while the soft segments are in most cases polyesters or polyethers [HOL00]. The thermoplastic polyurethanes on polyether basis have $T_{g(soft)}$ of the soft component about –40°C, while for the polyurethanes on polyester basis $T_{g\ (soft)}$ is about -60°C. Low T_g of the soft component is desirable, because it reduces the T_g of the whole co-polymer. The hard segments melt in the temperature range (190°C – 220°C), but by applying mechanical pressure the co-polymer can flow and take the form of the mold at lower temperatures.
The thermoplastic polyurethanes are fabricated by polycondensation reactions from long chain diols, short-chain diols (chain extender) and a linking monomer [HOL00].

Walopur ® and Platilon® U are commercially available thermoplastic polyurethane elastomer foils from Epurex Films GmbH, Walsrode, Germany. They are fabricated by extrusion of polyether- or polyester- urethanes on aromatic or aliphatic basis [EPU04]. The linking components are based on aromatic diisocyanates. They are flexible in a broad temperature range, plastisizer free, possess very good adhesion properties and assure sealing against liquids. They have good chemical resistance and can be glued or welded. The Walopur and Platilon foils are used in industrial applications such as car fabrication (seats, roofs, door seals), sport (clothing, shoes), building industry (isolation for roofs, pipes, hoses, transport bands etc.), medicine (mattresses, sticking plasters, prostheses).
The Walopur foils are complete or partially dissolved in polar solvents such as dimethylformamide, tetrahydrofurane or n-methylpyrrolidone. Some aromatic and polar aliphatic solvents (ketones, short-chain esters, halogenated hydrocarbons) cause reversible swelling accompanied with reduction in strength. The materials with higher soft component content are generally more susceptible to swelling. Alcohols partially dissolve the material, especially at elevated temperatures. The polyurethane elastomers possess good chemical resistance against diesel fuel, gasoline, kerosene, as well as against greases and lubricating oils.
The polyurethane elastomer foils based on ester lose partially their strength at temperatures higher then 60°C, because of hydrolytic degradation. The foils based on ether swell in hot water. At room temperatures prolonged contact with water or salt solutions cause no significant change of the properties of both ether and ester polyurethane foils. Weak bases and acids can have a prolonged contact with polyurethanes causing relatively low harm. Strong alkaline solutions, mineral acids, as well as organic acids and their water solutions are more aggressive to polyurethanes and can be used for a short time if an immediate water rinsing follows. The chemical resistance of Walopur foils against a number of standard solvents and acids is given in the appendix.
The thermoplastic polyurethane elastomers can be glued together by using n-methylpyrrolidone or dimethyl formamide (DMF). The TPUs can be glued to each

other, with other plastics or metals via glues on epoxy-resins base or two-component glues on modified polyester base with curing agent on diisocyanate basis [DOM98]. They can be welded by using high-frequency welding, hot air welding, ultrasonic welding or thermal impulse welding techniques.

The thermoplastic elastomers have the necessary elastic properties for achieving a reliable sealing between the microfluidic device and the quartz bio-chip. They possess good chemical resistance to the substances used in the bio-analytical system. Their thermoplastic properties allow fabrication of microfluidic devices by using hot embossing technology. The low cost of the material and the inexpensive fabrication technology allow the use of the microfluidic devices as disposables.

3.4 Biocompatibility

Since many microfluidic devices find application in the medicine, bio- and medical research, the biocompatibility is an important aspect [NGU02]. The biocompatibility should be discussed by taking into account the specific applications of the microfluidic system.

For in-vivo applications the material must be nontoxic and it must cause no inflammation or any other cellular response. Less stringent requirements could be set for in vitro applications. However, the material should not influence the biological substances in the system and the measurement itself by reacting, adsorbing, absorbing or destroying the biological samples. On the other hand, the material must be chemically resistant to the biological substances used in the sensor system. In most cases fluid is absorbed into the material causing so-called swelling. The swelling can lead to creation of microcracks and influences the mechanical properties of the material.

The biocompatibility is not a general property of the polymer materials, it must always be tested experimentally. The bio-analytical sensor system "S-sens" is designed for in-vitro applications and no medical tests have been carried out. The materials used such as PMMA (material for implants e.g. [KUR01], [GBU05]) and thermoplastic polyurethanes (used for catheter tubes and hoses) are suitable for in – vitro applications.

3.5 Fabrication of active valves

Integration of valves is a very important issue in the development of microfluidic devices. The valves are used to regulate and direct the fluid flow. There are two main types of valves – active and passive [NGU02].

The *passive valves* (also called check-valves) serve to let the fluid flow in one direction and prevent it to flow in the opposite direction. Such valves are usually part of micropumps. They are actuated from the fluid itself and cannot be regulated separately. Depending on the form of the valve seats, they can be fabricated as cantilever valves, membrane valves, bivalvular, diffuser/nozzle valves etc. [KOC00].

Active valves [NGU02] are used for the control of the fluidic flow. They consist of a valve seat, a body containing the fluid and an actuator. The flow is regulated by the actuator, which drives the valve seat. Depending upon the design the valves can be classified as normally open valves, normally closed valves and bistable valves. The bistable valves have non-defined off-mode position.

The active microvalves can regulate the flow in either digital or analog way. In case of the analog regulation the valve actuator varies the gap between the valve seat and the valve opening. In this way the flow resistance is proportional to the actuator signal if the inlet fluid pressure is kept constant. In the digital mode there are only two possible states: open and closed. There is a possibility for control of the flow rate in the open state by using either combination of digital valves or using a pulse-width –modulation (PWM) mode [NGU02].

Different actuation techniques have been used for operation and control of the active valves. The most common actuation principles are: piezoelectric, thermomechanical, pneumatic, thermopneumatic, electrochemical, electrostatic, electromagnetic and capillary force actuation [NGU02], [KOC00].
The following parameters are the most important ones for characterization of the microfluidic valves:

- *Closing force.* The necessary force that has to be generated from an actuator to close the valve (or to open a normally closed valve). Table 3.2 presents the pressure range generated by different types of actuators [NGU02]:

Table 3.2 Pressure range of actuator techniques used in microvalves [NGU02].

Pressure range [kPa]	Actuation Principle
1-100	Electromagnetic, Disk type piezoelectric, Electrostatic, Electrochemical
100-10000	Pneumatic, Thermopneumatic, Shape-memory alloy, Thermomechanic
>10000	Stack type piezoelectric

- *Chemical compatibility.* Microfluidic devices are often supposed to find application in the medicine, environmental and food analysis, chemistry etc. In many cases the samples can contain aggressive substances that react with the material of the valve. Important aspect is the use of polymer fluidic devices, because the samples are often in an organic solvent or in strong electrolytes.

- *Leakage ratio,* L_{valve} is the ratio between the flow rate in the closed state and the flow rate in the open state at a constant inlet pressure [NGU02]. In the ideal case the leakage should be zero.

$$L_{valve} = \frac{Q_{closed}}{Q_{open}} \qquad (19)$$

- *Valve capacity,* C_{valve} . This is the maximum flow of the valve at the highest possible pressure difference across the valve at open position [NGU02]:

$$C_{valve} = \frac{Q_{\max}}{\sqrt{\frac{\Delta p_{\max}}{\rho g}}} \qquad (20)$$

  Here, Q_{max} is the flow rate and Δp_{max} the pressure drop in the open valve, ρ is the density of the fluid, g is the gravity acceleration.

- *Power consumption.* This is the consumed input power of the valve in its active state.

- *Temperature range.* It is highly dependant on the materials and the actuation method.

- *Response time.* The response time of the valve is determined by the response of the actuator (see Table 3.3).

- *Stiction problems.* When the surfaces of the valve seat and the valve body are very smooth, as for instance with Si or SiO_2, they could stick together. For reduction of the friction, preliminary rinsing in deionized water, ethanol and toluene are usually done.

The proper actuation technique for the active valves should be chosen considering the specific applications. For the microfluidic disposable devices developed in this work, the reliability, simplicity and low cost were the most considered properties.

The development of a separate actuator for valves regulation as well as its integration in the fluidic device would lead to significant costs. That is why pneumatic driven valves have been chosen. Pressurized air can replace the actuator.

Table 3.3 Response time of actuation techniques used in microvalves [NGU02].

Response Time [s]	Actuation Principle
10^{-4} – 10^{-3}	Piezoelectric, Electromagnetic, Electrostatic
10^{-3} - 1	Thermopneumatic, Thermomechanic
>1	Pneumatic, Shape-memory alloy, Electrochemical

In comparison with the other valve types the pneumatic driven valves have the following advantages:
- simple concept.
- low cost.
- negligible temperature dependence.
- possibility to use the same material for the valves seat and fluidic channels. This solves the problem with the chemical resistance of the whole valve structure.

The principle disadvantage of the pneumatic actuated valves is the longer response times because of the external pneumatic supply system. In our case, the sample injection processes are in the range of tens of seconds to several minutes and the effect of the valve response time is negligible.

4 EXPERIMENTAL

4.1 Hot embossing technology

4.1.1 Hot embossing system HEX 03

The hot embossing technology has already become one of the most promising molding techniques for fabrication of non-electronic microdevices [HEC04]. It has shown some important advantages in comparison with the other micro-molding methods, for instance the injection molding, especially concerning the high aspect ratio of the fabricated structures, their size (down to 10 nm) and simplicity of the equipment. A scheme of the hot embossing process is shown in Fig. 4.1.

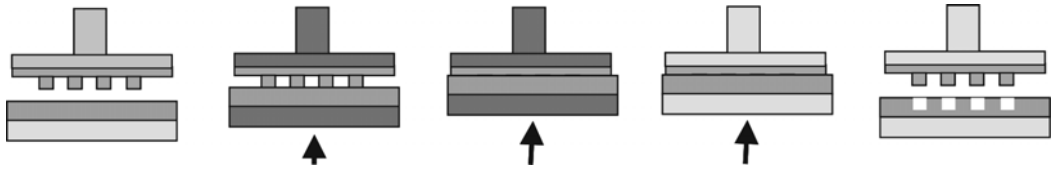

Fig. 4.1 Scheme of the hot embossing process technology. The foil is placed between the top and the bottom molds, they are heated, pressed, cooled and separated.

The hot embossing technology is suitable for structuring of thermoplastic materials. Thermoplastic material in form of a foil or substrate is placed between two plates (embossing tools). A negative image of the structures that are to be transferred into the polymer had been fabricated before on molds (master stamps). The molds are fixed in the embossing tools and heated up to temperatures well above the glass transition temperature of the polymer T_g. At this state the polymer is still not melted, but when sufficient embossing pressure is applied it flows and fills the cavities of the molds. In order to prevent inclusion of air bubbles into the polymer structure, the space between the tools (embossing chamber) must be evacuated. The whole system is then cooled down below T_g, the pressure is released and the molds are separated (demolding process).
During the hot embossing process the polymer flows a very short distance from the foil into the cavities. Hence, the temperature cycle is smaller in comparison with the injection molding process, where the melted polymer must be transported a long distance into the mold. The lower temperature difference leads to less shrinkage

during the cooling and reduced friction forces between the mold and the polymer during demolding. As a consequence, smaller features can be produced with the hot embossing technology. Furthermore, the embossed structures exhibit less stress in comparison with those fabricated by injection molding, because of the slower heating and cooling rates. This is especially useful for production of optical components such as lenses and wave-guides.

The hot embossing processes in this work have been performed with the hot embossing system HEX 03, Jenoptik Mikrotechnik GmbH [JEN03]. It consists of the following main components: *basic system unit, object and positioning system, vacuum system, measuring system, temperature control and electronics – software block*.

The *basic system unit* consists of a load frame, crossheads and drive. It applies and controls the force needed for the hot embossing processes. It allows embossing forces in the range of 200 kN.

Object and positioning system. The system HEX 03 is designed for double-sided hot embossing processes. The mold inserts can be mounted in the vacuum chamber on the tools on the top and on the bottom of the chamber (Fig. 4.2). The upper chamber part is fixed and does not move during the embossing processes. A VITON O-ring assures the sealing between the tools, when they come into contact. A vacuum chamber encloses both tools.
The parallelism between the tools is adjusted by two non-parallelism correction units. Each of them consists of two rotatable wedges. The non – planarities between the planes of the tools are compensated by rotation of the wedges against each other. The upper non-parallelism correction compensates the manufacturing tolerances in the built-in system components. The lower non- parallelism correction compensates the manufacturing tolerances in the tool holders and the tools themselves.
A demolding system is built in order to enhance the release between the tool and the molded material after embossing. It uses pressurized air that first seals off the bottom tool via a pneumatic cylinder. Subsequently, both tools move apart with low speed. The pressurized air enters the chamber via channel in the upper tool holder and acts as a demolding pressure.

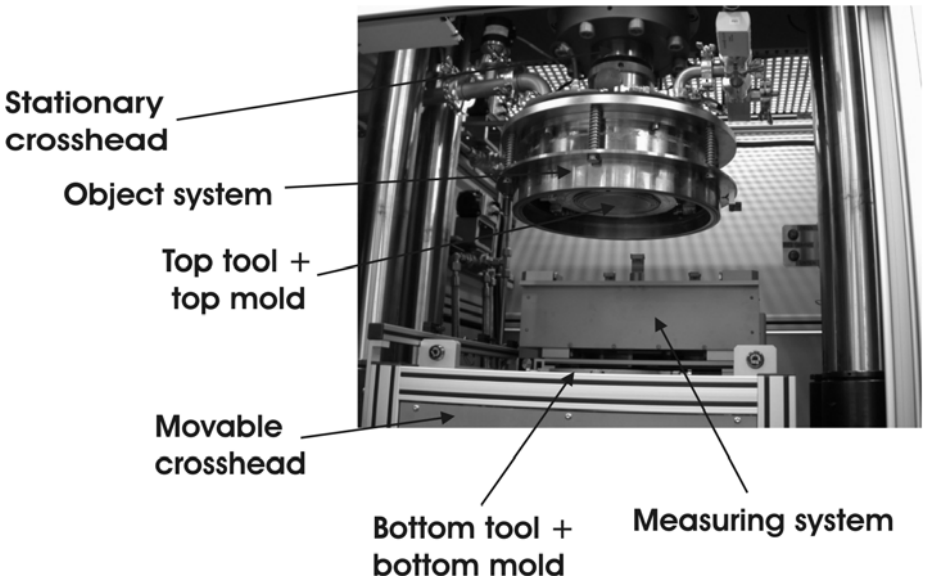

Fig. 4.2 Optical view of the hot embossing system HEX 03 (Jenoptik Mikrotechnik, Jena, Germany).

The VITON O-ring used for the sealing between the tools can be used for temperatures up to 220°C. If higher temperatures are needed a Chemraz sealing, resistant up to 320°C, can be mounted. The bottom tool holder is fixed at the lower heating/cooling unit. For double sided embossing, a special second holder was designed, which was fixed with screws to the bottom tool and has recess for the bottom mold.
The position of the bottom tool with respect to the top tool is adjusted by a sliding stage. The positioning is accomplished with two drives in x direction and one drive in y direction.

The measuring system consists of a microscope that is mounted on a microscope stage. The microscope is situated behind the chamber and enters the chamber between the tools for the alignment process. The microscope stage possesses drives with an integrated positioning system. The motion in x and y direction allows searching the alignment marks on the master stamp (left and right). The positioning system assures +/- 3 µm alignment between the top and the bottom tool. The microscope can work in "light" or "dark" field mode.

Temperature control. The cooling of the system uses heat transfer oil. It flows in special channels near the surface of the tool holders. The oil is then cooled by water in a storage tank. The oil system is split into two independent loops for a separate temperature control of the top and the bottom tool. A separate cooling system with water is used for temperature stabilization of the microscope with the microscope stage. The water is kept at 20°C by a refrigerated circulator.

The *electronic and software block* assures the electrical supply and the control of the embossing system. The control software is based on macro functions that can be combined into a complete operating program. There are image processing and control software, as well as software for position measurement and control for double side embossing processes.
Fig. 4.3 shows the changes of temperatures of the top tool and the bottom tool (substrate), as well as the embossing force during one of the embossing processes implemented in this work.

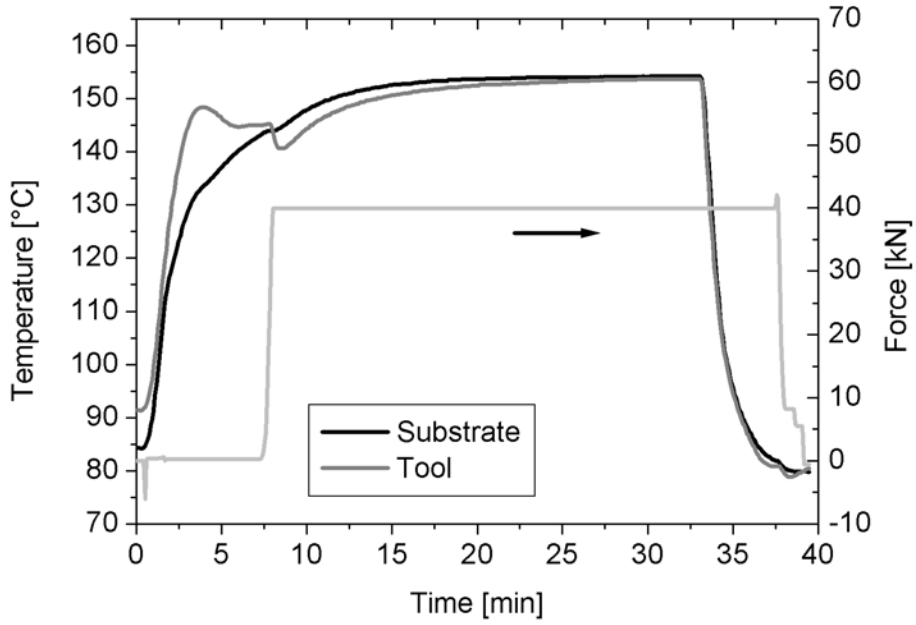

Fig. 4.3 Flow chart of a double-side hot embossing process. The temperatures of the top (tool, gray line) and the bottom (substrate, black line) mold are presented. The hell-gray line describes the embossing force.

4.1.2 Fabrication of the embossing molds

The embossing molds for the fabrication of the microfluidic devices in this work were fabricated by mechanical milling of brass with a CNC machine (DMU 50 eVolution, Deckel Maho Seebach GmbH, Germany). The milling cutters had diameters down to 200 µm. In order to reduce the sticking between the brass mold and the polymer the surface of the mold was additionally polished. The roughness R_a of the embossing molds was between 0.350 µm and 0.600 µm, determined with an optical measuring system MicroProf (FRT, Bergisch Gladbach, Germany).

The CAD drawings of the microfluidic devices fabricated in this work are shown in the Appendix.

4.2 "S-sens" bio-sensor system

The microfluidic devices that have been developed in this work, were fabricated for the use with the "S-sens" bio-analytical system. The "S-Sens" system is a fully integrated bio-sensor system for real-time and marker-free quantitative detection of molecular interactions. The system is built in a modular approach and uses two different types of sensors – surface acoustic waves (SAW) and impedance sensors.
The "S-sens" bio-analytical system combines the advantages of fully electronic detection with an advanced modular system design. The modular system design allows an easy exchange of the sensor chips and the fluidic handling system. Due to short analyte exchange times and high time-resolution (see Table 4.1), the S-sens sensor system is suitable for real-time kinetic characterization of molecular interactions. The sensor system can be used for real-time monitoring of binding and dissociation events with applications in bio-technological, pharmaceutical or chemical analytics. The small size and low weight make it an ideal for on-spot environmental studies and analysis.

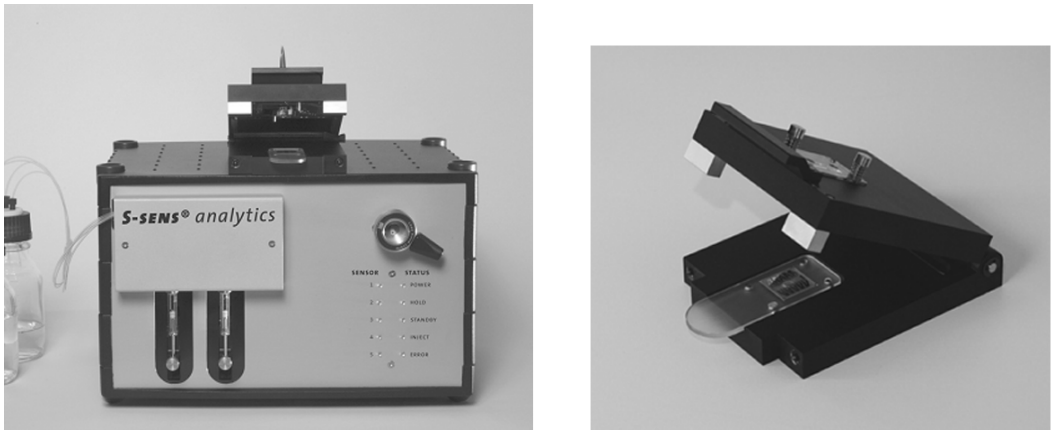

Fig. 4.4 Optical view of the S-sens bio-analytical system (left). Close view of the chip-reader unit (right).

The "S-sens" bio-analytical system consists of the following units:

chip-reader - includes fluidic cell module, chip-carrier and integrated high frequency electronic board (Fig. 4.4 , right). The chip-carrier enables precise positioning between the sensor chip, fluidic cell and the electronic board. The chip-reader allows measuring of 5 different sensor channels simultaneously. The electronic board contains a read-out electronics based on an IQ demodulator with integrated frequency synthesizer. The induction of acoustic waves and the read-out is assured by the in- and output interdigitated transducers (IDTs) and is controlled by a PC. The IDTs of the 5 SAW sensor elements are addressed by a multiplexer. The IQ

demodulator converts the radio frequency signal from the output transducer to a low frequency electrical signal. The electronic module measures a complex signal containing the phase and amplitude changes between the input and output IDTs. The read-out electronics allows 10 measurements per second on a sensor channel.
The fluidic device assures the contact between the sample analyte and the surface of the sensor. The chip-reader unit assures the connections between the macro-fluidic module and the fluidic cell as well as the contacts between the sensor chips and the read-out electronics.

fluidic handling system – controls the flow of analyte and buffer solutions over the sensor. It consists of two pumps (Tecan, Global FIA Inc., USA) and an auto-sampler unit. The autosampler allows an automated analyte injection.

software module – allows for fully automated measurements. It serves for system operation and control, programming of the automatic sample handling and the flow rates, calibration and data analysis. For setting up of special measurement sequences, for data recording and analysis and calibration routines, the system is connected to an external PC or Laptop with special software (Caesar, Bonn, Germany). The software module is able to visualize and record measurements for 5 sensor channels for 24 hours duration with a time resolution of better than 1 s.

The sensitivity of the bio-analytical system depends on the parameters of the sensors and the read-out electronics. The selectivity is assured by immobilization of special receptor molecules on the sensor surface, antibodies or aptamers (the binding mechanism is described in Section 2.3.2) that can specifically bind only one kind of molecule presented in the sample. The receptors bind the molecules of interest from the sample solution, while all other type of molecules flow through without causing an irreversible signal change. In this way the electronic detection is performed and no molecule labeling of any kind is necessary. The limit of detection (LOD) of the "S-sens" system was found to be 0.8 [pg/mm^2]. Some of the characteristic parameters of the system based on SAW sensors are given in Table 4.1.
The SAW sensors used in this work are based on horizontally polarized shear acoustic waves propagating in SiO_2 guiding layer on a quartz substrate.
The SAW chips have size 20 mm x 20 mm. They are fabricated by thin film technologies in a cleanroom environment. 500 µm thin ST cut quartz wafers were used as substrates [SCH04]. The IDTs were made of gold (300 nm) and 12 nm of chrome film as an adhesion layer. The optimal guiding layer thickness was 5.4 µm α-SiO_2 deposited by magnetron sputtering.
Each SAW chip contains 5 sensor elements. Each sensor element has an active surface area of 6 mm^2. The IDTs with a split-finger design include 10 finger pairs with a periodicity of P = 28 µm. The working frequencies are between 138 and 142 MHz.
The standard material for the active area is gold.

Table 4.1 Some characteristic parameters of the S-sens bio- analytical system.

Limit of detection (LOD)	0.8 pg/mm^2
Max. time resolution	5 points/s. channel
Offset between channels / sensors	< 3 %
Noise floor	0.02 ° (phase)
Drift at 25°C	0.1° phase/hour
Flow rate	12.5 – 500 µl/min
Flow cell volume	6 µl/channel
Total flow cell volume	30 µl
Analyte exchange time (burst mode)	5 s

An alternative substrate material for SAW applications is the $LiTaO_3$. It possesses higher piezoelectric coupling constant, leading to reduced number of the IDTs finger pairs and a broader frequency transmission peak [GIZ03]. The geometry of the $LiTaO_3$ based SAW chip allows smaller chip dimensions and lower production costs.

4.3 Macro-fluidic system for the "S-sens" apparatus

The macrofluidic system of the bio-sensor "S-sens" system allows a fully automated process control. It consists of:

1. *microfluidic unit* - includes modular fluidic device mounted on the chip-carrier.
2. *macrofluidic unit* - includes a syringe pumps (Tecan), autosampler (Sunchrom, Friedrichsdorf, Germany) with an integrated injection valve (Rheodine, Rohnert Park, CA, USA), PEEK capillaries with 0.1 mm inner diameter for the fluidic connections and a PMMA adaptor.

A scheme of the fluidic system is shown in Fig. 4.5.

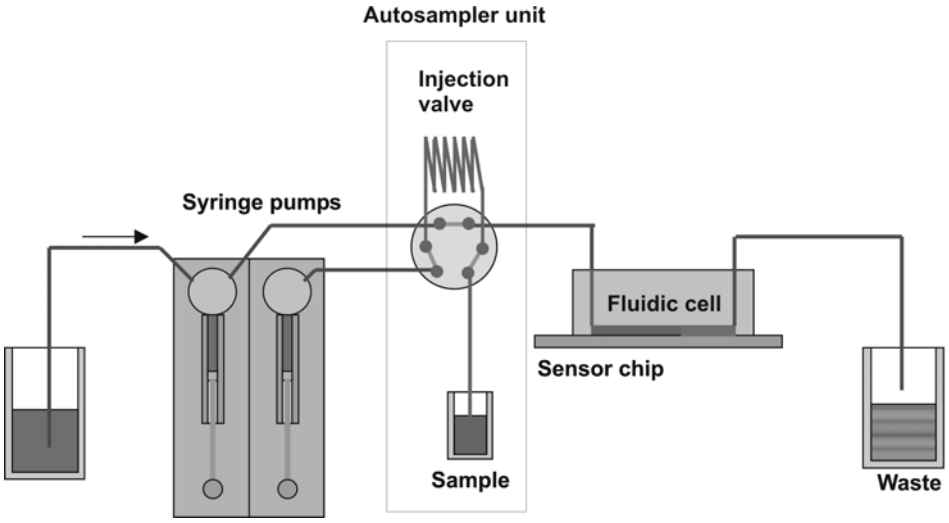

Fig. 4.5 Schematic fluidic system of the biosensor system. It contains two syringe pumps for the buffer (left one) and for the sample (right one). The injections are accomplished via a PC controlled autosampler unit with integrated injection valve.

The autosampler with an integrated injection valve has 200 or 500 µl sample loop. It ensures accurate and reproducible injections of sample solutions. The software unit allows programming of different injection sequences, adjustment of the flow rate of the sample (buffer), adjustment of the injection volumes, burst volumes and waiting times between the different injections.
For proper operation and for reliable and repeatable measurements, the following parameters of the fluidic system must be considered:

Dead volume [µl]. Total volume of all channels, cavities and fluidic connections that must be filled before the sample enters the micro-fluidic chamber over the sensor.

Off-time [s]. Minimum time between the end of one injection and the start of the next one. In the "S-sens" system it is set of 10 s. This time does not include the time needed from the autosampler for taking up the sample.
The dead volume and the off-time are parameters that are set for the system.

Waiting time [s]. Time between two injections that can be adjusted from the user. Usually this time is set in the range of 10 min. This time is needed for assuring that no rests of the previous sample remained in the system.

Injection mode (LQ, SQ, HQ). The reader module in combination with the autosampler unit can be used with different operation modes – LQ (low quality), SQ (standard quality) and HQ (high quality). In case of LQ mode, the sample volume taken from the autosampler contacts directly the buffer solution. This causes mixing between the sample and the buffer during taking the sample and the subsequent injection. As a result, the sample is diluted with buffer at the end of the injection. For this reason, by

using this mode the injection must be stopped before the whole sample volume flows into the fluidic chamber. The SQ modus includes a step of pooling of an air bubble from the autosampler pump just before the pool of the sample. The SQ mode can also lead to sample dilution, especially in case of measuring of electrolytes and using demineralized water as a buffer. The experiments have proven that two air bubbles with part of the sample liquid between them are necessary to fully prevent mixing of the sample and buffer solutions. This mode is called HQ and is presented in Fig. 4.6.

Flow rate [µl/min]. Volume of the fluid flowing through a cross-section of the fluidic channel per minute.

Sample volume [µl]. Volume of the sample solution.

Burst volume [µl]. Part of the sample volume that is injected with higher flow rate in order to reduce the fluidic exchange times. Burst is usually made at the moment at which the sample is entering the microfluidic chamber (*burst – in*) and at the moment of leaving the chamber (*burst – out*). In order to fix the burst parameters, the dead volumes between the injection valve and the input of the fluidic device must be calculated.
Flow rate, sample volume, burst volumes and injection mode can be defined by the user for the different injection sequences.

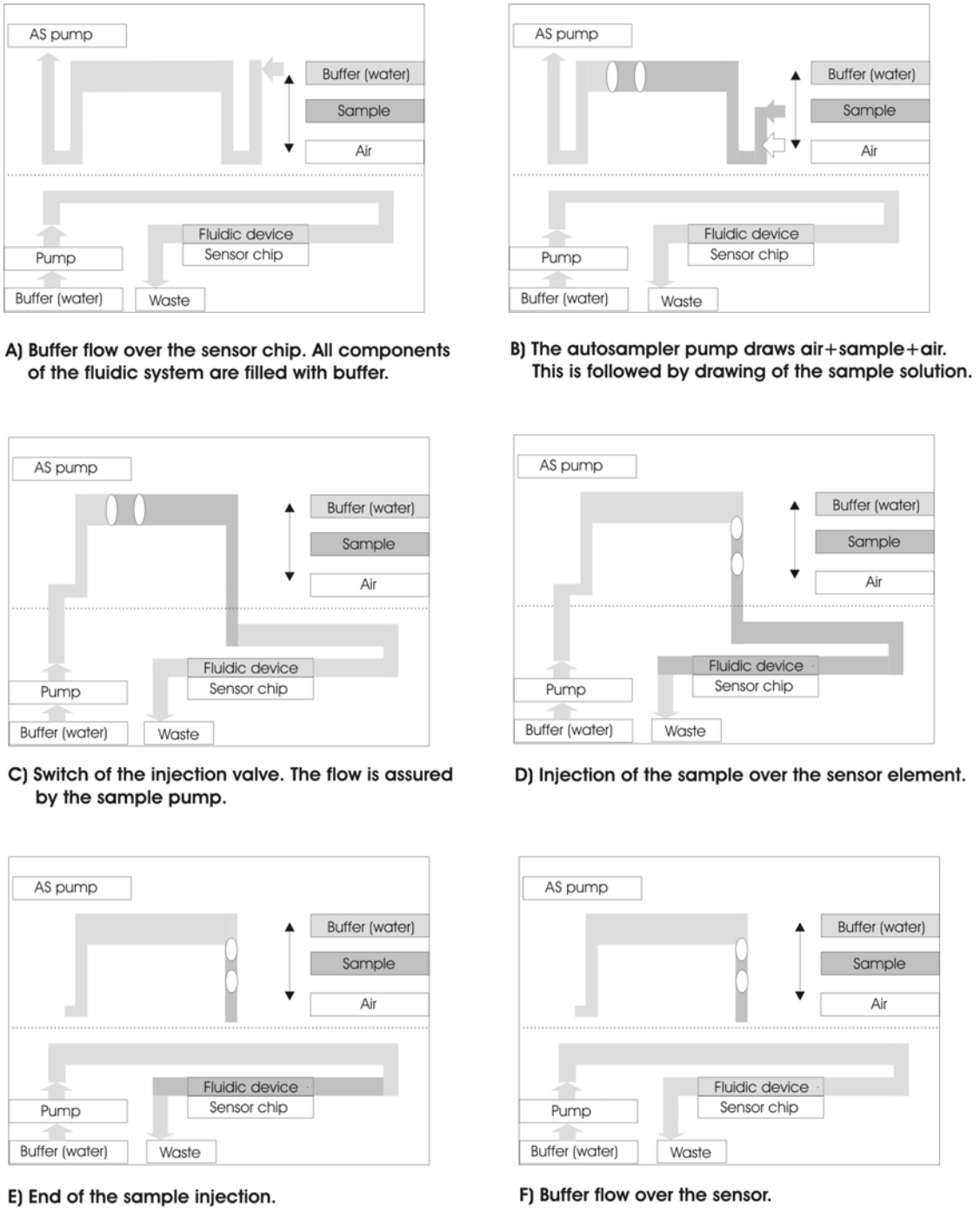

Fig. 4.6 Scheme of the steps for a sample injection by using high-quality (HQ) modus.

5 DEVELOPMENT OF MICROFLUIDIC DEVICES. RESULTS AND DISCUSSION

5.1 PMMA based fluidic devices

In the beginning of the sensor system development the fluidic devices were based on polymethylmethacrylate (PMMA). The material can easily be formed by mechanical milling, it is transparent and bio-compatible. As though PMMA is stiff and delivers no efficient sealing to the quartz SAW chip, additional sealing structures had to be integrated.

5.1.1 PMMA devices with a rubber sealing

Fig. 5.1 shows the first PMMA fluidic cell [SCH03]. It was fabricated by mechanical milling and consisted of two through holes for the connections with the PEEK capillaries and a chamber positioned over the all five SAW sensor elements.

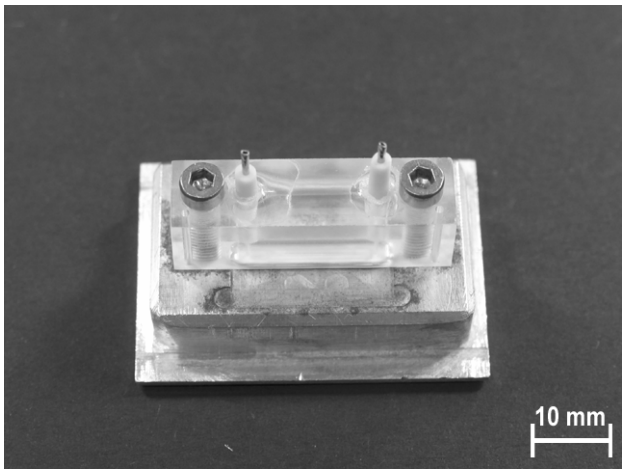

Fig. 5.1 Photograph of a PMMA fluidic cell with a "Viton" rubber sealing mounted on aluminum chip-carrier.

The chamber (18 x 5.4 x 0.7 mm) was surrounded by 1 mm wide groove channel in which a rubber "Viton" O-ring was placed. The cell was positioned over the sensor chip and fixed via two screws to a metal chip-holder to assure the sealing between the O-ring and the quartz chip. This fluidic device has the following disadvantages:

1. The volume of the chamber was 68 µl. It leads to long response times (> 10 s) of the sensor system and high sample consumption. For real-time bio-analytical measurements the chamber volume must be further decreased.
2. The rubber O-ring hampers a substantial reduction of the fluidic device geometries and cannot be used in case of more complicated shapes of the fluidic chamber (for instance for a separate sealing for every sensor).
3. The fluidic chamber does not allow for addressing the SAW sensors independently and can be used for immobilization of only one type of receptor molecules on the same bio-chip. For this reason, the surface passivation of the reference sensor must be performed outside the system. If the chip is regenerated with injection of NaOH, the passivation of the reference sensor will be destroyed as well.
4. PMMA device and the rubber O-ring are in direct contact with the sample and buffer solutions. Prolonged exposure to ethanol or NaOH reduces the life-time of the device. Even worse, the dissolved material can contaminate the sensor surface.
5. The fabrication of these devices is complicated and expensive, because the milling process is not suitable for a batch production. For this reason they cannot be used as fluidic disposables.

These disadvantages have initiated research and development towards smaller geometries of the fluidic devices, to alternative materials and to new fabrication technologies.

5.1.2 Devices with a silicone sealing

Alternative technologies have been developed in order to assure further miniaturization of the fluidic devices. Here, the elastomeric properties of silicone have been utilized.
First, fluidic devices were fabricated by combining mechanical milling of PMMA and a subsequent integration of a silicone sealing. The fluidic channel allows the serial flow over the sensor elements on the chip. The milling process of PMMA was performed with a milling system “Kosy” (Max-computer GmbH, Germany). The system consists of a CNC milling machine, positioning system for control in X, Y and Z directions and CAD/CAM software for computer control. Fig. 5.2 (left) shows me-

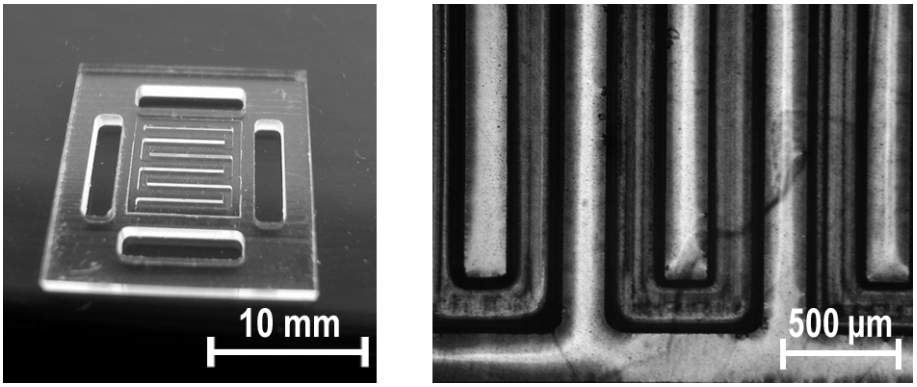

Fig. 5.2 Photograph of PMMA microfluidic device fabricated by mechanical milling (left). The cross-section of the fluidic channel is 300 x 300 µm. Four rectangular openings were foreseen for the contacts to the read-out electronic (left). In the next process, Sylgard 184 sealant is applied between the channels (right).

chanical milled device on a 1,5 mm thick PMMA plate. The fluidic channel with a cross-section of 300 x 300 µm was milled with a swivel stem 0.3 mm in diameter (Rexim Werkzeug GmbH, Germany) at a rotation speed of 5000 rpm and a feeding speed of 0.4 mm/s. The PMMA substrate was glued with a double-sided tape to another plastic substrate to assure proper milling of the openings for the electronic connections. The milling of the openings was done about 3 mm into the underlying plastic substrate in order to prevent the PMMA from breaking. The milling of the openings was done in three steps, each step removing material only 0,6 mm in depth for avoiding of PMMA overheating and melting. Isopropanol was used as a cooling agent during the whole milling process.
For comparison, similar devices were fabricated from diverse polymers such as PSU, PE, PP and PEEK. PSU has similar mechanical properties to that of PMMA, while PP and PE form "slivers" during the milling that led to poor quality of the structures. PEEK was easily milled, but is opaque and very expensive.

In order to assure the sealing of the milled fluidic devices with the sensor, a thin silicone elastomer film (Sylgard 184, Dow Corning, USA) was deposited in the areas between the channels (Fig. 5.2 right). Sylgard 184 is a two-component silicone encapsulant. The basic and the curing components were mixed in 10:1 ratio. The mixed elastomer was then deposited onto the areas between the fluidic channels by either stamping of the PMMA device against the silicone film or by using a dispensing system.
For the stamping process the mixed Sylgard 184 was spun on a silicon wafer (Spin-coater Delta 10, Süss MicroTec) in thicknesses in the range of 5 – 60 µm. The thickness was determined with a Tencor profilometer**.** The milled PMMA device was cleaned in an ultrasonic bath in a mixture of isopropanol/water 1:2 and treated in an oxygen plasma (P= 300 W, a partial oxygen pressure p_{O2} =1,1 mbar, 10 min). The plasma process was used to remove organic contaminants on the PMMA surface. The

PMMA device was then pressed against the silicone film, separated and left to cure at elevated temperature. In order to prevent the silicone flowing into the channels during the curing process, the PMMA device was placed in a way that silicone contacts a polyimide foil. It was found that with this technology Sylgard 184 forms more homogeneous layer.
A dispensing method was an alternative approach for silicone application around the fluidic channel. A dispenser 1500XL (GLT mbH, Pforzheim, Germany) was used. The mixed two components of Sylgard 184 were placed in a special cartridge with a dosage needle and by using pressurized air for controlled time the silicone was applied. Again, the sample was left to cure by contacting a polyamide foil.
The fluidic devices fabricated according to the described methods were manually tested and observed with an optical microscope.
Both methods have proven to be inappropriate for reliable fabrication of fluidic devices. The flow of the silicone into the fluidic channel was difficult to be completely avoided. This led to a low production yield. The optical control showed that Sylgard 184 films were comparatively smooth and homogeneous. However, considering the stress in the PMMA plate, no completely homogeneous contact between the silicone sealing and the sensor chip was achieved.
Better results were expected if the whole fluidic device was fabricated from elastic material. Elastic material could achieve better conformation between the fluidic device and the surface of the sensor chip. Furthermore, PMMA fluidic devices with silicone sealing cannot completely solve the problems mentioned in Section 5.1.1. For this reason, the next fluidic devices were fabricated from silicone.

5.2 Silicone fluidic devices

For the fabrication of silicone fluidic devices a rapid-prototyping fabrication process was implemented. An epoxy resin mold was designed, fabricated and used for molding of silicone (Sylgard 184). For the fabrication of the epoxy resin mold, a stereolithographical process was used.
Stereolithography is a method for fabrication of small complex and accurate parts with a resolution down to 20 μm. It is suitable for production of small numbers of complicated parts and is appropriate for mold fabrication [NGU02].
The configuration of the mold was designed by using a three dimensional (CAD) software. The datasets were then transferred to a stereolithography apparatus.
The 3D sample (mold) was built by curing a liquid epoxy resin layer by layer. The curing was accomplished by a directed UV beam, which was focused and guided on the resin surface. Fig. 5.3 (left) shows the epoxy resin mold fabricated by stereolithography.

The epoxy resin mold was subsequently used for molding of silicone for fabrication of microfluidic devices. A solvent free anti-sticking agent CIL Release 1711 E (Compounding Ingredients limited, UK) had been sprayed on the epoxy resin mold

in order to reduce the sticking between the silicone and the epoxy resin. For preventing air bubbles formation, the two-component silicone encapsulant Sylgard 184 was poured into the epoxy resin mold and cured in two steps: in the first step the elastomer was degassed in vacuum (100 mbar) at 25 °C for 15 min. In the second step the elastomer was cured at 70 °C for about 6 hours at atmospheric pressure. After curing, the silicone device was manually demolded by simple peeling of the cured silicone structures. Fig. 5.3 (right) shows the demolded silicone microfluidic device.

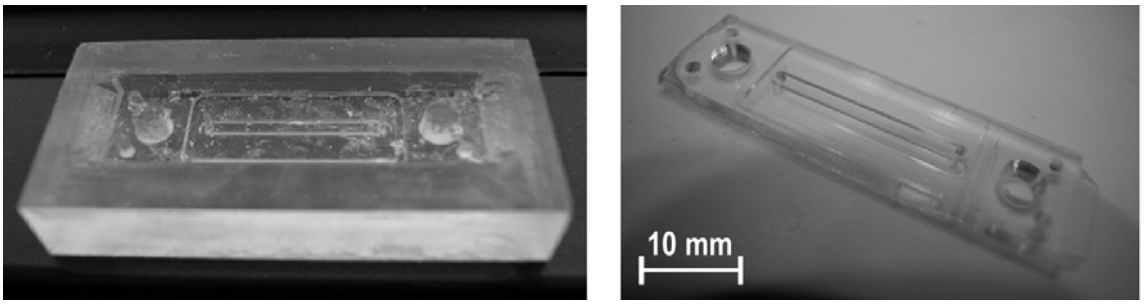

Fig. 5.3 Photograph of an epoxy resin mold (left) and molded PDMS fluidic device (right).

Although the first device was easily demolded and left almost no residues on the mold, the residues and the sticking problems have been steadily increasing with the next molding processes. Since the silicone is hardly soluble in organic solvents, the chemical cleaning without etching of the epoxy resin was difficult. The best results were achieved by mechanical cleaning of the silicone residues and an ethanol bath. However, if the mold structure is more complicated, with small dimensions, cleaning is not always possible. The problems with the cleaning of the epoxy resin mold reduced its lifetime, which additionally makes the fabrication more expensive. Therefore, the rapid prototyping process is suitable for a fast fabrication of limited numbers fluidic devices, but is not applicable to batch processes.

The silicone appears to be a suitable material for microfluidic applications for laboratory purposes, due to the fast fabrication process and excellent sealing properties. However, the insufficient mechanical stability of the silicone makes the handling of the microfluidic devices more difficult. This opinion is shared by another research groups [JAK98].

Considering afore mentioned disadvantages, alternative fabrication methods and materials were necessary. As described in Section 3, the combination of hot embossing technology and thermoplastic elastomer materials seemed to give an opportunity for fabrication of low cost fluidic disposables, able to deliver proper sealing and chemical resistance.

5.3 Fluidic devices based on thermoplastic polyurethane elastomers (TPUs)

5.3.1 Chemical tests of TPUs

As it was described in Section 3, the material of the microfluidic devices must be resistant against the sample and buffer solutions used in the analytical system.
The thermoplastic polyurethane elastomer foil Walopur 2201 AU (Epurex films GmbH) is fabricated on ether basis, the TPU foil Walopur VPT 2102 A has ester basis (see section 3).
The chemical resistance of these foils was tested by dipping of TPU samples into various standard substances and solutions which are typically used in bio-chemical experiments. The changes in the foils were optically and gravimetric observed.
The experimental results of ester- and ether-based TPUs are summarized in Table 5.1 and Table 5.2, respectively.

Table 5.1 Chemical resistance (at 37°C) of Walopur VPT 2102 A (on ester basis) against some standard substances and solutions used in the "S-sens" system (+ resistant, 0 moderate resistant (slight optical change), - not resistant).

	3 hours	3 days	1 week
Water	+	+	+
Ethanol 98%	+	+	-
Ethanol 70%	+	+	-
0.1 M NaOH	+	+	+
Glycine buffer pH 2.2	+	+	+
EDC/NHS	+	+	+
0.1 M KOH	+	+	+
Isopropanol	+	+	0
Selex buffer	+	+	+
PO_4 buffer	+	+	+
Acetic buffer pH 4.5	+	0	-
Sodiumcarbonate buffer	+	+	+

Table 5.1 represents the results from the chemical resistance tests of TPU foil Walopur VPT 2102 A (ester), 1 mm thickness, for different immersion times at 37°C. In the first 3 days, only the foils placed in acetic buffer pH 4.5 showed slight color change and became more opaque.
Table 5.2 represents the results from the tests of the Walopur 2201 AU (ether basis, 0.3 mm thickness).

Table 5.2 Chemical resistance (at 37 °C) of Walopur 2201 AU (on ether basis) against some standard substances and solutions used in the S-sens system (+ resistant, 0 moderate resistant (slight optical change), - not resistant).

	3 hours	3 days	1 week
Water	+	+	+
Ethanol 98%	+	+	+
Ethanol 70%	+	+	+
0.1 M NaOH	+	+	+
Glycine buffer pH 2.2	+	+	+
EDC/NHS	+	+	+
0.1 M KOH	+	+	+
Isopropanol	+	+	+
Selex buffer	+	+	+
PO_4 buffer	+	+	+
Acetic buffer pH 4.5	+	+	0
Sodiumcarbonate buffer	+	+	+

The Walopur VPT 2102 A (on ester basis) partially degrades in ethanol (100% and 70%), isopropanol and acetic buffer (pH 4.5), the Walopur 2201 (ether) was only slightly degraded in acetic buffer (pH 4.5).
The gravimetric tests showed 20-30% increase of weight for the foils immersed in ethanol and isopropanol, for the rest substances < 5% weight increase has been observed [STO05].
The chemical tests showed that the TPUs on ether basis possess a better chemical resistance against the tested substances. After the first three days, only the acetic acid caused small changes of the foils, while all the other substances caused no damage as determined by optical and gravimetric measurements. In the "S-sens" system, the microfluidic devices are exposed for a short period (2-3 min) to the cleaning substances (0.1 M NaOH, ethanol). More prolonged contact (1-2h) is needed with buffer solutions (SELEX buffer, PO_4 buffer).

In addition to the described chemical tests, microfluidic devices made from Walopur 2201 AU were used for a large number of real-time measurements of different biological samples. It has been found that the life - time of a single fluidic cell is more then 300 working hours and the chemical resistance allows high quality bio-analytical measurements. In order to skip the time-consuming and expensive sterilization process, as well as considering the negligible material costs, these devices are planned to be used as fluidic disposables.

5.3.2 Preparation of the embossing molds

For reduction of the sticking forces between the brass embossing molds and the TPU elastomer, an anti-sticking agent Antispread F 2/200 FK 60 (Dr. Tilwich GmbH, Horb (Ahldorf), Germany) was used. The anti-sticking agent is designed to reduce the friction forces between lubricating oils and metal or polymer surfaces [TILLW]. The low surface tension effect is observed on any surface, excluding PTFE. Antispread F 2/200 FK 60 consists of fluor-containing polymer as an active agent, dissolved in Fluorcarbide 60. During the evaporation of the solvent (about 10 s at 20 °C) the active agent polymerizes on the brass surface forming a network of fluorine-containing molecules that decrease the surface tension. The applied anti-sticking layer is about 10 nm thick and can be used at temperatures up to 200 °C.
The Antispread F 2/200 FK 60 was applied on the brass surface of the molds by dipping for 10 s or by using a pipette. Before the application of an anti-sticking layer the brass surface was cleaned from rests and impurities from the milling process. The cleaning was fulfilled in isopropanol in ultrasonic bath. The first hot embossing process with a certain mold also had a cleaning effect – since most of the impurities have better adhesion to the polymer than to the metal surface, they remained stuck to the embossed polymer foil. The cleaning effect reduced the sticking problems as well and during the following embossing cycles the sticking effect was much lower.

5.3.3 Single-side embossed fluidic cells

As it has already been discussed, the thermoplastic polyurethane elastomers combine high elastic properties with very good chemical resistance and excellent thermoplastic behavior. The use of a hot embossing process opens up the possibility for an inexpensive batch production. The first prototypes of polyurethane fluidic cells were embossed with a single embossing mold.

5.3.3.1 Optimization of the embossing parameters

The first fluidic design was used for optimization of the parameters of the hot embossing process of TPUs, as well as to demonstrate the sealing of TPU based devices.
The embossing molds for the fabrication of the single-side embossed fluidic devices were prepared by mechanical milling of brass. The mold for the first design of hot embossed microfluidic devices is shown in Fig. 5.4.

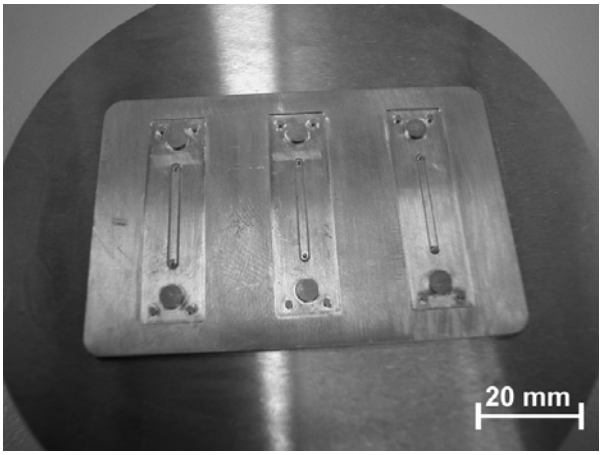

Fig. 5.4 Photograph of a brass embossing mold, fabricated by mechanical milling. The mold contains the negative images of three fluidic devices.

Each device consisted of two interconnects for the in- and outlet and a sealant structure that enclosed the fluidic chamber. The fluidic chamber was a reservoir (1 mm wide, 0.3 mm height, 16.65 mm long) that was to be positioned over the sensor area. The seal was 0.6 mm wide. For convenience, the single-side embossed fluidic devices will be called *fluidic cells*.

The hot embossing processes were performed with a HEX 03 machine using thermoplastic polyurethane (TPU) elastomer foils Walopur 2201 AU with a total thickness of 600 μm. The foil was positioned on an aluminum plate, which was attached to the bottom tool, while the brass mold was mounted into the top tool.

Hot embossing processes at different temperatures and pressures have been carried through. The results are summarized in Fig. 5.5.

The area of the embossing mold was 54 x 74 mm. Embossing forces in the range of 20 - 50 kN were used, that resulted in pressures in the range between 50 and 120 bar. At temperatures below the glass transition temperature of the polymer (T_g=135 °C) the structures were not properly embossed. The material was not soft enough to flow and fill the cavities of the mold. Temperatures higher than 160 °C led to low viscous state of the polymer and it was spread out of the embossing mold. Temperatures in the range between 135-155 °C gave structures with good conformation. However, the proposed openings for the fluidic in- and outlet were not open for the whole temperature range. For proper embossing of the openings, the temperature had to be increased over 145 °C for pressures of about 75 bar. At temperatures higher then 150 °C gas bubble formation in the TPU foil was observed (see Fig. 5.6) and areas with

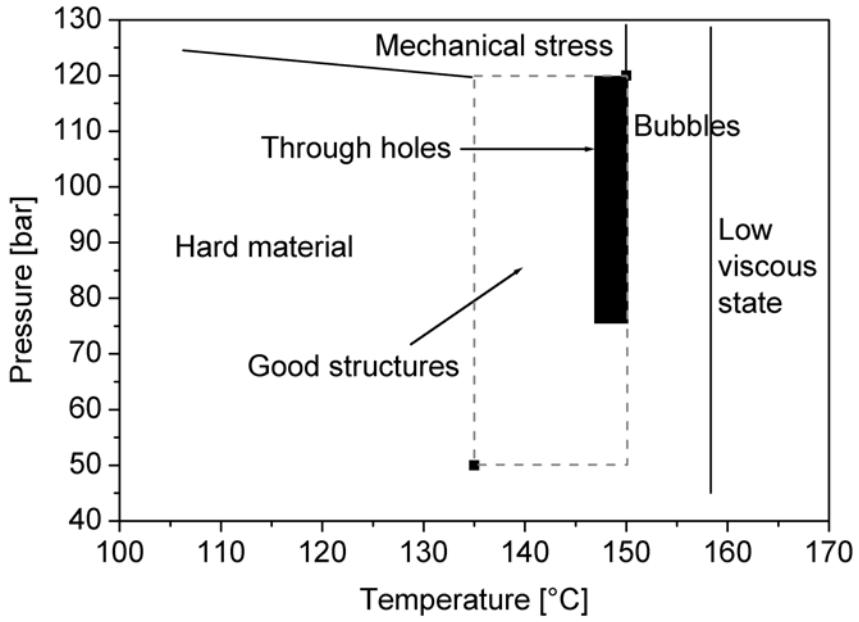

Fig. 5.5 Dependence of the quality of the embossed cells (from Walopur 2201) on the applied pressure (P) and temperature (T) for 15 min embossing time. The gray-lined box shows the area with good quality of the embossed structure. The black one shows the area with open through holes in the foil.

reduced transparency in the foil appeared. Finally, the optimal embossing parameters were fixed at P= 80-120 bar, T = 145-148 °C. The embossing time was about 15 min.

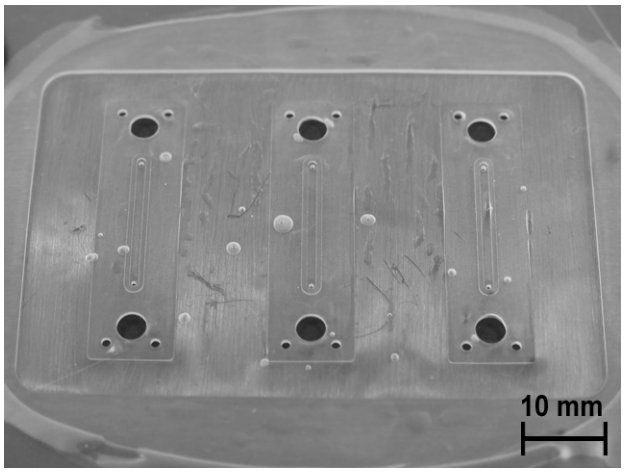

Fig. 5.6 Photograph of TPU fluidic devices, embossed at higher temperature (150°C). The overheating led to development of air bubbles.

In order to compensate deviations of the parallelism between the mold and the plane bottom embossing tool, high temperature silicone foils (200 µm thickness, Kunze Folien GmbH, Germany) were placed under the aluminum plate. An additional silicone foil and a thin polyimide foil (100 µm) were placed between the TPU material and the aluminum plate. The embossing assembly is shown in Fig. 5.7.

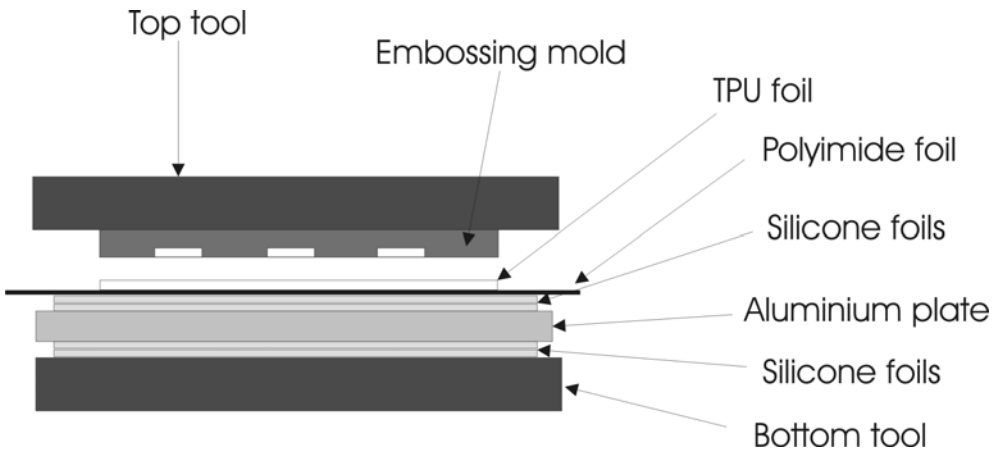

Fig. 5.7 Scheme of the assembly for single-side hot embossing of TPU fluidic devices.

The prototypes of the single-side embossed fluidic devices were used for tests of the sealing properties of the TPU material, as well as for testing of the fluidic connection between the PEEK capillaries and the fluidic device. Fig. 5.8 depicts a PMMA adaptor with through holes. The down side contains PEEK inserts for the capillary connections. The TPU fluidic device is bonded on the opposite side. The bonding process is described in section 5.3.3.2.

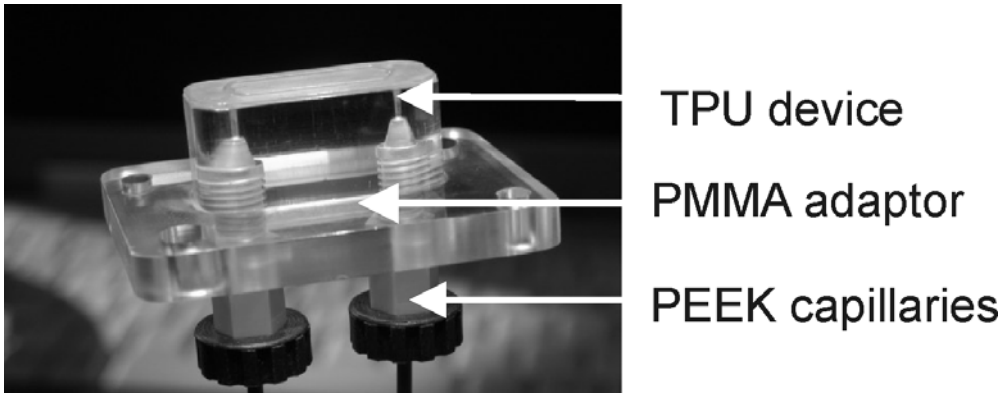

Fig. 5.8 Photograph of the PMMA adaptor with chemical bonded fluidic device.

The PMMA adaptor is then inserted in a corresponding slit of the chip-reader section of the "S-sens" system (Fig. 4.4). Thus, the TPU cell contacts the SAW chip positioned in the chip-carrier under the PMMA adaptor, while the fluidic connections remain on the top-side of the adaptor.

The construction of the chip-reader allows an exact positioning of the fluidic device, relative to the SAW sensor chip. A spring loaded mechanical force is applied on the top of the PMMA adaptor to assure the sealing. The force with which the TPU cell was pressed to the SAW sensor was 30 – 40 N (measured with FMI Force Gauge, FMI-200C_2, Alluris).
The fluidic inlet of the PMMA adaptor was connected with the autosampler unit, the outlet was connected to the waste bottle (see Fig. 4.5).

The tests of the TPU fluidic cells showed very good sealing properties. No leakages were observed for flow rates up to 150 µl/min.

5.3.3.2 Assembly

In order to provide for reliable connection between the TPU fluidic device and the PMMA adaptor, two different technologies were implemented. The first one used an UV curable glue, the second one was based on a chemical bonding process.
The ultraviolet (UV) curable glue Wellomer 4050 (Wellomer GmbH, Germany) is an one-component solvent free UV curing adhesive on acrylic basis, which possess strong adhesion to thermoplastic materials. The UV curing process can be accomplished if at least one of the surfaces to be glued is transparent for the UV light. The curing was performed with a UV point radiator Bluepoint 2.1 (Hoenle AG, Germany). The UV curing spectrum of Wellomer 4050 comprises the wavelengths in the range between 320 nm and 500 nm. The adhesion strength between TPU/PMMA after the gluing was sufficient. However, for microfluidic applications it is desirable to avoid the usage of additional substances like glues that can be source for particles generation. The particles can contaminate the fluidic channels and can be adsorbed at the sensor surface. For this reason, an alternative bonding process was performed.
The chemical bonding process with the organic solvent n-methylpyrrolidone (NMP) provided a very strong connection between the PMMA adaptor and the TPU fluidic devices. The TPU and PMMA are solved in NMP at a moderate rate. When NMP was applied on both surfaces they were slightly solved. Then, both surfaces were pressed to each other that allowed the solved TPU and PMMA molecules to mix in the solvent. When the solvent was completely evaporated, the area with mixed PMMA/TPU molecules exhibited a strong connection. The PMMA/TPU connection provided by the chemical bonding with NMP was stronger in comparison with the UV curable glue. In addition, the chemical bonding does not generate particles that contaminate the fluidic channels. Fig. 5.9 presents the applied chemical bonding technology.

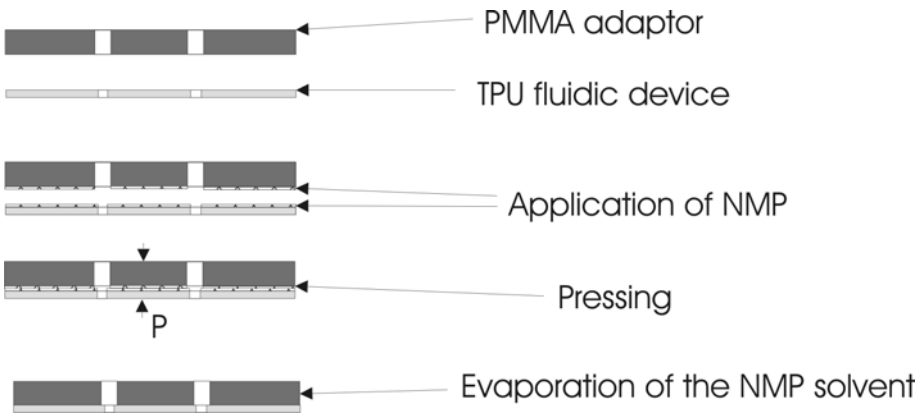

Fig. 5.9 Technology of the chemical bonding process of the embossed single-cell fluidic device to the PMMA adaptor.

During the following experiments, the chemical bonding with NMP showed no significant aging effects and the TPU/PMMA connection remained stable.

5.3.3.3 Design considerations for single-side embossed cells

Several designs of the fluidic cells were tested in real-time measurements in order to optimize the design of the fluidic chamber. Two embossing molds with different fluidic chamber configurations have been fabricated. Figure Fig. 5.10 shows one of the molds with six fluidic cells (left) and the embossed cells on TPU foil (right).

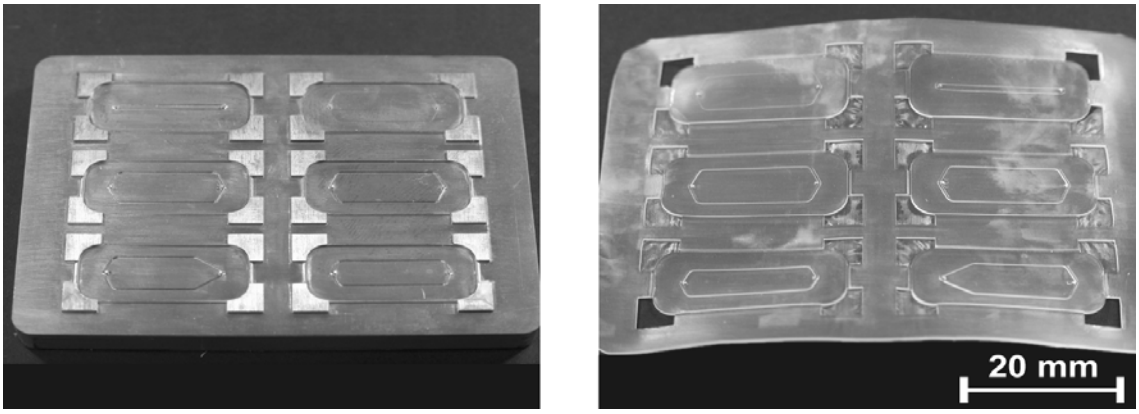

Fig. 5.10 Photograph of six different test configurations of the fluidic cells milled on brass mold (left) and embossed on TPU elastomer (right).

The parameters of the cells were chosen in a way to assure sealing properties with reduced chamber volume. In order to check the influence of different design parameters, one of the cells that had been successfully tested in real-time bio-analytical measurements was accepted as a *standard cell (S-Cell).* The other cells differed from the S-Cell by only one parameter. The design of the cells and their parameters are shown in Fig. 5.11 and summarized in Table 5.3.

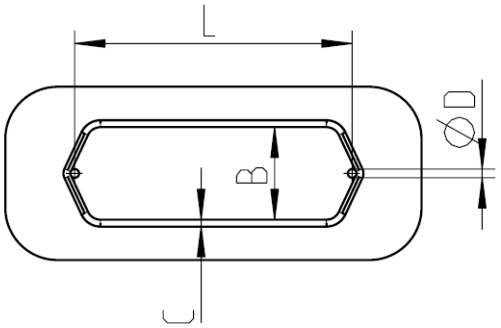

Fig. 5.11 Scheme of the parameters of the fluidic devices. Every device possesses in- and outlet, seal with different height H and width (C), different chamber width (B). The length L was equal for all samples (L = 16 mm). The diameter D of the through holes for the fluidic connections was 0.5 mm.

The different cells configurations were tested by injections of 20% glycerine (in water), Selex buffer (20 mM Tris-HCl with pH 7.4, 140 mM NaCl, 5 mM KCl and 1 mM $MgCl_2$) and demineralized water at different flow rates (20, 50, 80 µl/min). Water was also used as a running buffer between the injections. The SAW chip used for all measurements contained five sensor elements (Fig. 5.12).

Table 5.3 Dimensions of the test fluidic cells. Cell 4 has a narrow outlet for reduction of the fluid drain time. Cell 5 has three ellipse posts (0.3 x 0.2 mm) at the inlet.

Cell number	Chamber width [mm] (B)	Chamber height [mm] (H)	Seal width [mm] (C)
S-Cell	5.34	0.3	0.4
Cell 1	4	0.3	0.4
Cell 2	5.34	0.2	0.4
Cell 3	5.265	0.1	0.115
Cell 4	5.34	0.3	0.4
Cell 5	5.34	0.3	0.4

For assuring a proper basis for comparison, all measurements presented here were taken from SAW sensor 3. This is the sensor in the middle of the chip. The sensor at the inlet is number 1, the sensor at the outlet is number 5. The sensors 1 and 5 had higher deviations because of the position of the sealing or temperature effects from the fluid.
All the measurements were accomplished with flow rates 50 µl/min and burst step 150 µl/min.
Some of the cells were compared with respect to the value of the phase shift, signal-to-noise ratio (SNR) and rising time of the signal. The results are presented in Table 5.4.

The chamber of the **Cell 1** was chosen in a way to assure contact between the seal and the SAW chip outside the IDTs (Fig. 5.12).

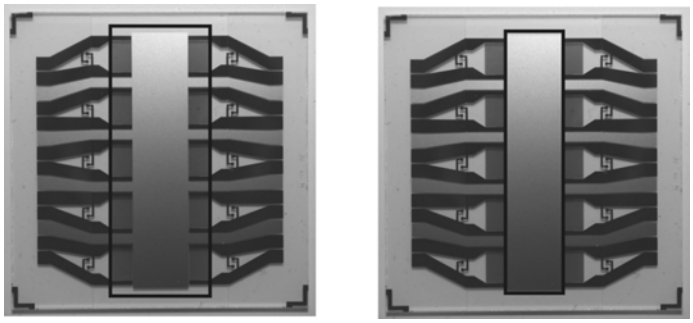

Fig. 5.12 Position of the chamber seal of the S Cell (left) and Cell 1 (right) on the SAW chip.

The design of Cell 1 aimed to prevent the contact between the IDTs and the liquid. A similar design has been reported earlier [JAK98].
Fig. 5.13 presents a comparison between S-Cell and Cell 1 for injection of 20% glycerine. The Cell 1 shows about 2.2 ° smaller phase shift and a Factor 10 lower SNR (Table 5.4). For Selex injection, the signals obtained with both cells show totally different behavior (Fig. 5.14). The sensor signal obtained with the S-Cell has a drop of more then 2.8 °, while the Cell 1 has a 1° increase and SNR only 2.4.
It is evident from the glycerine injection that by using Cell 1 the measuring signal is damped, with a higher SNR. The reason for this behavior is the position of the seal, which is pressed against the active sensor area and causes damping of the acoustic wave propagating in the guiding layer.
Cell 1 does not allow a contact between the Selex buffer and the IDTs. By using the S-Cell, the IDTs are in contact with Selex, which causes appearance of parasitic capacities with the conductive fluid (Fig. 2.4). The cross-talk between the parasitic capacities and the IDTs causes phase shifts of the measured signal.

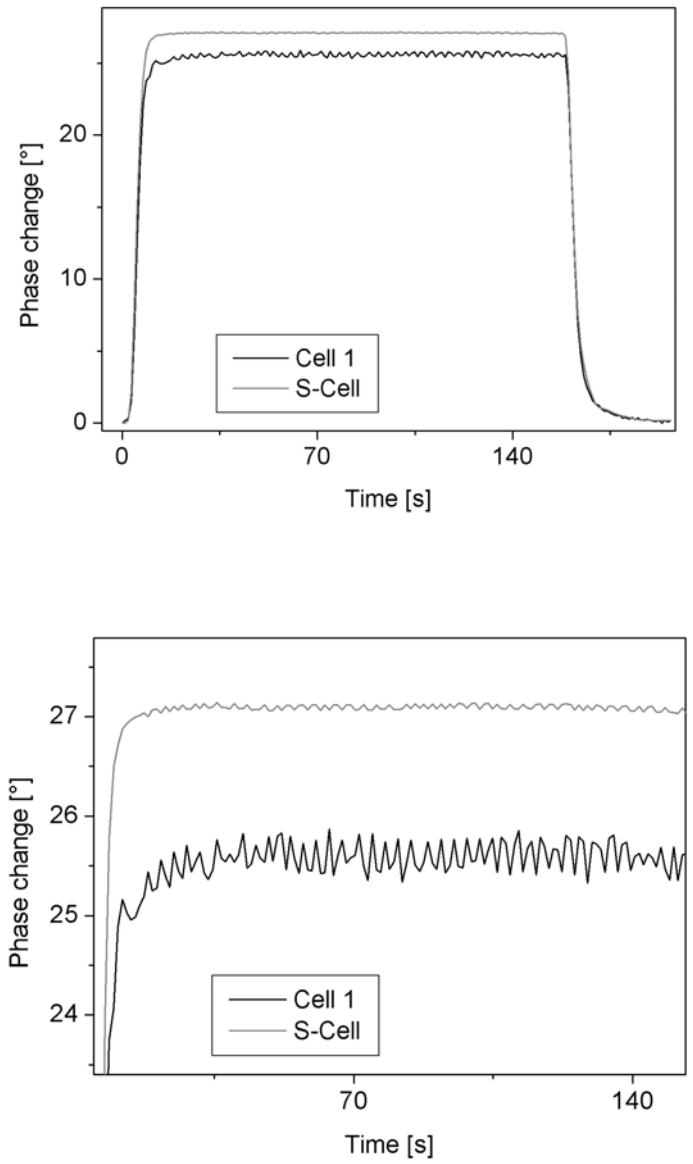

Fig. 5.13 Comparison between S-Cell and Cell 1 by injection of 20% glycerine (top). The magnified figure (bottom) shows the difference in noise.

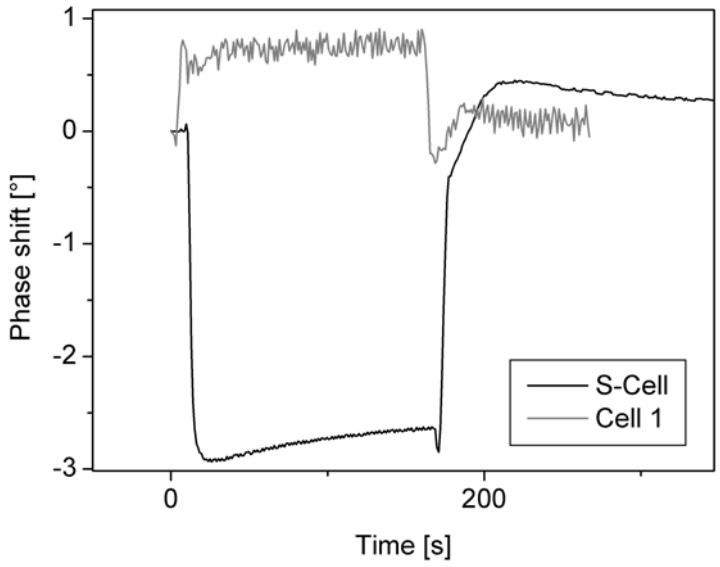

Fig. 5.14 Comparison between S-Cell and Cell 1 by injection of Selex buffer. The different direction of the phase shift can be explained with the different position of the seal according to the IDTs and the use of conductive liquid.

These results are in accordance with the already reported similar fluidic cell configuration [JAK98], where additional losses due to reflections and damping of the acoustic wave have been observed.

Cell 2 differed from the S-Cell only by its height (Table 5.3). The reduction of the cell volume by 33 % was supposed to reduce the fluidic exchange time (rising time). The rising time was more then 1 sec shorter than the rising time of the S-Cell (Fig. 5.15) for injection of 20 % glycerine (Table 5.4).
Fig. 5.16 shows SEM images of the inlet (outlet) area and a cross section of the sealing of Cell 2.

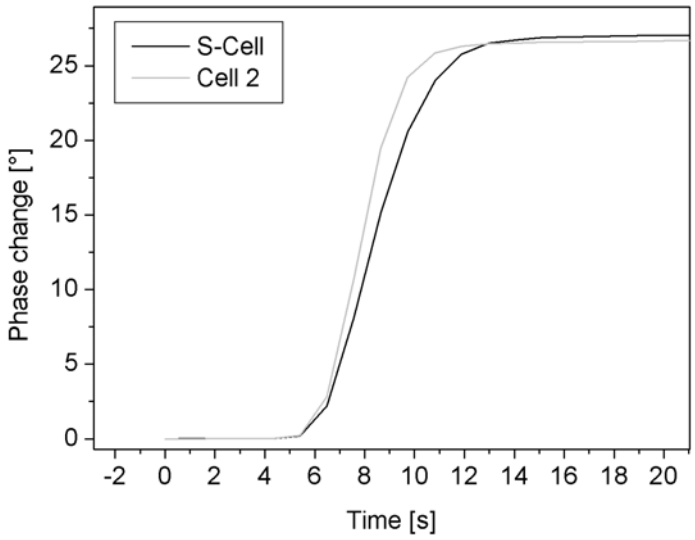

Fig. 5.15 Comparison between the rising times of the S-Cell and Cell 2. Cell 2 (33% less volume) reaches more than 1 s faster the new equilibrium state.

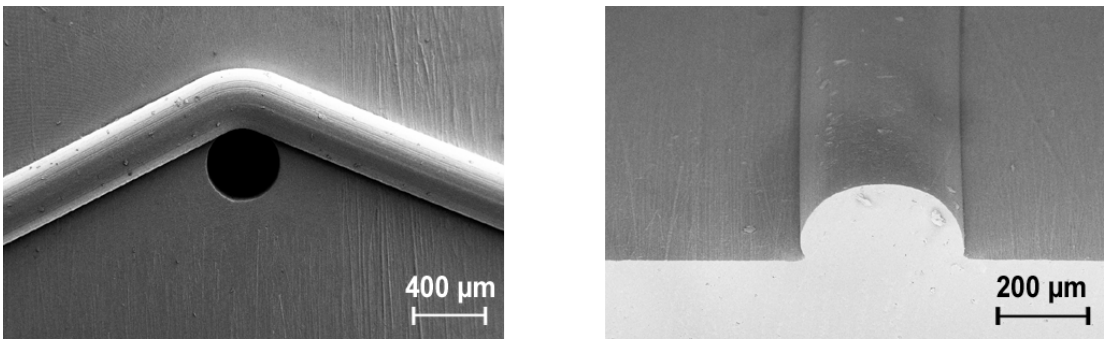

Fig. 5.16 SEM image of Cell 2. Inlet (outlet) area (left), cross-section of the seal (right). The cells were deposited with 100 nm Au for obtaining the image.

Cell 3 differed from the S-Cell by its height (Table 5.3). It had 66 % less volume than the S-Cell and the seal was 0.115 mm wide instead of 0.4 mm (S-Cell). The tests showed problems of removing of the air bubbles from the chamber. The reason could be that by causing pressure on the top of the cell, its roof contacts the sensor surface. Because of the small height, the sealing pressure was difficult to be adjusted without closing completely the chamber. If the pressure was not high enough, leakages were observed.

Cell 4 was designed with a narrower outlet. The aim was to enhance the drain speed of the liquid and to reduce the fluidic exchange times. With this design the seal

contacts the active area of sensor 5, which is located at the outlet of the chamber. Fig. 5.17 shows the signal change on sensors 3 and 5 of Cell 4 for 20 % glycerine injection.

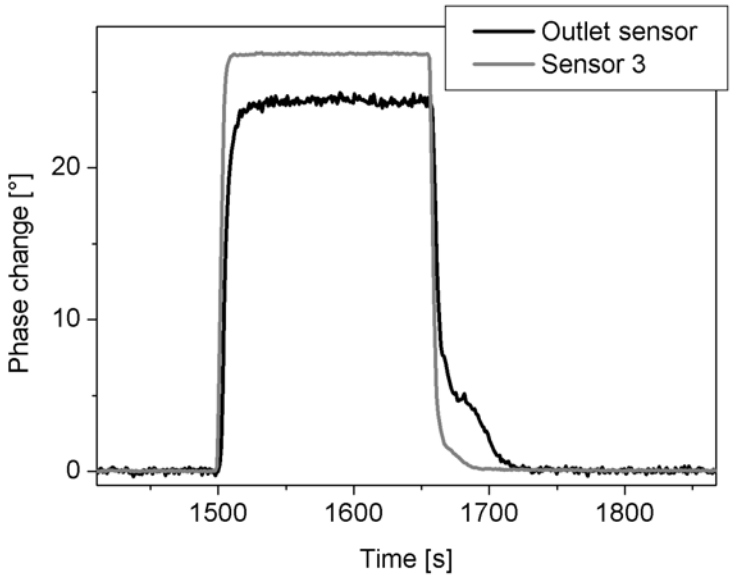

Fig. 5.17 Comparison of the signals from sensor 3 (middle) and 5 (outlet) with Cell 4, for 20% glycerine injection. The sharp outlet (black line) does not improve the exchange rates.

The sharp outlet did not lead to a sharper back slope of the signal from sensor 5. Furthermore, the shape of the sealing caused additional damping of the acoustic wave and the SNR for sensor 5 was 55, which is about 10 times lower than by using of the S-Cell. This result corresponds with the results from Cell 1, where the seal contacted the active sensor area and caused damping leading to SNR in the same range.
By comparison between the signal from sensor 3 of S-Cell and sensor 3 of Cell 4, no significant differences have been observed (not shown).

Cell 5 was designed with three ellipse posts at the inlet for homogenization of the fluid flow. It showed problems with removal of the air bubbles, which were concentrated near the posts.
The experiments showed that the sensors 1 and 5 had higher signal changes in comparison with the sensors 2,3 and 4. This is to be related to the specific geometry of the fluidic cell at the in- and outlet area. The shape of the sealing, as it was especially observed for Cell 4, influences the damping of the acoustic waves. The damping is higher when the sealing contacts the IDTs or the sensing area.
The S-Cell and Cell 2 showed the best signal to noise ratio and maximal phase shifts, without causing problems with air bubbles removal. Cell 2 had the advantage of higher fluid exchange rates, because of the smaller volume. The parameters of Cell 2 were subsequently used for the design of the chamber of the closed fluidic devices (see Section 5.4).

Table 5.4 Comparison between S-Cell, Cell 1 and Cell 2 considering their amplitude, signal to noise ratio (SNR) and rising time (s). The measurements were performed with 20 % glycerine and Selex buffer, flow rate 50 µl/min. All measurements were performed with Sensor 3.

Cell	Phase shift [°] 20% glycerine	Phase shift [°] Selex buffer	SNR 20% glycerine	SNR Selex buffer	Rising-time 20% glycerine, sec	Rising-time Selex buffer, sec
S-Cell	27.4	-2.8	548	55	8	8
Cell 1	25.2	1.0	50	2.4	8.5	8
Cell 2	25.9	-3.1	518	155	7	7

5.3.3.4 Influence of the flow parameters

As it was already discussed in Section 2, mass loading on the surface of the SAW sensor should cause only phase shifts, while the parameters of the fluid cause phase as well as amplitude changes. Fig. 5.18 shows the change of the amplitude and phase at subsequent injections of water, 20 % glycerine and Selex buffer at enhanced flow rates (80 µl/min). The measurement was performed with the S-Cell. The running buffer was demineralized water, flow rate 50 µl/min.

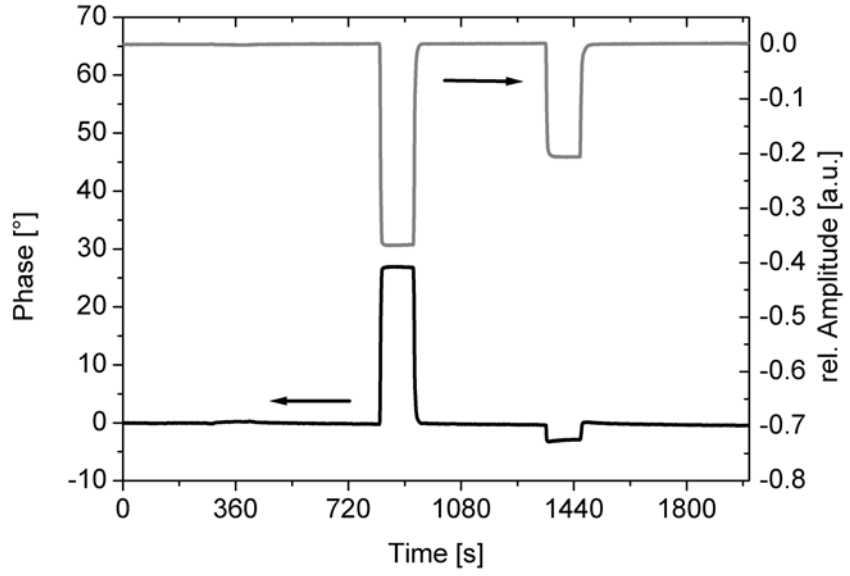

Fig. 5.18 Change of the phase and the amplitude of the sensor signal during water, 20 % glycerine and Selex buffer injection at flow rate 80 µl/min (measured with the S-Cell).

The injection of water at enhanced flow rate caused with the S-Cell a phase shift of 0.2°C. This change is due to the temperature effects on the sensor surface. At the same time no amplitude changes were observed. The Glycerine and Selex buffer injection caused phase as well as amplitude changes (Fig. 5.18) due to the different density viscosity product of the liquid (see Section 2). The same liquids were injected at flow rates 50 and 20 µl /min. The temperature effect caused by the water injection was weaker for the lower flow rates. In case of 20 % glycerine and Selex injections, no difference in phase and amplitude in comparison with the case with flow rate 80 µl/min was observed.

For real-time measurements of molecular interactions, it is desirable to achieve short fluidic exchange times. The exchange rate can be enhanced by a short-time increase of the flow rate at the beginning of the sample injection and before the end of the injection. Fig. 5.19 shows the signal for two injections of 20 % glycerine (Cell 2) with a flow rate 50 µl/min.

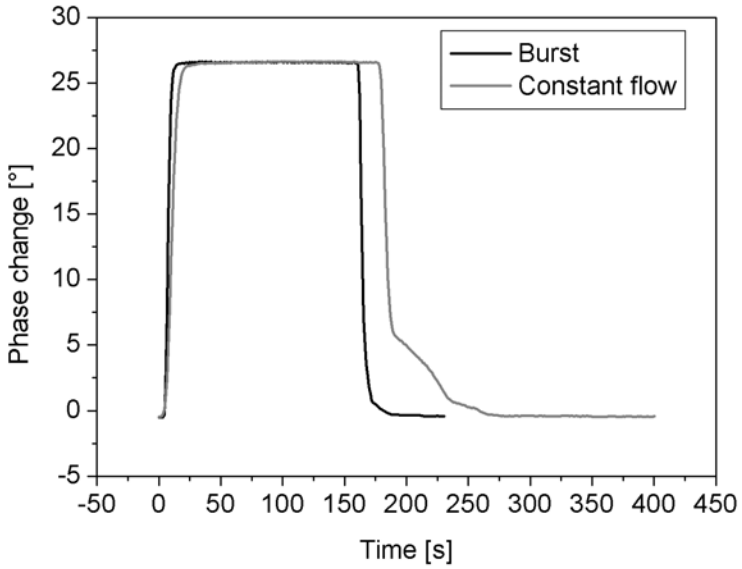

Fig. 5.19 Comparison between injections of 20 % glycerine with Cell 2 with burst 150 µl/min (black line) and without burst (gray line).

The black line describes the phase shift by using burst 150 µl/min, the gray one shows the phase shift without burst. The burst influences the front slope and much more significantly the back slope of the signal curve. The essential burst effect at the back front could be explained with the slower replacement of fluid with higher viscosity (20 % glycerine) by water in case of lower flow rates.

5.3.3.5 Temperature effects

As it has already been discussed, the temperature shift changes the liquid parameters and leads to deviations of the sensor signal. For this reason, it is important to keep the temperature constant during the measurements. In order to determine the temperature sensitivity of the SAW sensors, a Peltier element for temperature regulation of the sensor was used. It was mounted in a specially designed channel into the "S-sens" apparatus under the chip carrier (Fig. 5.20). The bio-sensor system was placed in a temperature stabilized box, allowing temperature deviations in the range of +/- 1 °C. The experiment was carried through with Cell 2 (Fig. 5.11, Table 5.3), using demineralized water as a running fluid. The water was degassed in vacuum and left for 2 h in the temperature stabilized box. The temperature in the box was kept constant (23 °C) during the experiment. The temperature of the Peltier element was changed in the range between 18 °C and 30 °C. The water flow rate was kept constant and the phase shifts at different temperatures of the Peltier element were measured. The dependence of the maximal phase shifts on temperature is shown in Fig. 5.21.

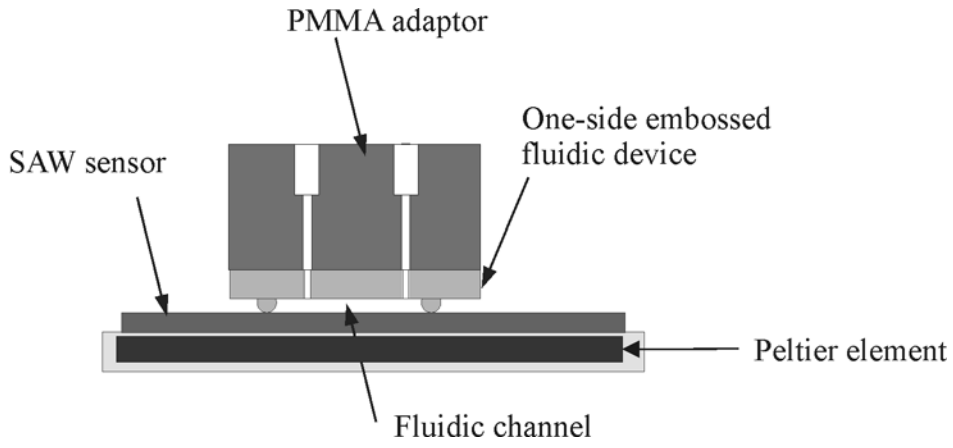

Fig. 5.20 Cross-section of the assembly of the chip-reader section of the S-Sens apparatus for measurements of the temperature stabilization with single-side embossed devices.

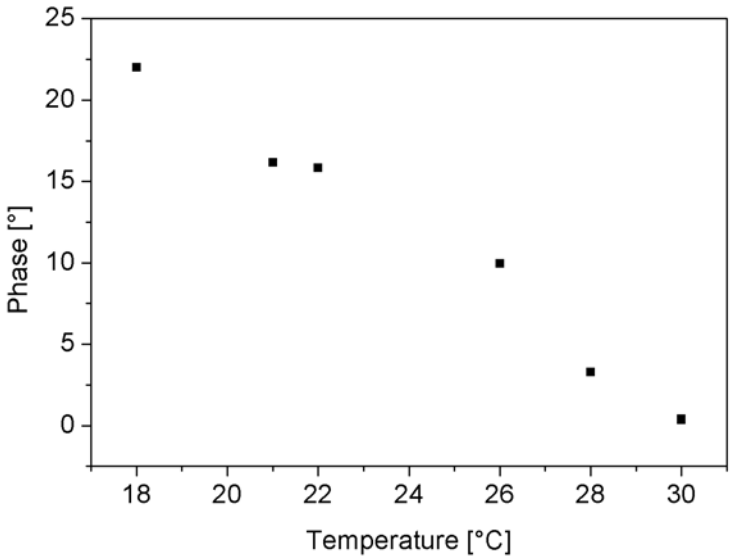

Fig. 5.21 Dependence between the phase shift and the temperature of the Peltier element. The buffer temperature was kept constant at 23°C.

In the temperature range 18 °C – 30 °C the change of the phase signal exceeds 20 °, which results in an average shift of more than 1.6 °/°C. This strong temperature dependence is included in the total sensor signal and results in an unacceptable errors. Hence, for reduction of the temperature effects, the temperature of the Peltier element should be kept constant and equal to the temperature in the box, as well as the buffer temperature. The temperature effects depend on the flow rates and increase with the increase of the flow rate.
Fig. 5.22 shows an experiment without using a Peltier element. The S-Sens apparatus was placed in the temperature stabilized box at 23 °C. Then water was injected with different flow rates between 40 - 200 µl/min and the phase change on every sensor element was measured. It is evident that the sensor at the inlet shows higher temperature deviations and the deviations decrease with every next sensor in direction outlet. This effect is observed for all flow rates and increases with the increase of the flow rate.

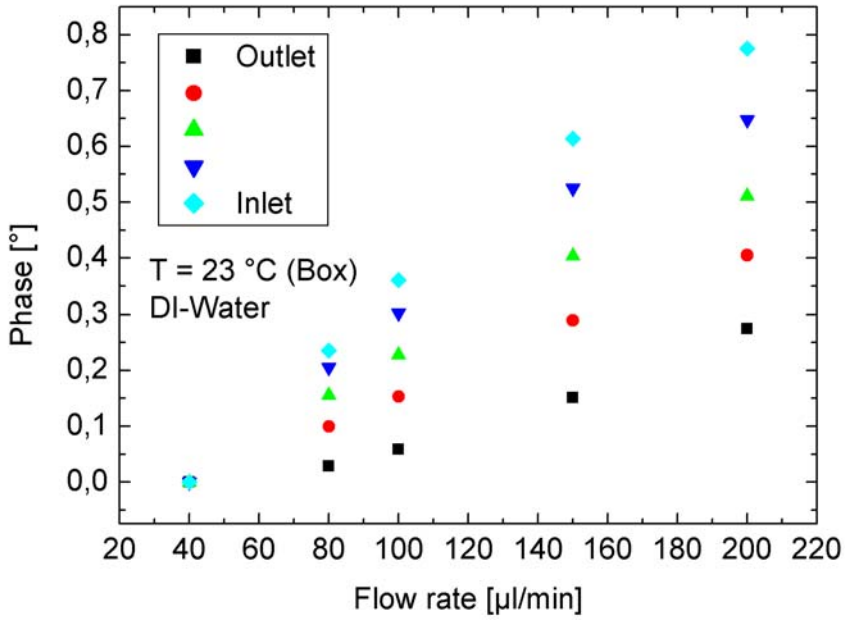

Fig. 5.22 Phase / Flow rate dependence of the five SAW sensors on a single chip. Deionized water was used as a fluid (Courtesy S. Glass, Caesar Internal report).

The surface of the sensor is warmer than the environment, because of the thermal diffusion from the electronic board. By increasing the flow rate, the liquid near to the sensor surface becomes colder. This leads to an increase of the density-viscosity product. Along the flow direction, the liquid is warmed up during the flow over the warmer sensor surface and the temperature difference between the sensor and liquid decreases in direction from sensor 1 to sensor 5.

Considering the results from the temperature dependence measurements, it was desirable to build the microfluidic system in a way assuring minimal temperature effects. One of the solutions was to design the fluidic channels to allow an equalizing of the sample temperature to the chip temperature before contacting the chip surface. This idea was realized by the fabrication of closed fluidic structures, described in Section 5.4.

5.4 Double-side embossed fluidic devices

Based on the successful development of single-side embossed microfluidic devices, the following section describes the development of sealed microfluidic devices fabricated by double-side hot embossing.
The fabrication of sealed fluidic channels reveals the following potential advantages:

- prevent the contact between the sample (buffer) solutions and the PMMA adaptor.
- flexible assembly of the fluidic device. No need for bonding with the PMMA adaptor
- better temperature stability
- possibility to integrate active fluidic parts into the channels
- allow in-situ immobilization of the receptor on the sensor surface.

5.4.1 Fabrication technology

Double-side hot embossing was employed for the fabrication of closed microfluidic devices. The double-side hot embossing allows creation of structures on both sides of a polymer foil. In this way, the fluidic devices contain a chamber (the reservoir that covers the sensors) embossed on the first side, while the fluidic channels are embossed on the opposite side of the foil. The fluidic channels are connected with the macro-fluidic system via embossed through holes into the foil that are closed from one side with another foil by a bonding process. The fluidic channels are in this way closed from the topside of the fluidic device. The sealing with the fluidic chamber and the openings for the channel connections remain on the bottom side of the foil.
The alignment between the top and the bottom molds was accomplished via the special alignment facilities of HEX 03 (see Section 4). The bottom mold was mounted into an additional plate fixed to the bottom tool.
The alignment process was accomplished in two steps. First, a dummy embossing process was carried out. A 1 mm thick PMMA plate was fixed to the bottom tool via polyimide tape. The position of the alignment marks on the bottom mold was detected via the microscope and stored by the software of the embossing system. Then the PMMA plate was embossed at 145 °C, 20 kN, 10 min. During the embossing process, the alignment marks on the top mold were replicated on the PMMA plate. Their position on PMMA was detected with the optical microscope. The difference between the position of the marks on the top and on the bottom molds is automatically calculated from the alignment software. The bottom plate is automatically driven to the correct position according to the calculated values.
The PMMA plate was preferred for the alignment process, because of high transparency. It allows easy observation of the surface of the bottom mold. Furthermore, the PMMA plate is harder than TPU foil and does not wrinkle. After the alignment, the PMMA plate was removed and the TPU foil was placed between the molds. The overall thickness of the TPU foil was 600 μm. The optimal embossing parameters for the Walopur material were already described (Fig. 5.5).
Fig. 5.23 represents a photograph of an embossed TPU foil with three fluidic devices.

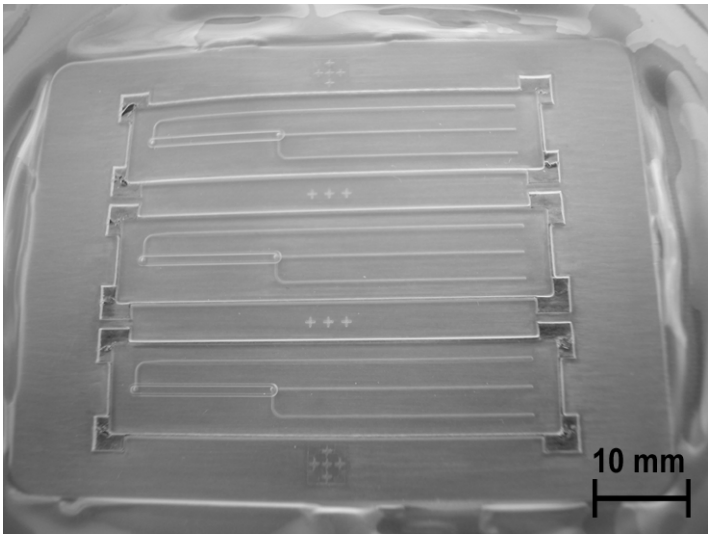

Fig. 5.23 Photograph of a TPU foil with double-side embossed fluidic devices. This test design contained no openings for the fluidic connections.

The embossed devices were cut off from the foil. The sealing of the channels from the topside was accomplished with 0.3 mm thick TPU foil. The bonding process was performed with the weak organic solvent NMP used for bonding of the single-side embossed cells to the PMMA adaptor (Fig. 5.9). In order to avoid damaging of the fluidic channels from the solvent, only the cover foil was treated with NMP. The both foils were then brought in contact manually on a plane surface. The applied pressure should keep the foils in contact and allow bonding of the areas between the channels. At the same time the channels must remain free. After 2 minutes the pressure was released and the foils were left at room temperature for 30 minutes to let the solvent completely evaporate. The fluidic channels were subsequently tested with a colored liquid.

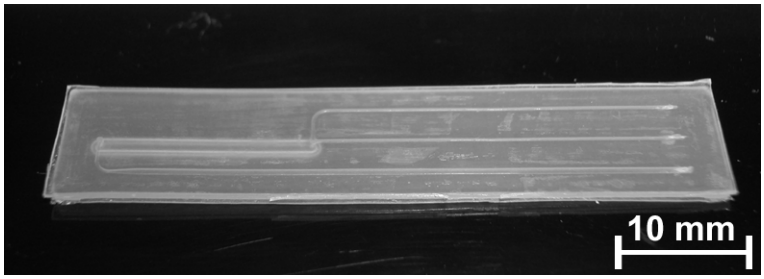

Fig. 5.24 Closed fluidic device, fabricated by double-sided hot embossing and subsequent chemical bonding process. The device has two inlets and one outlet aside.

Fig. 5.24 shows a closed double-side embossed device. The device has two inlets that can be switched by external valves and one outlet. Test with colored liquid has proven the sealing of the channels. No leakage or clogging was observed.

5.4.2 Devices for receptors immobilization

The double-side embossing process was also used for fabrication of a special microfluidic devices for immobilization of five different receptors on each of the sensor elements of the SAW biochip. The brass embossing molds were fabricated with the already described milling process. The first mold contained the sealing (0.2 mm height) surrounding the five fluidic chambers. Every chamber had a separate in- and outlet. The second embossing mold contained the inverse patterns of the fluidic channels (height 0.2 mm, width 0.2 mm). Both molds were aligned and the hot embossing processes were accomplished according to the above described process technology for double-side embossed devices. In order to compensate the non-planarities of the embossing molds, a 200 µm thick silicone foils (Kunze Folien GmbH, Germany) were placed between the embossing molds and the tools, into the top, as well as in the bottom embossing tool (Fig. 5.25).

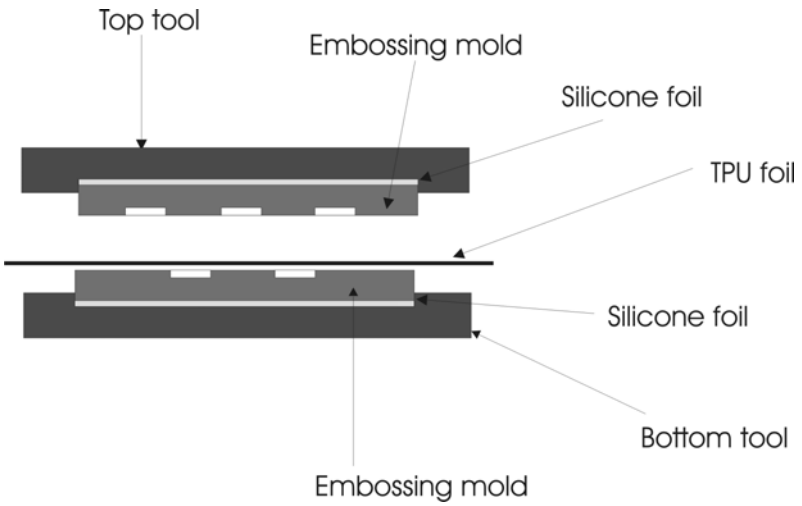

Fig. 5.25 Scheme of the assembly for double side embossing of TPU elastomers.

The above embossing assembly delivered structures with excellent conformation and through holes for 0.6 mm thick TPU foils. Fig. 5.26 presents a photograph of the molds for double-side embossing for devices for receptors immobilization.

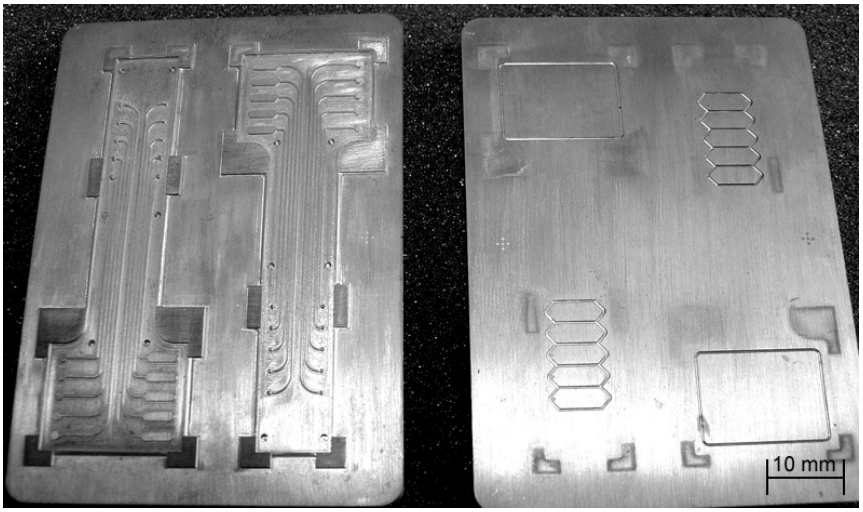

Fig. 5.26 Photograph of two molds for double side hot embossing. The design allows immobilization of five different receptors on the same bio-chip.

Fig. 5.27 presents a SEM image of a cross-section of the double-side embossed device. The embossed fluidic channels are seen on the top side, the sealing is on the bottom side of the fluidic device (Fig. 5.27 left).

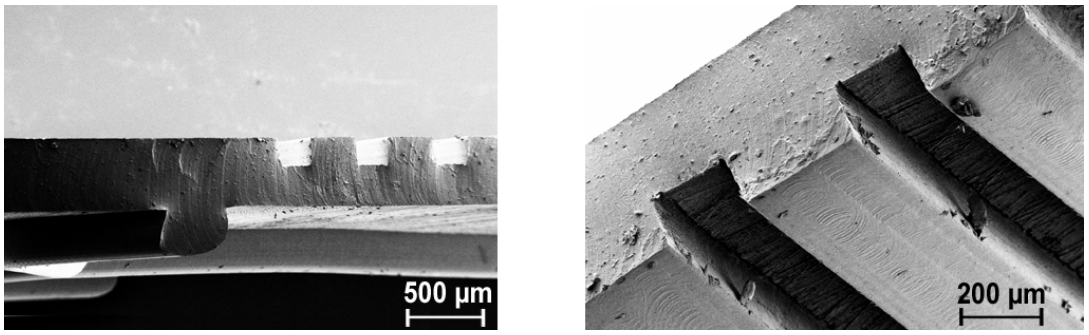

Fig. 5.27 SEM image of the cross-section of the fluidic device for receptor immobilization. 100 nm Au was deposited by thermal evaporation for obtaining the picture.

The fluidic devices for receptor immobilization were chemically bonded to a specially fabricated PMMA holder. A photograph of the bonded device is presented in Fig. 5.28. It can be positioned in a specially designed polypropylene (PP) fixture that holds the SAW chip.

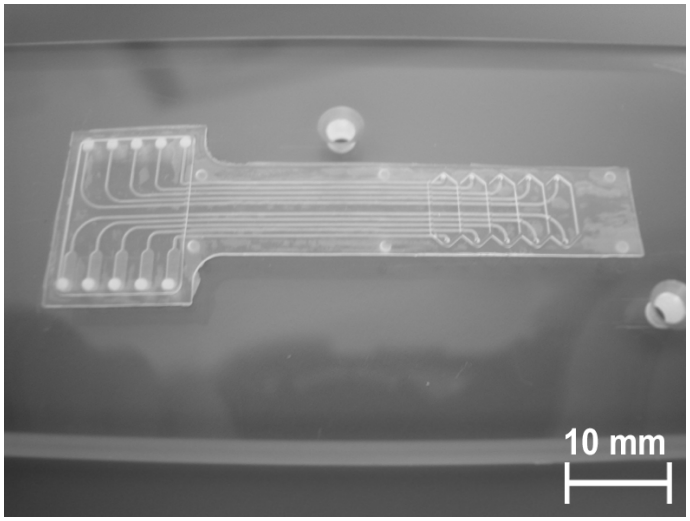

Fig. 5.28 Photograph of a fluidic device for immobilization of five different receptors on the same SAW biochip. The TPU device is bonded to PMMA carrier.

The first method was to spin the NMP on the PMMA holder by using a spin-coater (Delta 10, Süss MicroTec). This was not successful because of the non-symmetric shape of the holder and the resulting inhomogeneous NMP film. Another experiment was carried through by spinning of the NMP on a PDMS layer und subsequent "stamping" it on the TPU device. As in the first case, this led to insufficient homogeneity, partially because of the high evaporation rate of the NMP. The best results were achieved by applying the NMP on the PMMA adaptor by using a piece of soft paper. Since the sealing structure on the top hampers the application of homogeneous pressure to press the bonded pieces together, the bonding was done in a vacuum gel dryer. The upper part of the gel drier vacuum chamber consisted of an elastic foil that lies on the TPU foil and presses it to the PMMA adaptor. This method gave best results, but there were always leakages, because of bonding defects in the areas between the channels.
The design of the fluidic device proved to be not compatible with the chemical bonding processes. The space between the channels was only by factor of 2 wider than the channels themselves (the space width was 0.395 mm, the channel width was 0.2 mm.). The space between the channels had to be further increased. The channels were also comparatively long (more then 5 cm) that increases the possibility of defects during the bonding.

5.4.3 Devices for real-time measurements

The double-side hot embossing technology was also used for fabrication of closed microfluidic devices for real-time measurements with the S-sens system. For real-time measurements, the closed channels allow the fluid to flow a certain distance

over a plate temperature controlled by the Peltier element. It was expected that this design would decrease the temperature difference between the liquid and the sensor surface and result in reduced temperature effects in the sensor signal.
A TPU elastomer foil Walopur 2201 AU with thickness 0.6 mm was placed into the embossing assembly shown in Fig. 5.25. The optimal embossing parameters for good-shaped structures with through holes were: T_{top} = 148 °C, T_{bottom}= 148 °C, P_{emboss} = 100 bar, t = 28 min, T_{demold} = 80 °C.

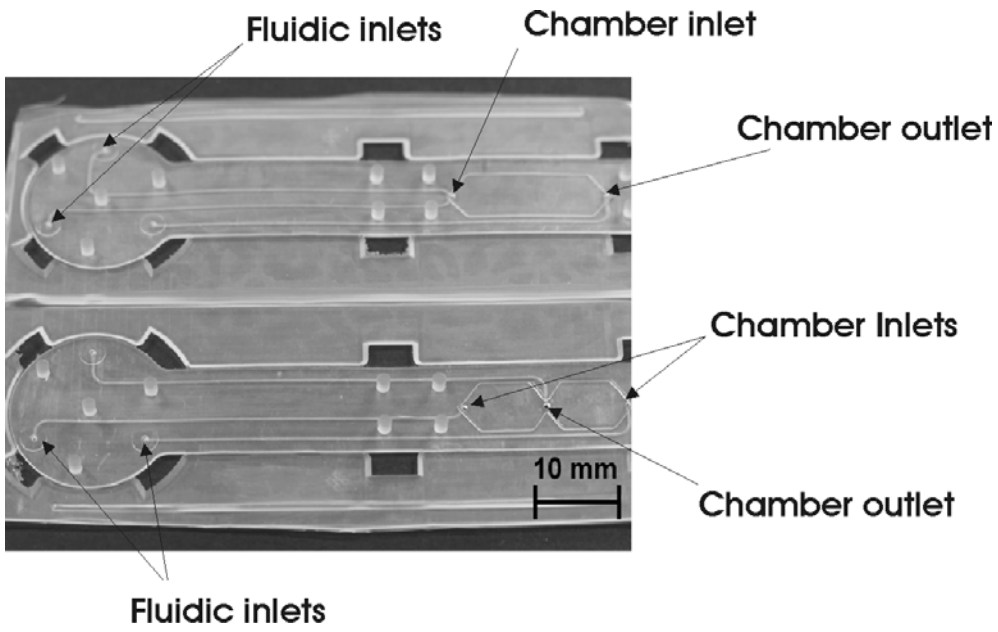

Fig. 5.29 Optical micrograph of two double-side embossed fluidic devices. The top one has two inlets for subsequent injection of different sample solutions. The chamber has only one inlet and one outlet. The bottom one has two chamber inlets on the opposite sides of the chamber and one outlet in the middle of the chamber.

Fig. 5.29 shows two double-side embossed devices with different design configurations. The parameters are listed in Table 5.5.

Table 5.5 Parameters of the double-side embossed fluidic devices for real-time measurements.

Device	Number of chambers	Number of inlets	Number of outlets	Channels cross-section, µm	Chamber height, µm
DS_1C_02	1	2	1	200 x 200	200
DS_2C_02	2	2	1	200 x 200	200

DS_1C_02 has the fluidic chamber configuration of the Cell 2 (see Table 5.3). The device has two inlets and one outlet situated on the opposite side of the chamber. The inlets serve for subsequent injection of two different sample solutions. The injection sequence is controlled by the use of external valves. The second fluidic device (DS_2C_02) has 2 chambers. The two inlets are located on the opposite sides of the chamber and the outlet is in the middle of the chamber. The seal was designed with a narrowing on both sides of the outlet, in order to prevent mixing of the receptor solutions.
DS_1C_02 was used for temperature stabilization measurements. It differs from the Cell 2 only by the longer fluidic channels, while the seal has the same shape.
DS_2C_02 was designed to serve for immobilization of two different types of receptor molecules on the same SAW chip. The different receptors solutions were injected simultaneously from the opposite sides of the chamber with the same flow rates (including the same burst rates). In this way the dynamic pressure on both sides of the outlet is equal and no cross-talk between the receptor solutions should take place. Experiments with a colored liquid have showed a very limited cross-talk between the chambers.

5.4.3.1 Assembly

The double-side embossed devices (Walopur 2201 AU) were bonded to another foil (Walopur 2201 AU) with thickness 300 µm for realization of sealed channels. The bonding process was already described in Section 5.4.1.
Thermal bonding was tested as an alternative bonding process. Hot embossing process was implemented to warm up the already embossed foil and the foil for the cover to temperatures that allow the both surfaces to "flow into each other". The processes were performed at low embossing pressure in order to prevent damaging of the already existing patterns. The double-side embossed device was placed on the bottom embossing mold, so that the embossed fixtures match their corresponding negative images on the brass mold. The TPU foil for the cover was placed on it. The use of foils from the same material is highly desirable, because both surfaces should have the same T_g. On the top side a plane embossing tool was used. The plane tool assured applying pressure only between the channels, because the plane of the channel bottom was located under the embossing plane. In order to prevent melting of the embossed foil, a temperature gradient was adjusted at which the bottom mold was kept at temperatures lower then the Tg, while the top tool was heated to temperatures above Tg, in order to allow the top foil to soften and to transfer heat to the top surface of the embossed foil. The temperatures varied between 125 – 130 °C for the top mold and between 70 and 110 °C for the bottom one. The embossing forces were between 4 and 10 kN. Each device has a surface area of 7.10^{-4} m^2.
The process parameters for Walopur 2201 AU foils that gave best results are: T_{top} = 125 °C, T_{bottom} = 80 °C, P = 5 kN, t= 180 s, $T_{deemboss}$ = 80 °C. This regime led to slightly deformed structures without sufficient bonding strength. When the temperature of the top mold was increased above 125 °C, the temperature difference T_{top} - T_{bottom} led

to enhanced stress into the TPU foil and caused wrinkling of the foils. The same results were observed with the increase of the embossing pressure. If the temperature was high enough to soften the material and strong bonding resulted, the thermal expansion led to changes of the dimensions of the embossed structures.

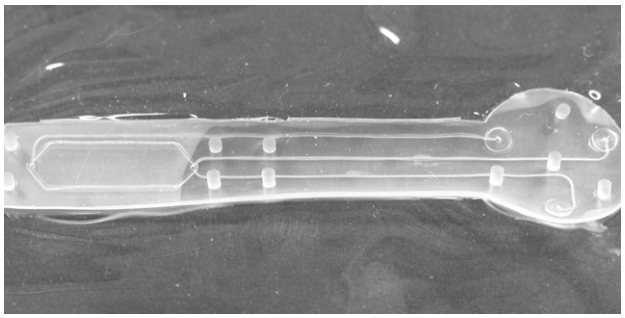

Fig. 5.30 Double-side embossed fluidic device, thermally bonded to a 300 µm TPU foil as a cover. The thermal bonding processes led to stress and deformation of the device.

In order to reduce the time interval in which the foils were prone to high temperature, experiments were made with applying the pressure while the foils are still at room temperature. This resulted at even more stress in the foil without sufficient bonding strength.

5.4.3.2 Temperature stability measurements with the double-side embossed devices

In this section, the closed fluidic device DS_1C_02 was tested in temperature stability measurements and compared with the fluidic Cell 2. Both devices have complete identical fluidic chambers. The design of the double-side embossed closed fluidic device and the way it is mounted in the "S-Sens" system give the sample liquid a possibility to flow over temperature stabilized area. The liquid partially equalizes its temperature to the surface temperature of the SAW sensor before entering the sensor area. Fig. 5.31 presents a scheme of the assembly of the S-sens system for temperature measurements with the double-side embossed (closed) fluidic devices.
The measurements with Cell 2 were performed with the assembly shown in Fig. 5.20. For comparison of the one-side embossed and the closed fluidic devices, the "S-sens" system was placed into a temperature stabilized box. The temperature could be regulated with an accuracy of +/- 1 °C. The running buffer was demineralized water that had been degassed in vacuum. The deminiralized water was placed in the temperature stabilized box 2 hours before the measurement. All measurements were

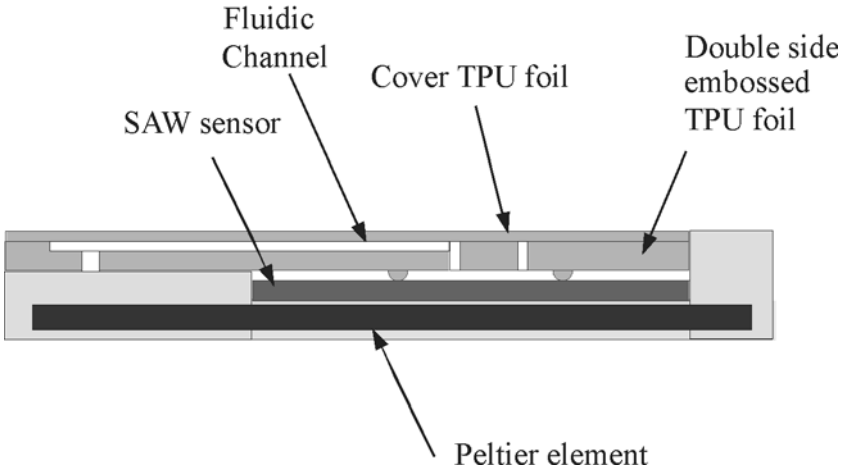

Fig. 5.31 Scheme of the chip-reader section of the "S-sens" apparatus with assembly for double-side embossed fluidic devices.

performed with the same SAW chip and the signals were taken from sensor 3. The temperature of the SAW biochip was regulated by using a Peltier element. The temperature of the Peltier element was first adjusted to be equal to the box temperature (23 °C). Hence, no temperature difference between the sensor surface and the running liquid existed. Afterwards, the temperature of the Peltier element (on the sensor surface respectively) was changed, while the box temperature (equal

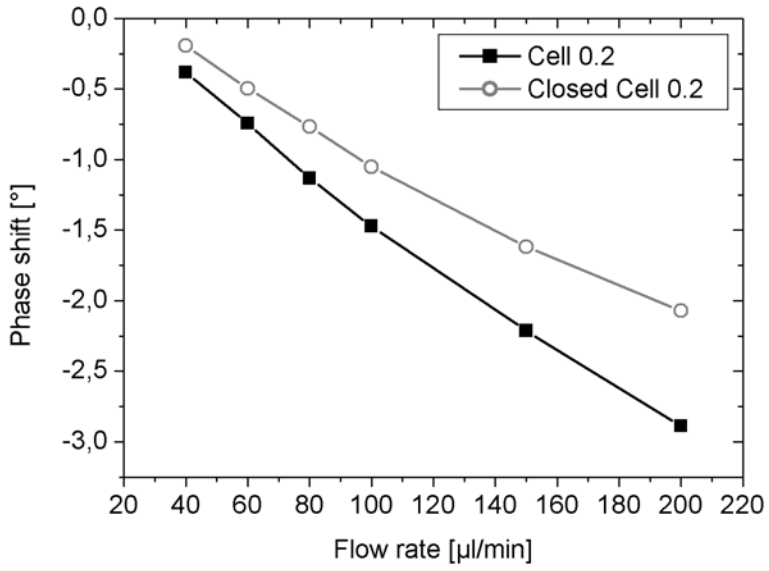

Fig. 5.32 Comparison between the phase shift for Cell 2 and the closed sell DS_1C_02 at different flow rates at temperature difference $T_{peltier} - T_{water}$ = -4.2 °C.

to the temperature of the running liquid) remained constant. Fig. 5.32 presents the phase change for both cells for different water flow rates at fixed temperature difference $\Delta T = T_{Peltier} - T_{water} = -4$ °C. The real (measured) temperature difference was $\Delta T' = -4.2$ °C for both cells. In this case the sensor surface was colder then the water.
Fig. 5.33 represents the phase shift at temperature difference $\Delta T = T_{Peltier} - T_{water} = +4$ °C. Here, the sensor surface was warmer then the running water. The measured temperature difference was $\Delta T' = 3.8$ °C for the Cell 2 and $\Delta T' = 3.6$ °C for the closed cell.

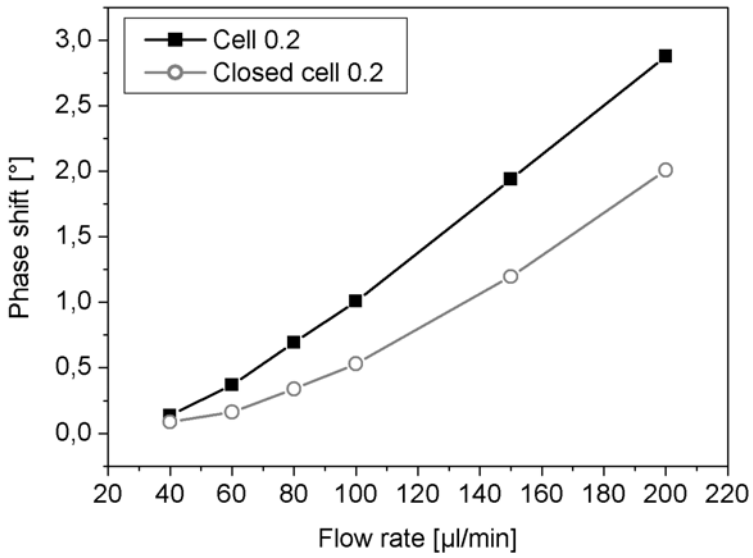

Fig. 5.33 Comparison between the phase shift for the Cell 2 and the closed cell DS_1C_02 at different flow rates at temperature difference $T_{peltier} - T_{water}$ = +4 °C.

Fig. 5.32 and Fig. 5.33 show that in both cases the use of closed fluidic devices led to smaller phase shifts in comparison with the single-side embossed devices at the same temperature differences. Furthermore, this effect was smaller for lower flow rates (40-60 µl/min) and became more significant at higher flow rates (80 – 200 µl/min). This observation can be explained with the flow of the water through the channels of the closed fluidic device that is located above the Peltier element. During the flow through these channels, the temperature of the water partially equalizes with the temperature of the sensors surface.

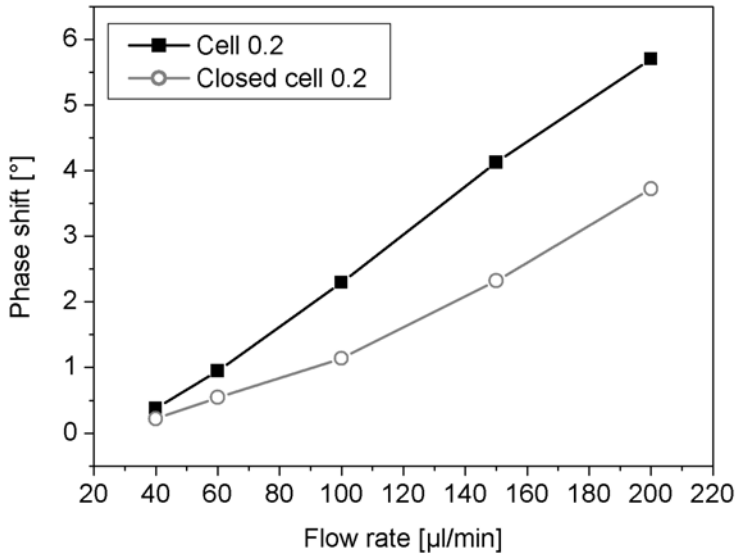

Fig. 5.34 Comparison between the phase shift for the Cell 2 and the closed cell DS_1C_02 at different flow rates at a temperature difference $T_{peltier} - T_{water} = 8$ °C.

The phase shifts for both devices for a temperature difference $\Delta T = T_{Peltier} - T_{water} = +8$ °C are shown in Fig. 5.34. The measured temperature difference was $\Delta T' = +7.6$ °C for the Cell 2 and $\Delta T' = +7$ °C for the closed cell. The corresponding curves for both devices have very similar slopes to those in case of +4 °C difference. Here, again the closed fluidic device delivers better temperature stability in comparison with the single-side embossed fluidic cell. The phase shifts for both curves differ by factor of 2 to the corresponding curves in case of 4 °C difference. As in the case with 4 °C difference, the difference between the signals taken from both cells enhances with the flow rate.
The phase shifts for both devices at temperature difference $\Delta T = T_{Peltier} - T_{water} = 0$ °C have been investigated. No significant difference between the signals was observed.

The experiments that have been carried out showed that the closed fluidic devices deliver better temperature stabilization and consequently reduce the contribution of undesired signals caused by temperature fluctuations. The difference in the temperature stability between the single-side embossed and closed fluidic devices increases with increasing of the flow rate of the running fluid.

6 INTEGRATION OF ACTIVE VALVES

6.1 Fabrication of active valves with PDMS

Fig. 4.5 shows that when using an external injection valve the liquid must flow a long way through the PEEK capillaries to the sensor. The volumes of the capillaries and the fluidic connections have to be filled before the liquid enters the fluidic chamber. These volumes are called dead volumes and lead to delay times during the liquid injection. The large dead volumes increase the sensor response time. Moreover, larger sample volumes are needed. The dead volume can be significantly reduced and the sensor response time decreased by integration of valves near to the sensor. By integration of valves into the microfluidic device, the influence of the macrofluidic parts with large dead volumes (such as long PEEK capillaries, injection valve, fluidic connections) can be eliminated. In addition, the decreased fluidic volumes also reduce the possibility of mixing and dilution between the sample and the buffer, as well as reduce the undesirable binding of sample (receptor) molecules to the walls of the capillaries. Another significant advantage of integrated microfluidic valves is that by their switching the flow can be guided in different directions in the chamber that allows coverage of the SAW sensors on the chip with different receptor molecules in flow through. In Section 3.5 a short review of microfluidic valves is presented.

Pneumatically driven active valves were chosen for the "S-sens" system. They are robust, reliable, do not depend on temperature and can be fabricated in a cost effective way. Low cost is of essential importance, because the microfluidic devices should be used as disposables. The disadvantages of the pneumatic active valves are the need of a source for pressurized air and their comparatively long response time. Here, the response time of the integrated valve depends on the response of the external pneumatic supply system that is slower than that of the pneumatic valve itself.
For the integration of active pneumatic valves into the microfluidic devices, a new design for molds for double-sided hot embossing was made [STO06]. The design of the fluidic chamber allows immobilization of two different types of receptor molecules on the SAW chip with 5 µl volume/sensor. The fluidic channels have cross-sections of 200 x 200 μm^2. During the embossing step, small reservoirs with a diameter of 500 µm and 1 mm had been formed in every channel between the inlet and the fluidic chamber (see Fig. 6.1). The reservoirs act as bodies of the pneumatic valves and they were designed in a way to fit into the already existing S-Sens system. For that reason, they are placed near to the inlets of the fluidic device. In the future, the apparatus design will allow the pneumatic valves to be located closer to the fluidic chamber. This will further decrease the dead volumes and contribute to the reduction of the response times.

The hot embossing process was similar to the already described fabrication of double-side embossed fluidic devices of TPU elastomer foils. After embossing, silicone was applied into the reservoirs in the channels. Here, a two-component silicone Elastosil RT 607 (red) (Wacker-Chemie GmbH, Munich, Germany) was used. The components A (containing platinum catalyst) and B (cross-linker) were mixed in 9:1 weight ratio and stirred thoroughly to homogenize. The mixture was degassed in a vacuum oven (15 mBar) at room temperature for 10 min. The silicone was taken out from the oven and poured into the reservoirs in the channels by using a dispenser system 1500 XL (GLT, Pforzheim, Germany) with dispense needles with diameter of 0.21 mm (EFD Inc., East Providence, RI, USA). Afterwards, the whole fluidic device was placed in an oven at atmospheric pressure and left to cure for 15 min at 100 °C. The adhesion of the silicone to the TPU was not very strong, but sufficient in order to sustain the pressure of the flowing liquid**.** The amount of silicone must be sufficient to fill in the reservoir in order to allow a proper functioning of the pneumatic valve. On the other hand, it must not flow into the fluidic channels, since this could lead to clogging, as well as to defects during bonding process.
The chemical bonding processes have been prepared using the described wet chemical welding technology. The silicone was not dissolved in the used organic solvent (NMP). Moreover, the silicone has hydrophobic properties and repels the NMP. For that reason, the areas of the TPU membrane (50 μm thick) located just above the reservoirs filled with silicone were not bonded to the silicone. A closed microfluidic device with four integrated silicone valves is shown in Fig. 6.1.

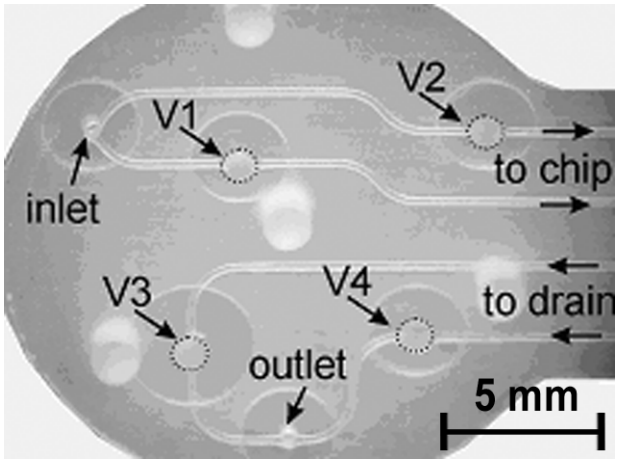

Fig. 6.1. Microfluidic device with 4 integrated silicone pneumatically driven valves. The valves (diameter 1 mm) are marked with dashed circle lines. The in- and outlets are connected from the backside.

The microfluidic devices are mounted in the S-sens system via a corresponding chip-holder, as shown in Fig. 6.2.

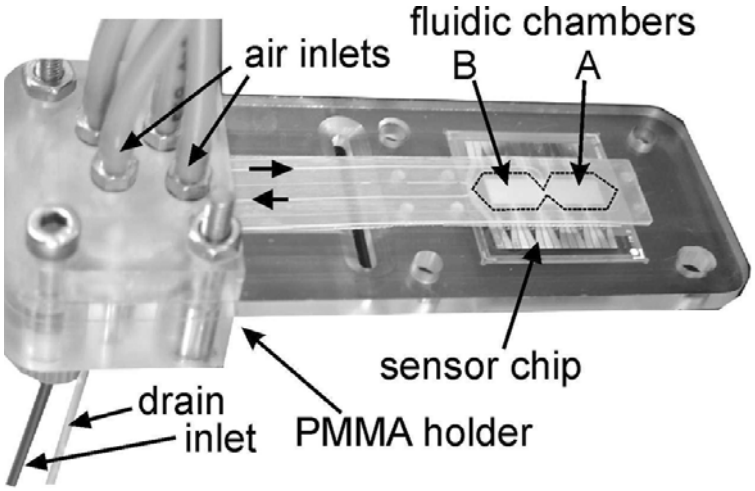

Fig. 6.2 Photograph of the chip-carrier with the connections for the pneumatic (from the top) and the fluidic system (from the bottom).

External pneumatic valves (Festo AG, Esslingen, Germany) used for switching of the fluidic valves were regulated with a 5 Volt TTL logic.
Fig. 6.3 depicts a cross-section of the chip holder with the mounted fluidic device. The sealant structure and the inlet are on the bottom side of the device, while the reservoirs for the valves are situated on the top. The silicone filled reservoir acts as body of the pneumatic valve, while the bonded TPU sealing foil (50 µm) acts as valve seat. The fluidic valve is normally open. Pneumatic pressure is applied through the air connections (Fig. 6.2, Fig. 6.3) in order to close the valve. If the corresponding pneumatic valve is open, pressurized air (P = 4-6 bar) causes a bending of the polyurethane membrane (50 µm thick) and closes the channel. When the pneumatic valve is switched off, the fluidic valve opens under the pressure of the liquid flow. The position of the sealing forming two fluidic chambers (A and B) over the bio-chip is marked in Fig. 6.2 with a black line. The total volume of the fluidic chamber is 25 µl.

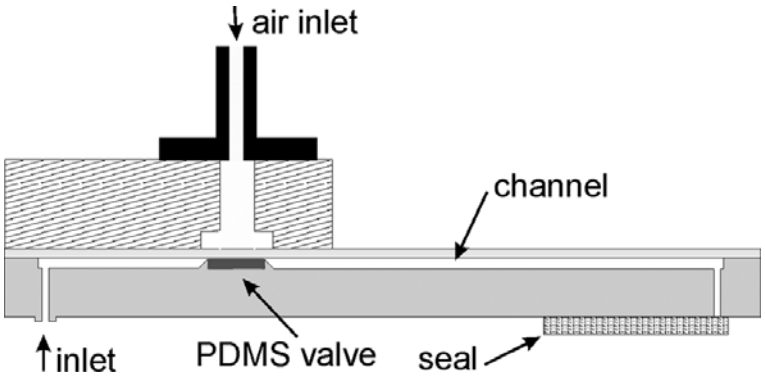

Fig. 6.3 Cross-section of the fluidic device and the adaptor for the pneumatic connections.

The four fluidic channels with four active valves and two chambers allow biological solutions to be directed into either chamber A or B or into both chambers simultaneously by switching of the corresponding active fluidic valves. A scheme of the fluidic flow regulation is shown in Fig. 6.4. Table 6.1 shows the TTL logic.

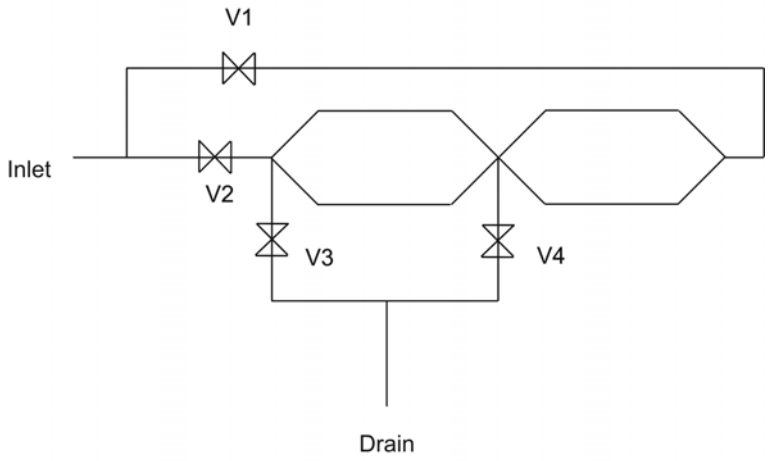

Fig. 6.4 Scheme of the liquid flow regulation via integrated fluidic valves.

The valves V1 and V2 control the inward flow into chamber A or B, whereas the valves V3 and V4 control the outlet drain. By switching of the outlet valves, either the outlet between the chambers, or the outlet of chamber B (left side) can be used as drain.
The fluidic valves were first tested with colored liquid (Data not shown). No valve leakages have been observed.

Table 6.1 TTL logic for the regulation of the integrated fluidic valves (0 means "closed", 1 means "open").

TTL	V1	V2	V3	V4	Process
000	0	0	0	0	xx
001	1	0	1	0	measurement
010	1	0	0	1	Immobilization chamber A
011	0	1	0	1	immobilization chamber B
100	0	1	1	0	by-pass
101	0	0	0	1	xx
011	1	1	0	1	xx
111	1	1	1	1	xx

Before carrying through bio-analytical measurements with the microfluidic devices with integrated valves, the dead volume of the whole fluidic system (macro- and micro- unit) was determined by tests with 0.5 M NaCl. The dead volume was calculated by measuring the time needed for the salt solution to flow from the sample cartridge to the first SAW sensor at a certain flow rate. The determination of the dead volumes is of essential importance for adjusting the time of the burst steps. The volume of the used PEEK capillaries was 20 µl, the volume of each fluidic channel of the device was 2 µl and the volume of a single chamber was about 15 µl. The burst should start exactly in the moment, when the sample solution (buffer) enters the fluidic chamber.

The aim of these experiments was to prove the function of the integrated valves. For that reason, the current configuration of the "S-sens" system was used. In the future configurations of the bio-analytical system, the valves are going to be integrated nearer to the fluidic chamber. Additional reservoirs for the sample are going to be designed into the fluidic device, which will reduce the sample volume.

Here, several different real-time macromolecular interactions have been measured by using the TPU based devices with integrated valves. All injections were carried out by using 200 µl substance volume, 40 µl /min flow rate with burst-in and burst–out steps 150 µl/min.

6.1.1 Glycerine injection

Fig. 6.5 shows an experiment with 5 % glycerine in water. Deminiralized water was used as a running buffer before and between the glycerine injections. First, the fluidic valves were switched in position 1001 (Table 6.1). In this position valves V1 and V4 were opened, valves V2 and V3 were closed. The flow was guided through chamber A. 5 % glycerine was injected and caused about 6° phase shift on the sensor A. No change of the signal of sensor B was observed.

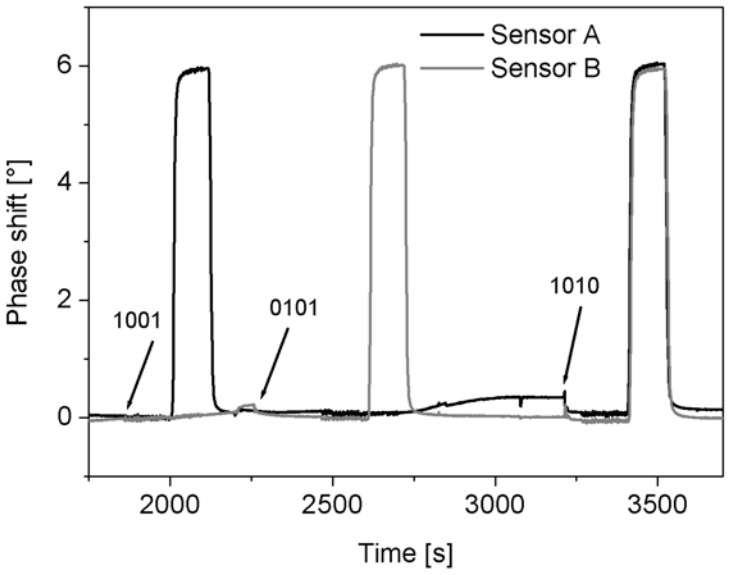

Fig. 6.5 Test of the integrated microfluidic valves with injection of 5% glycerine (in water) subsequently in chamber A, chamber B, and in both chambers A and B simultaneously. The arrows show the moment of valves switches.

After the end of the glycerine injection the pneumatic valves were switched in position that corresponded to opening of fluidic valves V2 and V4, while V1 and V3 were closed. The following 5 % glycerine injection caused 6 ° phase shift on sensor B. Sensor A showed no change.
In the next step, the pneumatic valves were switched in a way, assuring opening of fluidic valves V1 and V3, and closing V2 and V4. The flow was guided through both chambers. The glycerine injection caused 6 ° phase shift for both sensors A and B.
This experiment has proven the proper functioning of the fluidic valves. No glycerine was detected into the neighbor chamber, which was an evidence for good sealing of the valves.
In the next measurements, the integrated fluidic valves were tested for a real-time detection of intermolecular interactions.

6.1.2 Thrombin – antithrombin binding [STO06]

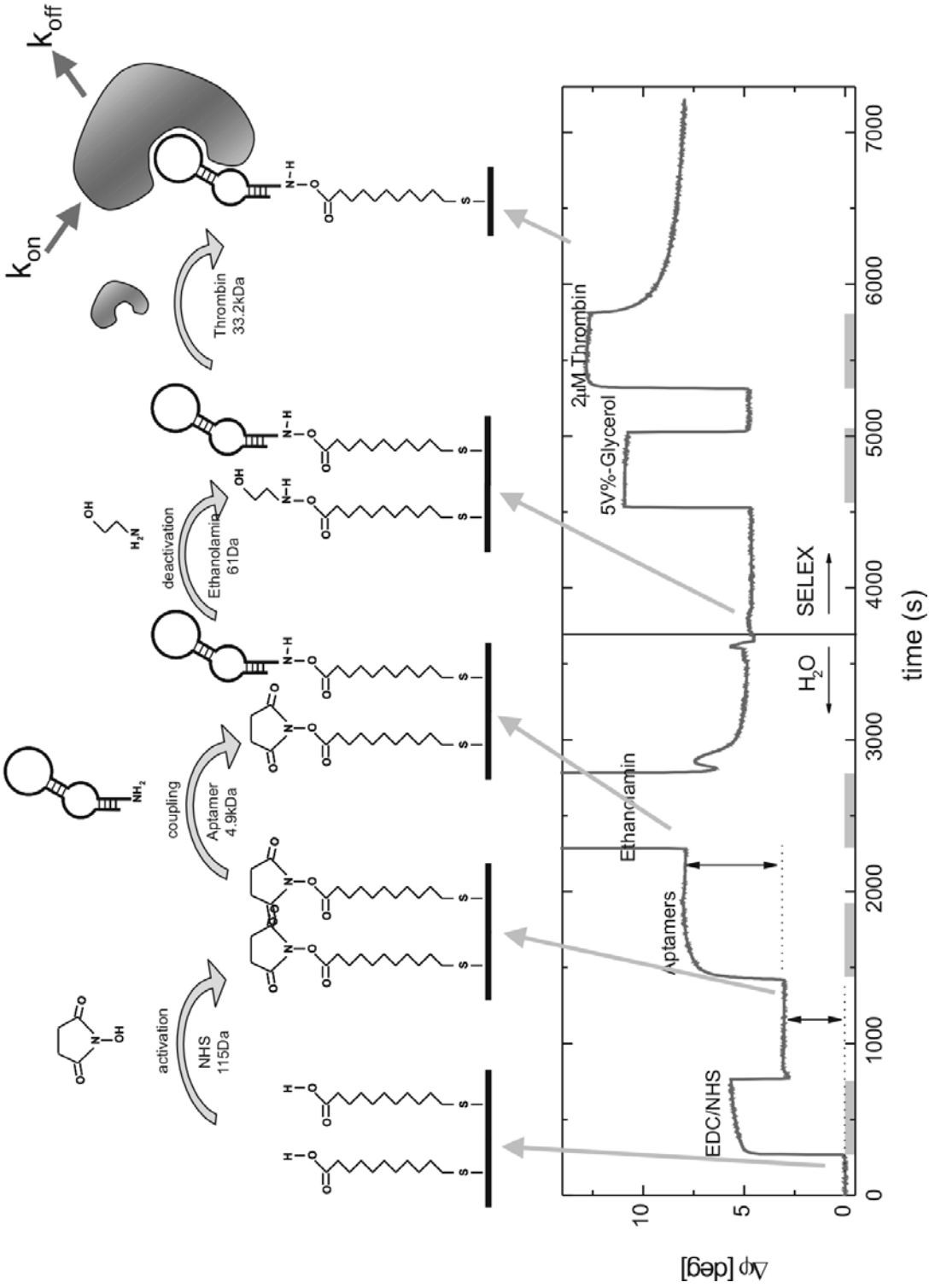

Fig. 6.6 Scheme of the chemical processes taking place on the sensor surface. This includes SAM activation, coupling of the receptor, deactivation and, after a buffer change, thrombin detection.

The interaction between thrombin and anti-thrombin is a typical antigen – antibody binding. The gold sensor chip surface had been externally alkanethiol covered with a self-assembled monolayer (SAM) of 11 mercapto-undecanoic acid (Aldrich). The alkanethiols possess terminal carboxyl groups (COOH) (Fig. 6.6). Then the sensor chip and the fluidic device were mounted onto the chip-carrier and placed into the "S-sens" system. The chip was exposed to a continuous flow of demineralized water until the phase signal stabilized. The fluidic valves were switched to a position that guides the flow only through chamber A. The carboxyl groups of the SAM on the sensors in chamber A were activated with 200 µM EDC (1-Ethyl-3-(3-dimethylaminopropyl)-carbodiimide) and 50 mM NHS (N-Hydroxysuccinimide). Fig. 6.6 presents a scheme of the chemical processes taking place on the sensor surface.

This activation process was followed by injection of anti-thrombin antibodies with a concentration of 0.25 µM. The anti-thrombin immobilization led to 9 ° phase shift on sensor A, while no signal change of the sensor B was observed (Fig. 6.7).

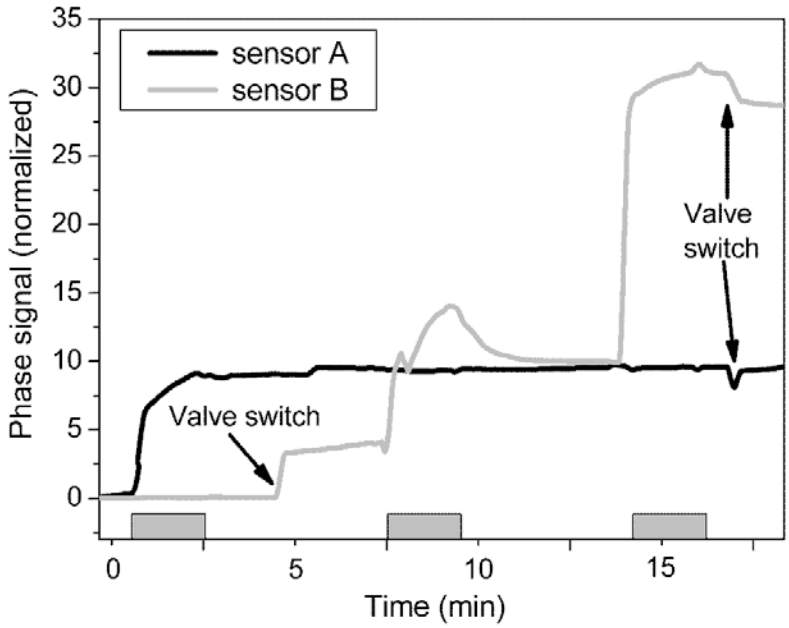

Fig. 6.7 Phase signal of sensors A and B for the immobilization process of anti-thrombin antibodies (chamber A) and BSA (chamber B). The gray boxes mark the injection cycles of thrombin antibody, EDC/NHS activation and BSA immobilization respectively. The arrows indicate the valve switches.

After 4 minutes, the fluidic valves were switched to a position to address only chamber B. The switching caused a slight signal change on sensor B, which was due to slight displacement of the seal on the sensor surface, as well as due to temperature drift. Before switching, the water buffer in chamber B did not flow. The flow of the entering water possibly changes the temperature on the sensor surface. The SAM on the sensors in chamber B was also activated with EDC/NHS mixture and

subsequently bovine serum albumin (BSA) with a concentration 10 µM was injected. The BSA protein was used to block the surface of sensor B to make use of this sensor as reference. On sensor B, a 5 ° phase change during the activation process and 22 ° phase shift during the BSA immobilization was observed. At the same time, no signal change on sensor A was detected.
After the anti-thrombin antibody and BSA immobilization, the terminated NHS-esters on the SAM have to be deactivated. Otherwise they react with the following samples causing unspecific binding events. In order to deactivate the NHS-esters, the fluidic valves were switched to guide the flow over both chambers (TTL position 001, Table 6.1) and 1 M ethanolamin (pH 8.5) was injected. This process was followed by a buffer change from H_2O to PBS buffer. Then, a sample of 500 nM thrombin was injected. Fig. 6.8 displays the phase change of sensors A and B for the thrombin injection.

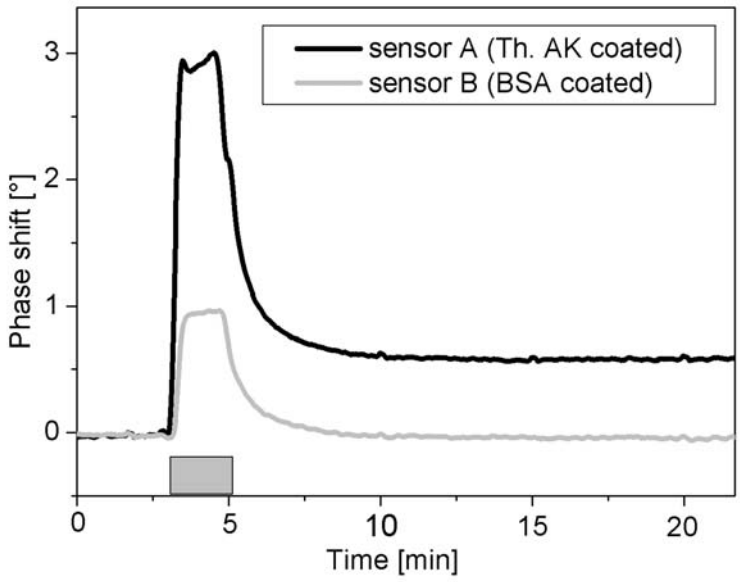

Fig. 6.8 Sensor response to thrombin injection of the thrombin antibody coated sensor A and the BSA coated sensor B. Only sensor A shows irreversible phase shift due to specific binding process. The gray box indicates the injection time.

Only sensor A with the immobilized anti-thrombin antibodies shows an irreversible phase change of 0.6 ° after the injection, as indicated in Fig. 6.8. This phase shift is attributed to specific binding of thrombin to its antibody. At the same time the BSA coated sensor B shows no irreversible phase change after the injection, which is due to a complete coverage of the sensor surface with BSA.

The experiments with thrombin demonstrated the proper functioning of the integrated active fluidic valves with pneumatic actuation for experiments detecting intermolecular binding events. The sensors in both chambers were covered with

different receptor molecules by switching of the fluidic valves, without any cross contamination. This proves the lack of any detectable leakage of the valves.

The integrated valves were further tested with other combinations of macromolecules such as DNA/RNA binding and thrombin binding on DNA/RNA.

6.1.3 DNA-DNA binding

The integrated fluidic valves were tested for detection of DNA-DNA binding events as well. First, the SAW chip was first covered with a SAM of 11 mercapto-undecanoic acid. The chip was placed into the S-sens system and water was flown over the sensor surface. All sensors were activated with EDC/NHS mixture in flow through. Then the fluidic valves were switched (1001) to address chamber A. 5 µM BRCA1-NH_2 DNA-linker (*BRCA1 – BReast CAncer susceptibility gene 1)* (5`-NH2-AGGACACTGT-3`) was injected. This resulted in a more then 3.5° phase shift of the signal on sensor A, while no change on sensor B was observed (Fig. 6.9).

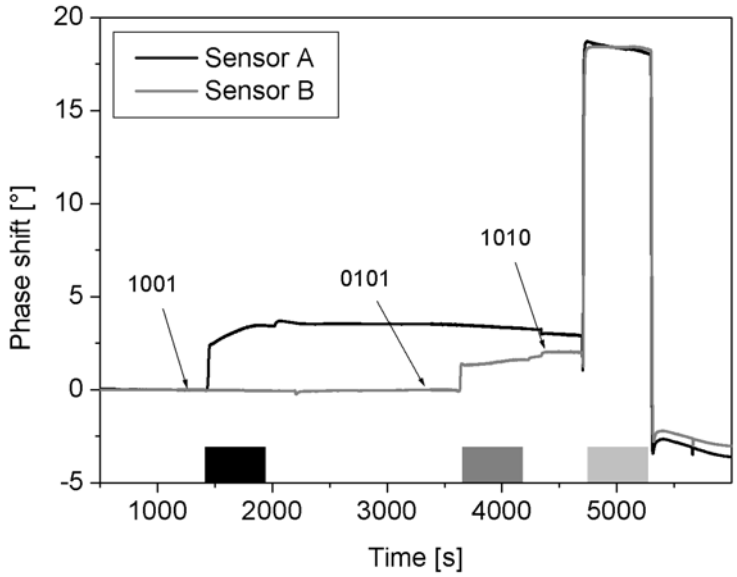

Fig. 6.9 Immobilization of BRCA1-NH_2 linking receptor on sensor A (black line) and PTCH-NH_2 linking receptor on sensor B (gray line), followed by deactivation with Ethanolamine / Ammonium acetate. The arrows show the valves switch.

The fluidic valves were switched in position 0101 to address chamber B and immobilize 5 µM PTCH – NH_2 linker (*PTCH – Homologous to PaTCHed segment polarity gene in Drosophilia melanogaster*) (5`-NH2-CTCCCCGGTC-3`). A 1.6° phase change on sensor B was detected. At the same time, the signal of sensor A showed a

slight drop. This drop can be explained with temperature fluctuations, because no water is flowing over the sensor A.
The fluidic valves were switched again to guide the flow through both chambers (position 1010) and the non-reacted NHS groups on the SAM were deactivated in 1 M Ethanolamine (pH 8.5). Sensor A showed 15.6°, sensor B 16.4° phase shift. After the deactivation process, the sensor signals of both sensors dropped under their levels before the deactivation step.
After the deactivation process, the running buffer (water) was changed to DNA binding buffer (10 mM Tris-HCl pH 8.3; 1.5 mM $MgCl_2$; 50 mM KCl). The samples were diluted in the DNA binding buffer as well. At first, 2 µM BRCA1-2G was injected (5`AAGGGCCTTCACAGGGTCCT-3`). It was expected not to bind to the immobilized receptors. In fact, the detected signals from sensors A and B showed no irreversible binding (Data not shown).
In the next step, 2 µM BRCA1-2T (5´-AAGGGCCTTCACAGTGTCCT-3) was injected in both chambers. The injection resulted in more then 0.31° phase shift on sensor A with immobilized BRCA1-NH_2 (see Fig. 6.10). At the same time, a phase change of more then 0.17° on sensor B was observed. The sensor shift on sensor B was due to unspecific binding of BRCA1-2T to the PTCH-NH_2.

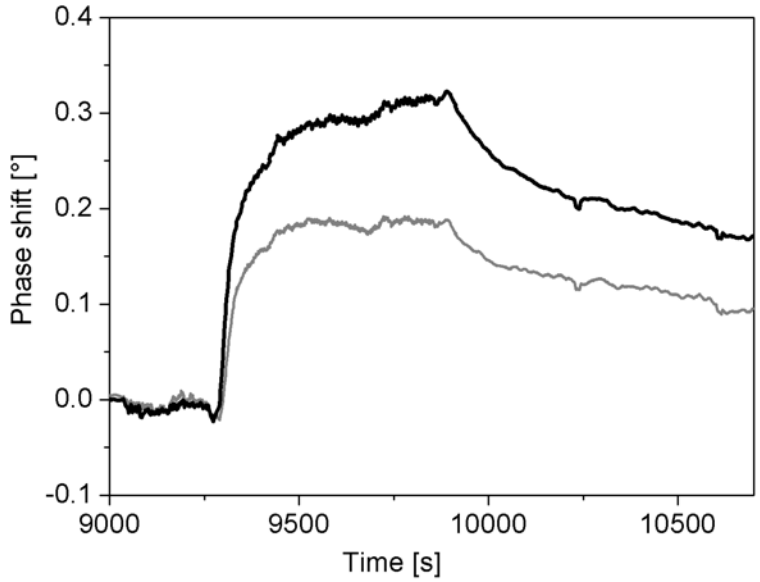

Fig. 6.10 Sensor signal from sensor A (black line) and B (gray line) during injection of BRCA-2T.

6.1.4 Binding of DNA and RNA to an anti-thrombin receptor

The above described microfluidic device with integrated valves with pneumatic actuation was also tested for binding of DNA and RNA molecules on sensors placed in different fluidic chambers. The experimental setup was the same as described for the three previous experiments.
The SAW biochip was covered with SAM of 11 mercapto-undecanoic acid and mounted on the chip holder of the S-sens system. The valves were switched into position to inject 100 % ethanol (C_2H_5OH) into both chambers to remove air bubbles out of the system. The chamber A was addressed by switching the valves (1001) and the SAM layer was activated with the EDC/NHS. The process was followed by injection of 2 µM RNA α-thrombin aptamer. The next valves switching addressed chamber B (0101). A SAM activation with EDC/NHS was accomplished, followed by injection of 5 µM DNA aptamer. The fluidic valves were switched again for both chambers (1010) and NHS-esters were deactivated by injection of 1M ethanolamine, pH 8.5.
The process of binding of DNA and RNA aptamers to the SAM should result in surface that enables specific binding of thrombin. However, defects on the sensor surface can result in an incomplete coverage of the gold surface with SAM.

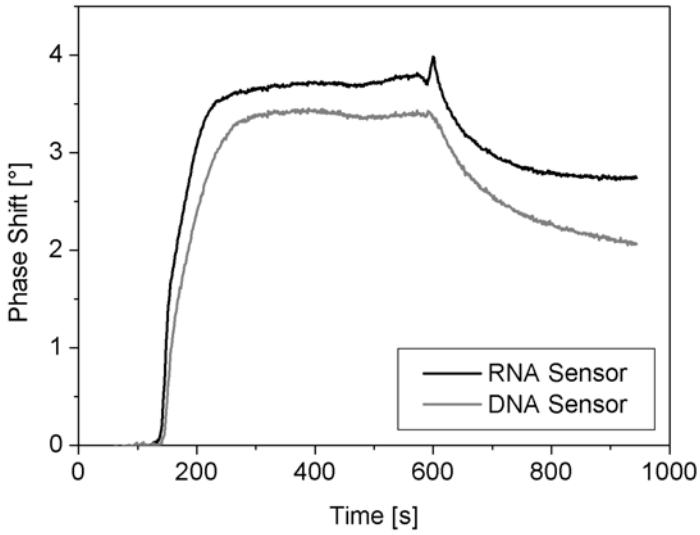

Fig. 6.11 Reaction of the RNA and DNA covered sensors to 100 nM Thrombin injection. The sensors were immobilized in flow through by using the integrated active pneumatic valves.

The defect areas can catch molecules from the sample and cause unspecific binding events. In order to neutralize these defects on the surface, 1000 nM elastase was injected. The elastase is used to eliminate non-specific binding [GRO04]. Elastase and thrombin belong to the same family of serine proteases and elastatse was used in this case to quantify the non-specific binding on the DNA and RNA covered surface.

Elastase covers most of the defect areas and the RNA/DNA aptamers remain free for specific binding events. The process was followed by a number of thrombin injections with concentrations 20 nM, 100 nM, 500 nM and 1000 nM. After every thrombin injection, the aptamer surface was regenerated with 0.1 N NaOH.
According to Galas et. al. [GAL05] the pneumatically controlled microfluidic valves with PDMS membranes show diffusion of air through the PDMS, that leads to air bubble formation into the liquid. We have not observed an additional formation of air bubbles into the fluidic system caused by the pneumatic system and penetration of air through the TPU membrane. In our approach, the PDMS structures act only as a body of the fluidic valve.
We have not observed any sticking effects between the valve seat and the valve body. The hydrophobic properties of silicone can be the reason for this effect. However, sticking problems could appear at higher working frequencies.

7 SUMMARY AND OUTLOOK

7.1 Summary

The aim of the work was to develop a fluidic handling system for the S-Sens bio-analytical system. The fluidic system has to have a high chemical resistance and to assure reliable flow of the sample and buffer solutions over the SAW sensor chip. The volume of the fluidic devices had to be small enough to assure real time bio-analytical measurements with fluidic exchange times less than 10 s. Active fluidic valves had to be integrated into the fluidic devices for control of the direction of the fluid flow. They had to give the possibility for immobilization of different receptor molecules on the same bio-chip.
The S-sens system is built in a modular approach. The bio-sensor chips can be recycled. For this reason, the microfluidic devices had to be easily separated from the chip. These devices have to be used as disposables. Thus, the material of the fluidic devices and the fabrication technology used had to allow an inexpensive batch production.

Two main approaches for the fabrication of the microfluidic devices have been tested.

The first one used the elastic properties of silicone elastomer (Sylgard 184) either to seal PMMA based mechanical milled devices or to fabricate silicone devices by stereo-lithography. The PMMA based devices did not show efficient sealing properties. Moreover, the PMMA material is not resistant against the chemical substances used in the system. The devices made of silicone had excellent sealing properties. However, they did not have sufficient mechanical stability and stereo-lithography is not suitable for batch fabrication.

For the second approach, alternative elastomeric materials have been utilized. They have good chemical resistance and thermoplastic properties, which allow fabrication processes by using injection-molding or hot embossing technology.
Commercially available thermoplastic polyurethane (TPU) elastomer foils proved to be a suitable material. The chemical resistance against a range of standard chemical substances used for bio-analytical analysis was tested. TPU foil Walopur 2201 showed excellent resistance against all the substances for more the 72 hours at 37°C. After 168 hours only the acetic buffer pH 4.5 caused slight changes in the transparency of the foil. Some of the substances were absorbed by the TPU material, which was determined by gravimetrical measurements.
The thermoplastic elastomer foils were used for fabrication of single- and double-side embossed devices. The embossing molds were fabricated by mechanical milling

process. The embossing parameters were optimised for achieving of structures with good conformation and openings in the foil for the fluidic connections.
The single-side embossed fluidic devices (cells) were used for real-time measurements with the S-Sens bio-analytical system. A number of cell designs were used for optimisation of the proper position of the seal to the IDTs of the SAW chip, the height and the shape of the fluidic cell. By using the single-side embossed cells, the temperature stability of the sensor signal was determined. The signal deviation for temperature changes proved to be dependant on the position of the sensor element on the chip, as well as on the flow rate. For the same temperature difference between the sensor surface and the liquid, the deviation increased with increase of the flow rate. The temperature deviation decreased in direction of the fluid flow, because of thermal equalization between the sensor and the liquid. The dependence of the sensor signal on the liquid parameters was investigated and discussed.
The double-side hot embossing process was employed for the production of closed microfluidic devices. The embossed fluidic channels were closed with an additional chemical bonding process. The experiments showed that the chemical bonding delivers stronger connection in comparison with the other bonding techniques, without damaging the existing structures on the foil and delivers no source of contamination of the fluidic channels.
The enclosure of the sample liquids within the TPU channels prevents their contact with other components of the chip reader unit. The design of the closed microfluidic devices allows the sample to flow about 5 cm over a thermally stabilized area, which improved the temperature stability of the sensors signal in comparison to the usage of single-side embossed cells. The improvement varied for the different flow rates and was up to 30% for flow rates of 200 µl/min. Both types of fluidic devices showed fluidic exchange times in the range of 7-8 s.
For reduction of the fluidic dead volumes and for a decrease of the fluidic exchange times, active fluidic valves have been integrated into the fluidic channels. The pneumatically driven valves were designed as round reservoirs (d = 500 µm and 1mm), which were filled with silicone and then sealed with a cover TPU foil. By switching the valves, the flow can be driven in a way that the sensor elements on the same biochip are immobilized with two different receptor molecules. The proper function of the integrated pneumatic valves was proven with a number of real-time macromolecular interaction measurements such as thrombin/anti-thrombin, thrombin/DNA etc.

7.2 Outlook

In the future, several different aspects of the fabrication of the micro-fluidic devices, which are in strong connection with the development of the other modules of the S-Sens bio-analytical system, will be addressed.
In the next generation of the S-Sens apparatus, the quartz-based SAW chips will be replaced with SAW sensors fabricated on $LiTaO_3$ substrate. The $LiTaO_3$ based SAW

sensors show higher coupling coefficients of the acoustic waves. This allows a reduction of the number of the IDT pairs and as a consequence - reduction of the chip dimensions.
The dimensions of the fluidic components should be also decreased. The resolution of the mechanical milling process used for the embossing molds is less then 100 µm and can be employed for the new fluidic design as well (Fig. 7.1).

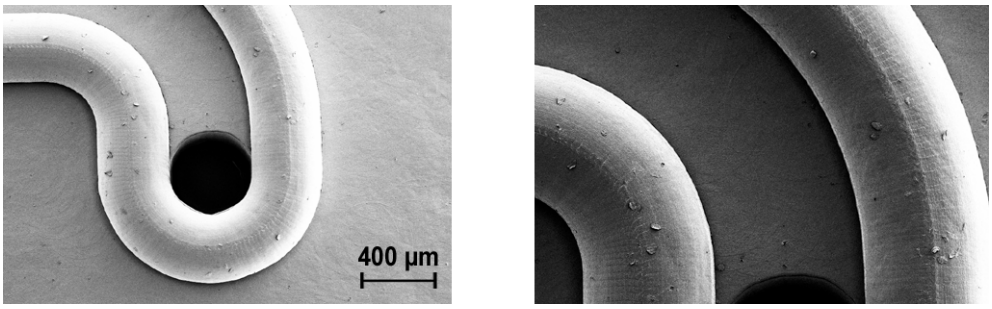

Fig. 7.1 SEM image of a test device for the $LiTaO_3$ based SAW sensors. The devices were embossed in Walopur foil and deposited with 100 nm gold for obtaining the SEM image. The diameter of the openings is 400 µm.

The hot embossing technology of thermoplastic elastomers proved to be very reliable method for fabrication of fluidic devices. If the microfluidic devices have to be used in water at higher temperatures (70-80°C) or in strong acid or alkali solutions, the TPUs are not suitable. If materials with higher chemical resistance are needed, thermoplastic elastomers on polyolefine basis (polyethylene, polypropylene) can be used.
The sealing of the fluidic channels with a cover foil by chemical bonding process was done manually. The bonding is accomplished over the whole surface of the foil and is prevented over the valve seat by the deposited silicone. However, the manual process is the reason for a low yield of the fabricated closed fluidic devices with integrated pneumatic valves. There are alternative methods for bonding of polymer materials, such as ultrasound welding or laser welding that have the potential to deliver automatized and high-quality welding.

In the case of ultrasound welding both foils are joined together by pressure and ultrasound waves cause internal friction and heating of the polymers e.g. [CHE05]. The areas that are to be welded have to be designed for the vibrating tool.

In the case of *laser welding*, the upper material is transparent for the laser beam. The bottom material absorbs the laser beam and is directly heated. The heat is transported to the upper layer and both layers heat up and melt. The laser welding process does not generate any particles.
In comparison to the chemical bonding process, the laser welding could achieve more homogeneous sealing, reduced damage of the channels profile, as well as the possibility to selectively weld areas of the polymer with resolution less then 100 µm.

The polymer welding is usually accomplished with either diode laser (wavelengths 808, 940, 980 nm) or with Nd:YAG laser (wavelength 1064 nm). The Nd:YAG laser is suitable for widths of the welding bonds less then 100 µm. The quality of the welding depends on the absorption coefficient of the welded material [VIT00].

Preliminary tests for laser welding of the thermoplastic polyurethanes have already been accomplished with a welding system "PolyScan" (Rofin – Baasel Lasertech, Germany) (Fig. 7.2). It includes a diodes pumped Nd:YAG laser SWD-Y75 with maximum average power output up to 75 W. The microfluidic structures had been embossed on black foils with a thickness of 600 µm. Best results were achieved with 300µm transparent PU as a cover. The processes were performed with a scan speed 20 mm/s and laser power of 1-2 W. The width of the weld bond was about 70 µm.

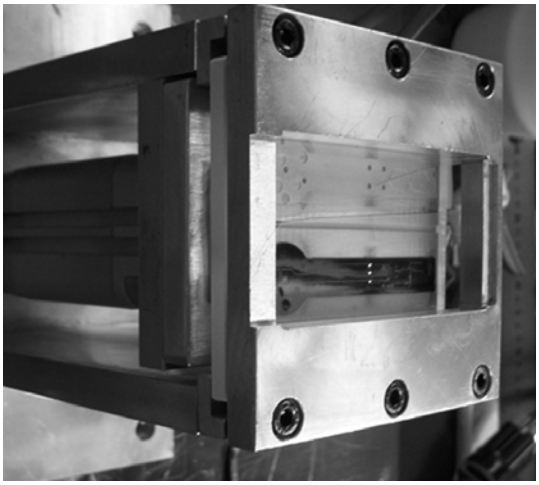

Fig. 7.2 Welding of TPU foils (600 µm black / 300 µm transparent) with Nd:YAG laser SWD-Y75, (Courtesy of Rofin – Baasel Lasertech, Germany).

A good mechanical contact between the foils is essential for the welding quality since air bubbles can prevent the contact and particles can lead to deflection of the laser beam. Additional work is needed to optimize the fixture assuring a reliable contact between the foils.

Polymer based sensors

Future work should be also focused on integration of the bio-analytical sensors and the microfluidic devices into one disposable unit. For this purpose, the bio-sensor should be fabricated on a plastic substrate.
The physical principle of the SAW sensors is based on a piezo-electrical substrate. For this reason, if the bio-sensors should be made on plastic, other sensor principles have to be employed.

One of the possibilities is to use impedance sensors [MAL05]. They are based on the change of the capacitance between two electrodes when deionized water is replaced by macromolecules with different dielectric constant ε. For achieving a high sensitivity, the gap between the electrodes should be in the range of 50-150 nm. Impedance sensors have been developed at Caesar by using a sacrificial layer technology with three lithographical processes.
Patterns with such dimensions could be also fabricated with one metalization process by usage of alternative writing methods.

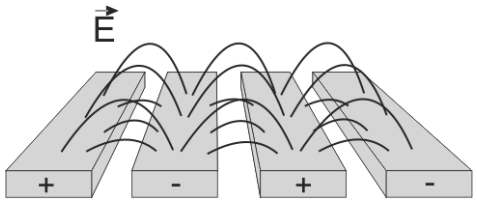

Fig. 7.3 Schematic drawing of the electrode structure showing the electric field lines above the electrodes.

One of these methods is the nanoimprinting lithography (NIL). Here, serial writing techniques (e-beam or focused-ion-beam (FIB) lithography) are used for production of a negative image of the desired pattern on a master stamp. This process is very slow and expensive. Next, the pattern is transferred into a functional layer by replication process. The replication takes usually several minutes. Thus, it can be easily scaled up to a batch production and the whole writing and replication technology becomes economically feasible.
A scheme of the nanoimprinting process is shown in Fig. 7.4.
The NIL is similar to the hot embossing process. However, with the decrease of the structure dimensions in the micrometer and nanometer range, especially with the reduction of the polymer thickness, additional technological problems have to be solved such as deviation of the residue layer thickness, mass transport etc.
Preliminary tests for the fabrication of the electrodes for the impedance sensor have been carried through. A stamp with the images of the impedance sensors with interdigitated electrodes was fabricated at X-Lith GmbH, Ulm, Germany. Electron-beam lithography and dry etching were used for production of the pattern with 320-340 nm deep structures on 4 -inch SOI wafer. The master stamp was designed for RIE structuring of the gold layer through a resist mask.

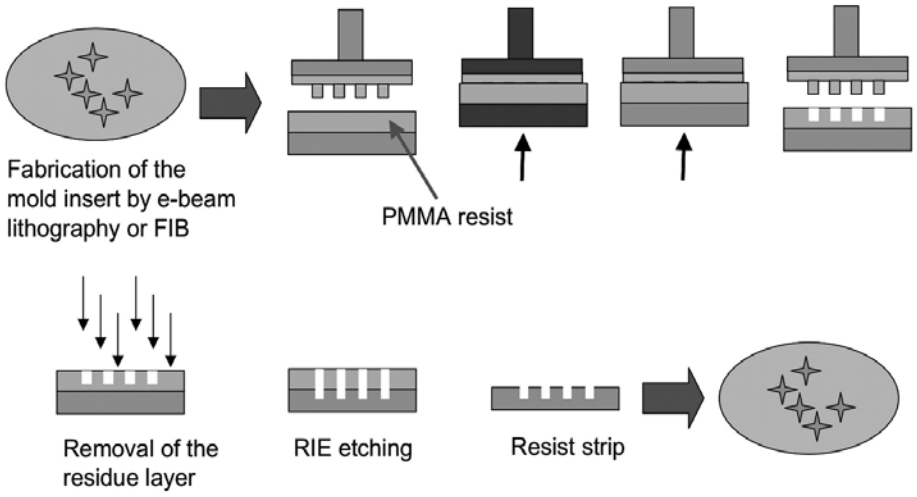

Fig. 7.4 Scheme of the nanoimprinting process technology.

The nanoimprinting processes were performed with two chips as master stamps, each ~1,5 x 2 cm. The first chip contained 4 reference electrodes (20 µm wide, 40 µm pitch) and 10 interdigitated electrodes (125 nm wide, 250 nm pitch). On the second one there were 4 reference electrodes (20µm wide, 40 µm pitch) and 10 interdigitated electrodes (250 nm wide, 500 nm pitch). Fig. 7.5 represents a SEM picture of the interdigitated electrodes (250 nm) and an optical micrograph of one of the master stamps.

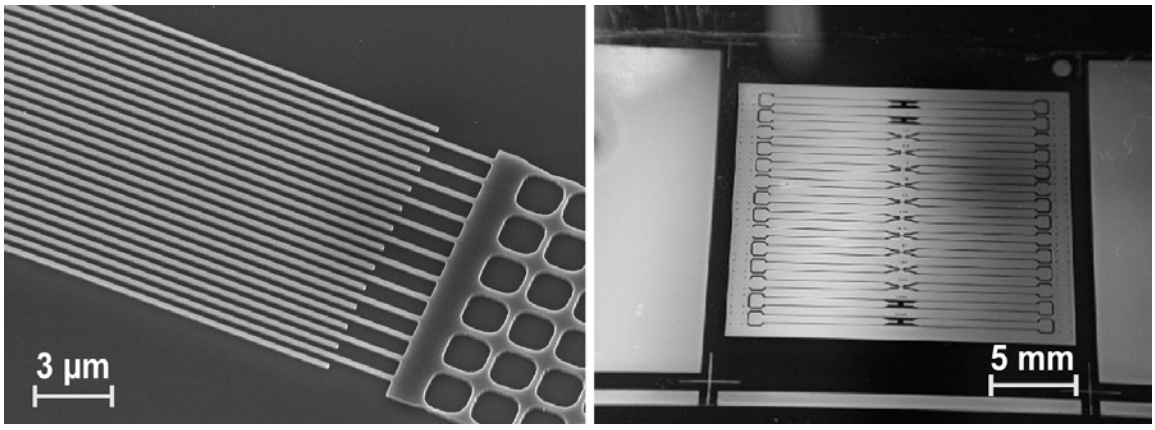

Fig. 7.5 SEM image (left) and optical micrograph (right) of a master stamp for nanoimprinting processes. The electrodes are 125 nm wide, pitch 250 nm. Courtesy of X-Lith (Ulm, Germany).

For the replication process, nanoimprinting resist mr-I 8030 (Micro resist technology GmbH, Berlin, Germany) was used. The resist is specially designed to better withstand plasma processes and allow proper etching of the residual layer (Fig. 7.6).

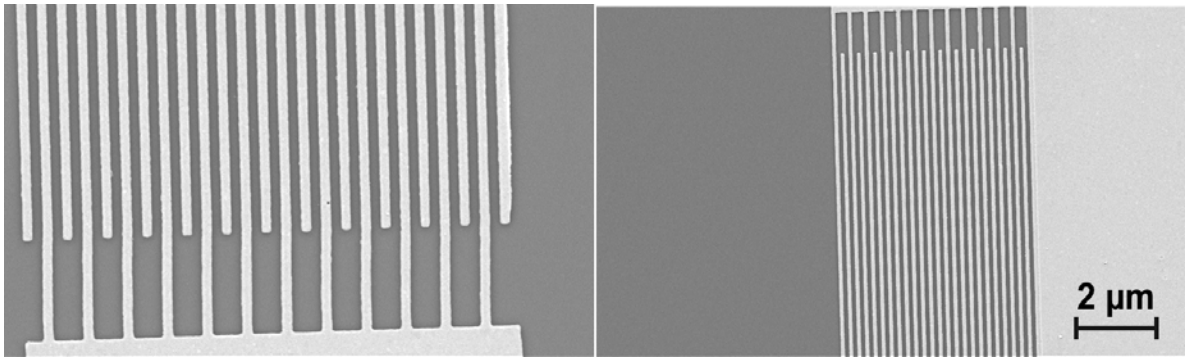

Fig. 7.6 SEM image of IDEs fabricated by NIL lithography and lift – off technique with resist mr-I 8030.

The results have shown a substantial quality difference between the micrometer and nanometer sized structures. Furthermore, differences of the filling factor on both sides of the interdigitated electrodes have been observed. The best NIL results have been achieved with mr-I 8030 spun in 350 nm thickness on glass substrates.

The quality and the feature size of the nanoimprinting process is mainly dependant on the master stamp fabrication technology. It has been proven to reliably replicate structures down to 20nm. The nanoimprinting technology requires homogeneous distribution of the pressure and temperature over the whole wafer. For that reason the parallelism between the stamp and the substrate is of essential importance. In order to overcome the parallelism problems and to partially compensate the wafer surface roughness, the use of an oil-balance system [HEI00] or pressurized air [Fa. Obducat, Sweden] have been reported.

Preliminary experiments for the integration of the microfluidic device into a plastic-based bio-chip have been accomplished. Fig. 7.7 (left) shows optical view of interdigitated electrodes of gold fabricated on PMMA wafer. A 20 µm deep fluidic channel was embossed then in the PMMA subtrate and sealed with a 500 µm thick PDMS membrane. The sealing was tested with a colored liquid (Fig. 7.7right).

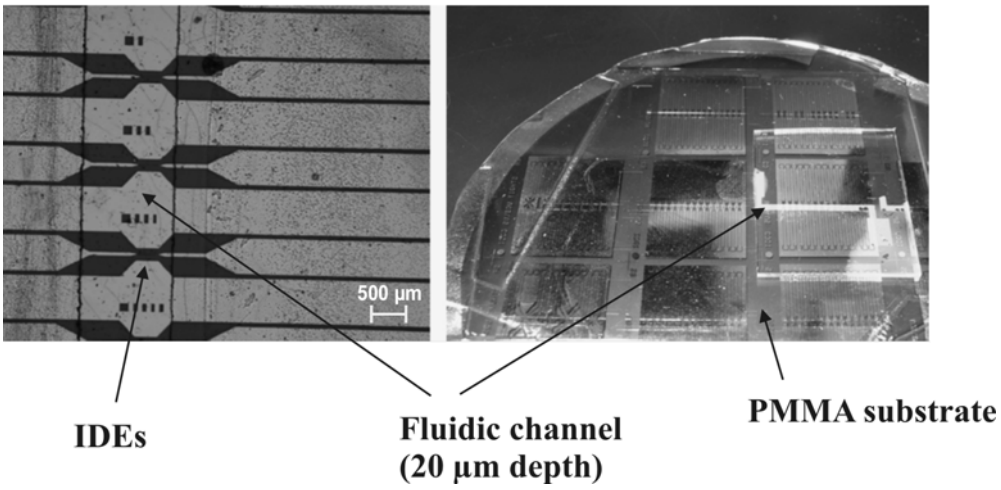

Fig. 7.7 Optical micrograph of interdigitated electrodes fabricated on PMMA substrate. 20 µm deep fluidic channel was subsequently embossed into the substrate. The whole chip was then covered with PDMS cover with thickness ~ 500µm. The so closed fluidic channel was tested with a color liquid (right).

The above experiments aimed to prove the possibility for the fabrication of all-on-plastic biochip. The future work will be focused on employment of the microfabrication technologies for production of the bio-sensor on a polymer substrate and their integration with plastic-based microfluidics. The aim is to develop a technology for the production of disposable all-on plastic chips for bio-analytical measurements.

8. LITERATURE

ABU94 Byfield R.A., Abuknesha M.P.: Biochemical Aspects of Biosensors, Biosens. Bioelectron., 9, 1994, 373-399

AND03 Andersson H., van den Berg A.: Microfluidic devices for cellomics: a review, Sens. Actuator B-Chem., 92, 2003, 315-325

ATE05 Atencia J., Beebe D.J.: Controlled microfluidic interfaces, Nature, V 437, 2005, 648-655

AUR02 Auroux P.-A., Iossifidis D., Reyes D.R., Manz A. : Micro Total Analysis Systems. 2. Analytical Standard Operations and Applications, Anal. Chem., 74, 2002, 2637-2652

BAL97 Ballantine D.S., White R.M., Martin S.J., Ricco A. J., Zellers E.T., Frye G.C., Wohltjen H.: Acoustic wave sensors: Theory, Design and Physico-Chemical Applications, Academic Press, San Diego, 1997

BAL00 Baller M.K. et al.: A cantilever-array based artificial nose, Ultramicroscopy 82, 2000, 1-9

BAR97 Bart J.C., Judd L.L., Kusterbeck A.W.: Environmental immunoassay for the explosive RDX using a fluorescent dye-labeled antigen and the continuous-flow immunosensor, Sens. Actuator. B-Chem., 38-39, 1997, 411-418

BAR01 Barie N. and Rapp M.: Covalent bound sensing layers on surface acoustic wave (SAW) biosensors, Biosens. Bioelectron. 16 (2001), 979-987

BAS98 Baselt D.R., Lee G.U., Natesan M., Metzger S.W., Sheenan P.E., Colton R.J.: A biosensor based on magnetoresistance technology, Biosens. Bioelectron. 13, 1998, 731-739

BAS04 Bashir R.: BioMEMS: state of the art in detection, opportunities and prospects, Adv. Drug Deliv. Rev., 56, 2004, 1565-1586

BEC82 Becker E.W., Ehrfeld W., Munchmeyer D., Betz H., Heuberger A., Pongratz S., Glashauser W., Michel H.J., Siemens V.R.: Production of separation Nozzle Systems for Uranium Enrichment by a combination of X-ray Lithography and Galvanoplastics, Naturwissenschaften, 69, 1982, 520-523

BEC99 Becker H., Gartner c.: Mikrosystemtechnik in den Life Sciences, Physikalische Blatter, 55, 1999, 51-53

BEC02 Becker H., Locascio L.E.: Polymer microfluidic devices, Talanta, 56, 2002, 267-287

BIA06 www.biacore.com

BOU96 Bousse L.: Whole cell biosensors, Sens. Actuator B-Chem., 34, 1996, 270-275

BOW02 Bower D.I.: An introduction to polymer physics, Cambridge University Press 2002

CAL05 Calleja M., Nordstrom M., Alvarez M., Tamayo J., Lechuga T.M., Boisen A.: Highly sensitive polymer based cantilever sensors for DNA detection, Ultramicroscopy, 105, 2005, 215-222

CHE05 Cheng Yue, Truckenmüller R., Ahrens R., Rogge T.: Entwicklung and Herstellung einer chemisch inerten Mikropumpe, scientific report, 2005, Forschungszentrum Karlsruhe

CHO02 Chovan T., Guttman A.: Microfabricated devices in biotechnology and biochemical processing, Trends Biotechnol., Vol.20, 3, 2002, 116-121

DOM98 Domininghaus H.: Die Kunststoffe und ihre Eigenschaften, 5th Edition, Springer Verlag, Berlin, 1998

DUJ96 Du J., Harding G.L., Ogilvy J.A., Dencher P.R., Lake M.: A study of Love-wave acoustic sensors, Sens. Actuator A-Phys., 56, 1996, 211-219

EPU04 Epurex Films GmbH, Walopur and Platilon Product sheet

FER03 Ferreira H.A., Graham D.L., Freitas P.P, Cabral J.M.S.: Biodetection using magnetically labeled biomolecules and arrays of spin valve sensors, J. Appl. Phys., V 93, 10, 2003, 7281-7286

FIA97 Fiaccabrino G., de Rooij N.F., Koudelka-Hep M.: On chip generation and detection of electroluminescence, Anal. Chim. Acta, 359, 1998, 263-267

FIS98 Fister J.C., Jacobson S.C., Davis L.M., Ramsey J.M: Counting single chromophore Molecules for Ultrasensitive Analysis and Separations on Microchip Devices, Anal. Chem., 70, 1998, 431-437

GAL05 Galas, J.-C., Studer V., Chen Y.: Characterization of pneumatically activated microvalves by measuring electrical conductance, Microelectron. Eng. 78-79, 2005, 112-117

GAU02 Gautschi, G.: Piezoelectric sensorics, Berlin, Springer Verlag, 2002

GBU05 Gbureck U., Grübel S., Thull R., Barralet J.E.: Modified PMMA cements for a hydrolysis resistant metal-polymer interface in orthopaedic applications, Acta Biomater., 1, 2005, 671-676

GEO02 George E.Y., Meixner L., Scheithauer W., Koppi A., Drost S., Wolf H., Danapel C., Feller K.A.: Chemiluminescence multichannel immunosensor for biodetection, Anal. Chim. Acta, 457, 2002, 3-12

GER60 Gerthsen C., Kneser H.O.: Physik – ein Lehrbuch zum Gebrauch neben Vorlesungen, 6th Edition, Springer Berlin-Göttingen-Heidelberg, 1960

GIL01 Gilchrist K.H., Barker V.N., Fletcher L.E., DeBusschere B.D., Ghanouni P., Giovangrandi L., Kovacs G.T.A.: General purpose, field-portable cell-based biosensor system, Biosens. Bioelectron., 16, 2001, 557-564

GIM94 Gimzewski J.K., Gerber C., Meyer E., Schlittler R.R.: Observation of a chemical reaction using a micromechanical sensor, Chem. Phys. Lett., 217, 1994, 589-594

GIZ96 Gizeli E., Lowe C.R., Liley M., Vogel H.: Detection of supported lipid layers with the acoustic waveguide device: application to biosensors, Sens. Actuator B-Chem., 34, 1996, 295-300

GIZ97 Gizeli E., Liley M., Lowe C.R., Vogel H.: Antibody binding to a Functionalized Supported Lipid Layer: A Direct Acoustic

Immunosensor, Anal. Chem., 69, 1997, 4808-4813

GIZ03 Gizeli E., Bender F., Rasmusson A., Saha K., Josse F., Cernosek R.: Sensitivity of the acoustic waveguide biosensor to protein binding as a function of the waveguide properties, Biosens. Bioelectron., 18, 2003, 1399-1406

GLA03 Glass S.: S-sens Data Analysis, Caesar Annual report 2003

GLA04 Glass S.: S-sens Data Analysis, Caesar Annual report 2004

GOM02 Gomez R., Bashir R., Bhunia A.K.: Microscale electronic detection of bacterial metabolism, Sens. Actuator. B-Chem., 86, 2002, 198-208

GRA93 Gravesen P., Branebjerg J., Jensen O.S.: Microfluidics – a review, J. Micromech. Microeng. 3, 1993,168-182

GRA01 Gray S:A:, Kusel J.K., Shaffer K.M., Shubin Y.S., Stenger D.A., Pancrazio J.J.: Design and demonstration of an automated cell-based biosensor, Biosens. Bioelectron., 16, 2001, 535-542

GUB04 Guber A.E., Heckele M., Herrmann D., Muslija A., Saile V., Eichhorn L., Gietzelt T., Hoffmann W., Hauser P.C., Tanyanyiwa J., Gerlach A., Gottschlich N., Knebel G.: Microfluidic lab-on-a-chip systems based on polymers – fabrication and application, Chem. Eng. J., 101, 2004, 447-453

HAN01 Hansen K.M., Ji H.F., Wu G., Datar R., Cote R., Majumdar A., Thundat T. : Cantilever-Based Optical Deflection Assay for Discrimination of DNA Single-Nucleotide Mismatches, Anal. Chem., 73, 2001, 1567-1571

HAN05 Hansen K.M., Thundat T.: Microcantilever Biosensors, Methods, 37, 2005, 57-64

HAR92 Harrison D.J., Manz A., Fan Z., Lüdi H., Widmer H.M.: Capillary Electrophoresis and Sample Injection Systems Integrated on a Planar Glass Chip, Anal. Chem., 64, 1992, 1926-1932

HEC04 Heckele M., Schomburg W.K.: Review on micro molding of thermoplastic polymers, J. Micromech. Microeng., 14, 2004, R1-R14

HEI00 Heidari B., Maximov I., Montelius L.: Nanoimprint lithography at the 6 in. wafer scale, J. Vac. Sci. Technol., B 18(6), 2000, 3557-3560

HIN91 Hintsche R., Moller B., Dransfeld I., Wollenbereger U., Scheller F., Hoffmann B.: Chip biosensors on thin-film metal electrodes, Sens. Actuator. B-Chem., B4, 1991, 287-291

HIN95 Hintsche R., Kruse C., Uhlig A., Paeschke M., Lisec T., Schnakenberg U., Wagner B.: Chemical microsensor systemsfor medical applications in catheters, Sens. Actuator. B-Chem., B27, 1995, 471-473

HOL96 Holden G., Legge N.R., Quirk R., Schroeder H.E: Thermoplastic elastomers, 2nd Edition, Carl Hanser Verlag, Munchen, 1996

HOL00 Holden G.: Understending of Thermoplastic elastomers, Carl Hanser Verlag, Munchen, 2000

HOS00 L`Hostis E., Michel Ph.E., Fiaccabrino G.C., Strike D.J., de Rooij N.F., Hep M.-K.: Microreactor and electrochemical detectors fabricated using Si and EPON SU-8, Sens. Actuator. B-Chem., 64, 2000, 156-162

ILI00 Ilic B., Czaplewski D., Craighead H.G.: Mechanical resonant

immunospecific biological sensor, Appl. Phys. Lett., 77, N3, 2000, 450-452

JAC01 Jackman R.J., Floyd T.M., Ghodssi R., Schnidt M.A., Jensen K.F.: Microfluidic systems with on-line UV detection fabricated in photodefinable epoxy, J. Micromech. Microeng., 11, 2001, 263-269

JAK98 Jakoby B., Vellekoop M.J.: Viscosity sensing using a Love-wave device, Sens. Actuat. A, 68, 1998, 275-281

JEN03 Hot embossing system HEX03, Operating manual, Jenoptik Mikrotechnik GmbH, 2003

JEN06 Jensen K.F.: Silicon-Based Microchemical Systems: Characteristics and Applications, MRS Bulletin, 31, 2006, 101-107

JIA04 Jianrong C., Yuquing M., Nongyue H., Xiaohua W., Sijiao L.: Nanotechnology and biosensors, Biotechnol. Adv., 22, 2004, 505-518

JOE93 Joensson U., Fagerstam L., Löfas S., Steinberg E., Karlsson R., Frostell A., Markey F., Schindler F.: Introducing a Biosensor Based Technology for Real-Time Biospecific Interaction Analysis, Ann. Biol. Clin. , 51, 1993, 19-26

JON05 De Jong L.A.A., Uges D.R.A., Franke J.P., Bischoff R.: Receptor-ligand binding assays: Technologies and Applications, J. Chromatogr. B, 829, 2005, 1-25

JOS01 Josse F., Bender F., Cernosek R.W.: Guided Shear Horizontal Surface Acoustic Wave Sensors for Chemical and Biochemical Detection in Liquids, Anal. Chem., 73, 2001, 5937-5944

KAN85 Kanzawa K.K, Gordon J.G.: Frequency of a quartz microbalance in contact with fluid, Anal. Chem., 57, 1985, 1770-1771

KEN06 Kenis P.J.A., Stroock D.: Materials for Micro- and Nanofluidics, MRS Bulletin, V.31, 2006, 87-94

KOC00 Koch M., Evans A., Brunnscheiler A.: Microfluidic Technology and Applications, Research Studies Press LTD, Baldock, Hertfordshire, UK 2000

KUL03 Kulmala S., Suomi J.: Current status of modern analytical luminescence methods, Anal. Chim. Acta, 500, 2003, 21-69

KUR01 Kurosaka D., Kato K.: Membranous proliferation of lens epithelial cells on acrylic, silicone and poly(methyl methacrylate) lenses, J. Cataract. Refract. Surg., V 27, Is. 10, 2001, 1591-1595

LAK95 Lake L.C.S., Golden J.P., Patonay G., Narayanan N., Ligler F.S.: Use of three longer-wavelength fluoropores with the fiber-optic biosensor, Sens. Actuator . B-Chem., 29, 1995, 25-30

LAN02 Lange D., Hagleitner C., Hierlemann A., Brand O., Baltes H.: Complementary Metal Oxyde Semiconductor Cantilever Arrays on a Single Chip: Mass-Sensitive Detection of Volatile Organic Compounds, Anal. Chem., 74, 2002, 3084-3095

LAN99 Landweber L.: Experimental RNA evolution, Trends Ecol. Evol., 14, 1999, 353-358

LEH01 Lehmann M., Baumann W., Brischwein M., Gahle H.J., Freund I., Ehret

I.R., Drechsler S., Palzer H., Kleintges M., Sieben U., Wolf B.: Simulteneous measurement of cellular respiration and acidification with a single CMOS ISFET, Biosens. Bioelectron., 16, 2001, 195-203

LÖH05 Löhndorf M., Schlecht U., Gronewold T.M.A., Malave A., Tewes M.: Microfabricated high-performance microwave impedance biosensors for detection of aptamer-protein interactions, Appl. Phys. Lett., 87, 243902, 2005

LUP01 Luppa P., Sokoll L.J., Chan D.W.: Immunosensors-principles and applications to clinical chemistry, Clin. Chim. Acta, 314, 2001, 1-26

MAD97 Madou M.J.: Fundamentals of Microfabrication, CRC Press LLC, Boca Raton, Florida, 1997

MAI73 Maines J.D., Paige E.G.S.: Surface-Acoustic-Wave components, Devices and Applications, Ultrasonics propagation, 120,10, 1973, 1078-1110

MAL05 Malave A., Tewes M., Gronewold T., Loehndorf M.: Development of impedance biosensors with nanometer gaps for marker-free analytical measurements, Microelectron. Eng., 78-79, 2005, 587-592

MAN90 Manz A., Graber N., Widmer H.M.: Miniaturized total chemical analysis systems : A novel concept for chemical sensing, Sens. Actuator B-Chem., 1, 1990, 244-248

MAN90A Manz A., Miyahara Y., Miura J., Watanabe Y., Miyagi H., Sato K.: Design of an open tubular column liquid chromatograph using silicon chip technology, Sens. Actuator B-Chem., 1, 1990, 249-255

MAR91 Martin S.J., Granstaff V.E., Frye G.C.: Characterization of a Quartz Crystal Microbalance with simultaneous Mass and Liquid loading, Anal. Chem., 63, 1991, 2272-2281

MAR93 Martin S.J., Frye G.C., Ricco A.J.: Effect of surface roughness on the Response of Thickness-Shear Mode Resonators in Liquids, Anal. Chem., 65, 1993, 2910-2922

MAR94 Martin S.J. Frye G.C., Senturia S.D.: Dynamics and Responce of Polymer-Coated Surface Acoustic Wave Devices: Effect of Viscoelestic properties and Film Resonance, Anal. Chem. 66, 1994, 2201-2219.

MAR94A Martin S.J., Frye G.C., Wessendorf K.O.: Sensing liquid properties with thickness-shear mode resonators, Sens. Actuator A-Phys., 44, 1994, 209-218

MCH00 McHale G., Lücklum R., Newton M.I., Cowen J.A.: Influence of viscoelesticity and interfacial slip on acoustic wave sensors, J. Appl. Phys., 88, 12, 2000, 7304-7312

MEN97 Menz W., Mohr J.: Mikrosystemtechnik für Ingenieure, Weinheim, VCH 1997

NGU02 Nguyen N.-T., Wereley S. : Fundamentals and Applications of Microfluidics, Artech House Inc., Norwood, MA, USA, 2002

NEW03 Newton M.I., McHale G., Martin F.: Experimental study of Love wave devices with thick guiding layers, Sens. Actuator A-Phys., 109, 2004, 180-185

PAN98 Pancrazio J.J., Bey Jr. P.P., Cuttino D.S., Kusel J.K., Borkholder D.A.,

Shaffer K.M., Kovacs G.T.A., Stenger D.A.: Portable cell-based biosensor system for toxin detection, Sens. Actuator B-Chem., 53, 1998, 179-185

PAT02 Patel P.D.: (Bio)sensors for measurement of analytes implicated in food safety: a review, Trends Anal. Chem., V 21, 2, 2002, 96-115

PIZ97 Pizziconi V.B., Page D.L.: A cell based immunobiosensor with engineered molecular recognition, part 1: design feasibility, Biosens. Bioelectron.,12, 1997, 287-299

RAI01 Raiteri R., Grattarola M., Butt H.-J., Skladal P.: Micromechanical cantilever based biosensors, Sens. Actuator B-Chem., 79, 2001, 115-126

REY02 Reyes D.R., Iossifidis D., Auroux P.-A., Manz A. : Micro Total Analysis Systems. 1. Introduction, Theory and Technology, Anal. Chem., 74, 2002, 2623-2636

RIF03 Rife J.C., Miller M.M., Sheehan P.E., Tamanaha C.R., Tondra M., Whitman L.J.: Design and performance of GMR sensors for the detection of magnetic microbeads in biosensors, Sens. Actuators A-Phys., 107, 2003, 209-218

ROD96 Rodahl M., Kasemo B.: Frequency and dissipation-factor responses to localized liquid deposits on a QCM electrode, Sens. Actuator B-Chem., 37, 1996, 111-116

ROY00 Royer D., Dieulesaint E.: Elastic waves in solids II, Berlin Springer, 2000

SAH03 Saha K., Bender F., Rasmusson A., Gizeli E.: Probing the Viscoelasticity and Mass of a surface bound Protein Layer with an Acoustic Waveguide Device, Langmuir, 19, 2003, 1304-1311

SAN00 Sanders G. H. W., Manz A.: Chip-based Microsystems for genomic and proteomic analysis, Trends Anal. Chem., Vol. 19, N6, 2000, 364-378

SAU59 Sauerbrey G.: Verwendung von Schwingquarzen zur Wägung dünner Schichten und zur Mikrowägung, Zetschrift für Physik 155, 1959, 206-222.

SCH93 Schomburg W.K., Fahrenberg J., Maas D., Rapp R.: Active valves and pumps for microfluidics, J. Micromech. Microeng., 3, 1993, 216-218

SCH94 Schomburg W.K., Vollmer J., Büstgens B., Fahrenberg J., Hein H., Menz W.: Microfluidic components in LIGA technique, J. Micromech. Microeng. 4 (1994), 186-191

SCH95 Schomburg W.K., Maas D., Bacher W., Büstgens B., Fahrenberg J., Menz W., Seidel D.: Assembly for micromechanics and LIGA, J. Micromech. Microeng. 5, 1995, 57-63

SCH99 Schomburg W.K., Ahrens R., Bacher W., Martin J., Saile V.: AMANDA – surface micromachining, molding, and diaphragm transfer, Sens. Actuator A-Phys., 76, 1999, 343-348

SCH03 Schlensog, M.D.: Entwicklung und charakterisierung eines Love-Wellen Biosensors, GCA-Verlag, Herdecke 2003

SCH04 Schlensog M.D., Gronewold T.M.A., Tewes M., Famulok M., Quandt E.: A Love-wave biosensor using nucleic acids as ligands, Sens. Actuator B-Chem., 101, 2004, 308-315

SCO95 Scouten W.H., Luong J.H.T., Brown R.S: Enzyme or protein immobilization techniques for applications in biosensor design, Trends Biotechnol., 13, 1995, 178-185

SEI93 Seiler K., Harrison D.J., Manz A.: Planar Glass Chips for Capillary Electrophoresis: Repetitive Sample Injection, Quantitation and Separation Efficiency, Anal. Chem., 65, 1993, 1481-1488

SEY05 Seydack M.: Nanoparticle labels in immunosensing using optical detection methods, Biosens. Bioelectron. 20, 2005, 2454-2469

STE97 Steinschaden A., Adamovic D., Jobst G., Glatz R., Urban G.: Miniaturized thin film conductometric biosensors with high dynamic range and high sensitivity, Sens. Actuator B-Chem., B44, 1997, 365-369

TES97 Tessier L., Schmitt N., Watier H., Brumas V., Patat F.: Potential of the thickness shear mode acoustic immunosensors for biological analysis, Anal. Chim. Acta, 347, 1997, 207-217

TILLW Antispread F 2/200 FK 60, Application report, Dr. Tillwich GmbH, Horb (Ahldorf), Germany

VIT00 Vitez I. Z-.: Laser processing for microelectronics packaging applications, Microelectron. Reliab., 41, 2001, 563-570

VOD01 Vo-Dinn T., Cullum B.M., Stokes D.L.: Nanosensors and biochips: frontiers in bio-molecular diagnostics, Sens. Actuator B-Chem., 74, 2001, 2-11

WEB01 http://www.silicones-science.com/chemistry.html

WEI98 Weiss M., Welsch W., v. Schickfus M., Hunklinger S.: Viscoelastic Behavior of Antibody Films on a Shear Horizontal Acoustic Surface Wave Sensor, Anal. Chem., 70, 1998, 2881-2887

WEI03 Weigl B. H., Bardell, R.L., Cabrera C.R.: Lab-on-a-chip for drug development, Adv. Drug Deliv. Rev., 55 (2003), 349-377

WHI74 White F.M.: Viscous Fluid flow, McGraw-Hill, New York, 1974

WIL00 Willemsen O.H., Snel M.M.E., Cambi A., Greve J., De Grooth B.G., Figdor C.G.: Biomolecular interactions measured by atomic force microscopy, Biophys. J., 79, 2000, 3267-3281

WOO99 Woodbury C.P. Jr., Venton D.: Methods for screenining combinatorial libraries using immobilized or restrained receptors, J. Chromatogr. B, 725, 1999, 113-137

ZHA06 Zhang X., Haswell S.J.: Materials Matter in Microfluidic devices, MRS Bulletin, V.31, 2006, 95-99

Personal publications:

STO05 Stoyanov I., Tewes M., Glass S., Koch M., Löhndorf M.: Low-cost and chenical resistant microfluidic devices based on thermoplastic elastomers for a novel bio-sensor system, MRS Symp. Proc., Vol 872, J11, 2005, 4.1-4.6

STO05_A Stoyanov I., Tewes M., Glass S., Gronewold T., Koch M., Löhndorf M.:

Development of micro-fluidic interfaces for a surface acoustic wave (SAW) biosensor system, Proc. Micro Total Analysis Systems 2005, Vol. 2, 2005, 1152-1154

STO06 Stoyanov I., Tewes M., Koch M., Löhndorf M.: Microfluidic devices with integrated active valves based on thermoplastic elastomers, Microelecrtron. Eng. 83, 2006, 1681-1683

APPENDIX

Chemical resistance of the TPUs (Epurex GmbH, Walsrode, Germany)

Medium	**Temp.** °C		**Walopur 2102** Polyester TPU Shore A 93	**Platilon U04** Polyester TPU Shore A 86	**VPT 7107** Polyester TPU Shore A 85	**Walopur 2201 / 4201 / Platilon U073** Polyether TPU Shore A 85 / 87
Aceton	RT	Q	0	0	0	0
Ammoniak 10-prozentig	RT		+	+	+	+
Anilin	RT	Q	-	-	-	-
ASTM - Öl 1	80		+	+	+	+
ASTM - Öl 2	80		+	+	+	+
ASTM - Öl 3	80		0/+	0/+	0/+	+
Benzin, "normal"	RT	Q	+	+	+	+
Benzin, "super"	RT	Q	0/+	0/+	0/+	0/+
Benzol	RT	Q	0	0	0	0
Butylacetat	RT	Q	0	-	-	0
Cyclohexanol	RT	Q	0	0	0	0
Dieselöl	RT	Q	+	+	+	+
Dimethylformamid	RT	Q	-	-	-	-
Ethylacetat	RT	Q	-	-	-	-
Ethylalkohol	RT	Q	0	0	0	0
Ethylether	RT	Q	+	+	+	+
Essigsäure, 20-prozentig	RT		0	0	0	0
Fluorkohlenwasserstoff	RT	Q	+	+	+	+
Isopropanol	RT	Q	0/+	0/-	0	0/+
Kerosin	RT	Q	+	+	+	+
Kalilauge, 10-prozentig	RT		+/0	+/0	+/0	+/0
Kochsalzlösung, konz.	RT		+	+	+	+
Methanol	RT	Q	0/+	0/+	0	0/+
Methanol/Benzin, 15/85	RT	Q	+/0	+/0	+/0	+/0
Methylenchlorid	RT	Q	-	-	0/-	-
Mineralöl	80		+	+	+	+
Natronlauge, 10-prozentig	RT		+/0	+/0	+/0	+/0
N-Methylpyrrolidon	RT	Q	-	-	-	-
Perchlorethylen	RT	Q	+/0	-	+/0	+/0
Phenol	RT	Q	0	0	0	0
Salpetersäure, 20-prozentig	RT		-	-	-	-
Salzsäure, 20-prozentig	RT		0/-	0/-	0/-	0/-
Schwefelsäure, 20-prozentig	RT		0/-	0/-	0/-	0/-
Seewasser	RT		+	+	+	+
Tetrachlorkohlenstoff	RT	Q	0	0/-	0/-	0
Trichlorethylen	RT	Q	0/-	-	0/-	0/-
Tetrahydrofuran	RT	Q	-	-	-	-
Toluol	RT	Q	0/-	-	-	0/-
Wasser	RT 80 100		+ 0 0/-	+ 0 0/-	+ 0 0/-	+ +/0 0/+

\+ = über längere Zeit beständig

0 = kurzzeitiger Kontakt unter bestimmten Voraussetzungen möglich

\- = unbeständig, starker Angriff oder löslich

Q = Quellung / reversibel; die mechanischen Eigenschaften werden im gequollenen Zustand vermindert. (gilt für alle Typen)

Die angegebenen chemischen Beständigkeiten beziehen sich auf naturfarbene Folien. Die aus den Lagerungsversuchen ermittelten Ergebnisse können nur als unverbindlicher Hinweis gelten. Unsere anwendungstechnische Beratung in Wort, Schrift und durch Versuche erfolgt nach bestem Wissen, gilt jedoch nur als unverbindlicher Hinweis, auch in bezug auf etwaige Schutzrechte Dritter und befreit Sie nicht von der eigenen Prüfung der von uns gelieferten Produkte auf ihre Eignung für die beabsichtigten Verfahren und Zwecke. Anwendung, Verwendung und Verarbeitung der Produkte erfolgen außerhalb unserer Kontrollmöglichkeiten und liegen daher ausschließlich in Ihrem Verantwortungsbereich.

07/02

Schnitt A-A

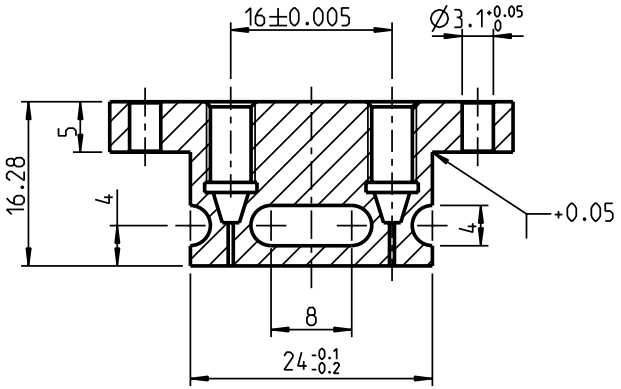

Schnitt B-B

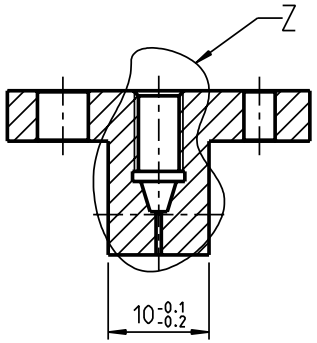

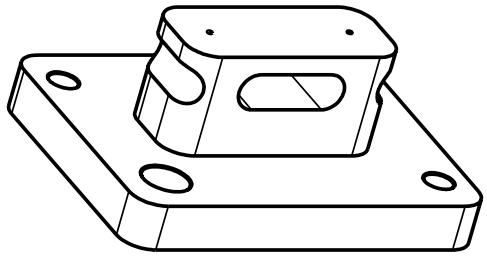

Z
4:1

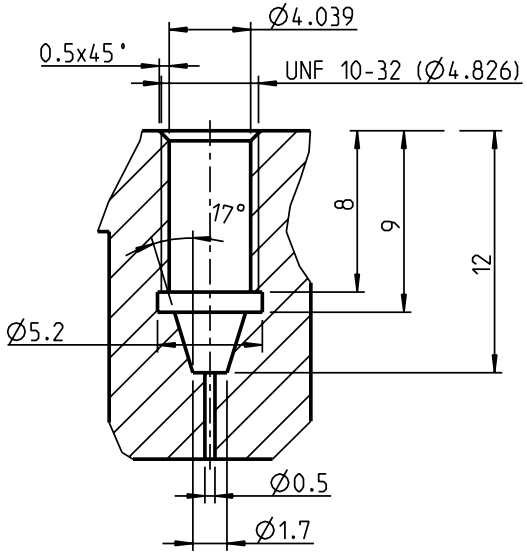

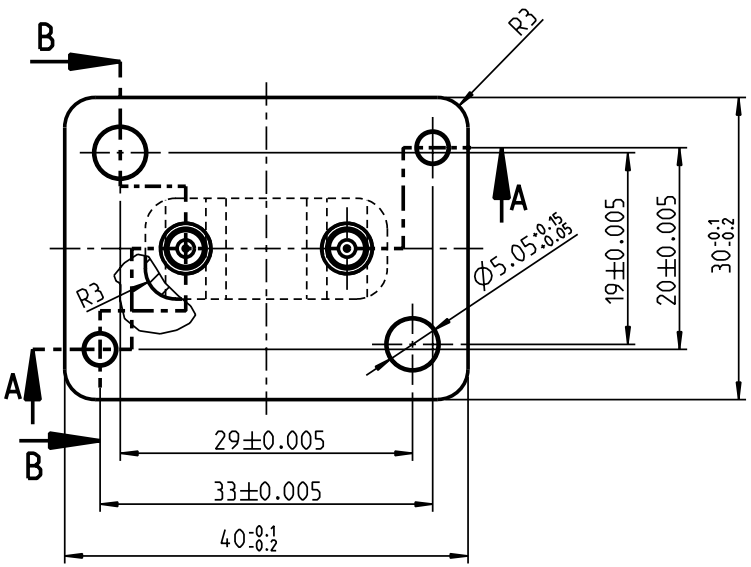

+0.05 -0.1

Rz 6.3

Dateiname des Zeichnungsobjektes: FLUIDIK		Dateityp: PART	Dateiname der Zeichnung: Z_FLUIDIK
	Allgemeintol. DIN ISO 2768-m-H	Werkstück -kanten DIN 6784	Maßstab 2:1 / Gew.: kg
			Werkstoff: PMMA
			Halbzeug:
	Datum	Name	Benennung: Fluidik(thermisch) (Chipreader)
	Bear. 05.08.2004	Lampert	
	Gepr.		
	Norm		
			Zeichnungsnummer: 3-50084-2.1.4.3 / Blatt 5 / Bl.8
Zust. Änderung Datum Nam	(Urspr.)		(Ers.f.:) (Ers.d.:)

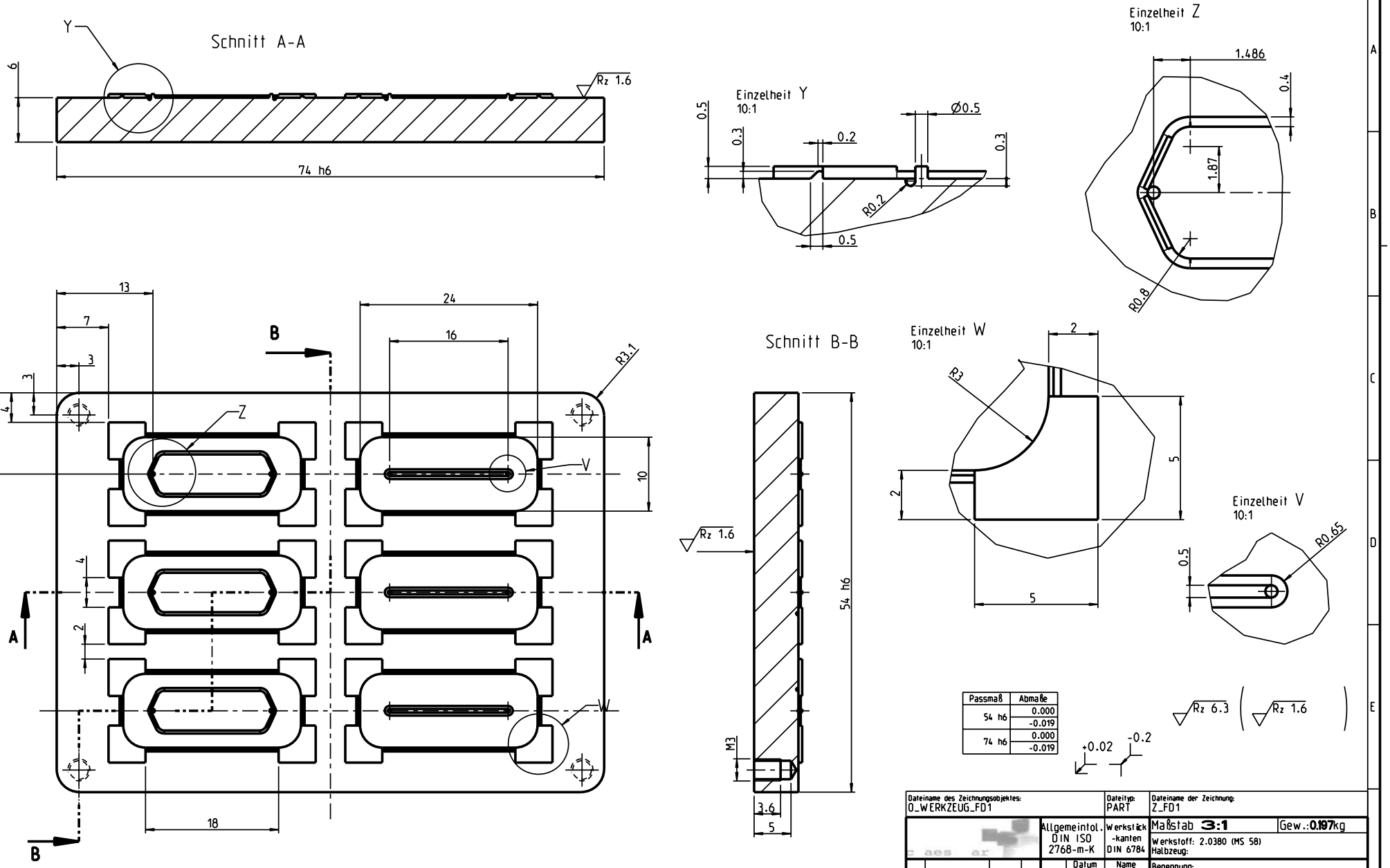

Passmaß	Abmaße
54 h6	0.000
	-0.019
74 h6	0.000
	-0.019

Dateiname des Zeichnungsobjektes: O_WERKZEUG_FD1		Dateityp: PART	Dateiname der Zeichnung: Z_FD1
	Allgemeintol. DIN ISO 2768-m-K	Werkstück -kanten DIN 6784	Maßstab 3:1 / Gew.: 0.197kg
			Werkstoff: 2.0380 (MS 58) Halbzeug:
	Datum / Name		Benennung: oberes Werkzeug (Einseitig) (für 2 Sensortypen)
	Bear. 14.01.2004 Lampert		
	Gepr. - -		
	Norm		
			Zeichnungsnummer: 2-50082-3.14.2 / Blatt 1 / 1 Bl.
Zust. Änderung Datum Nam	(Ursp.)		(Ers.f.:) (Ers.d.:)

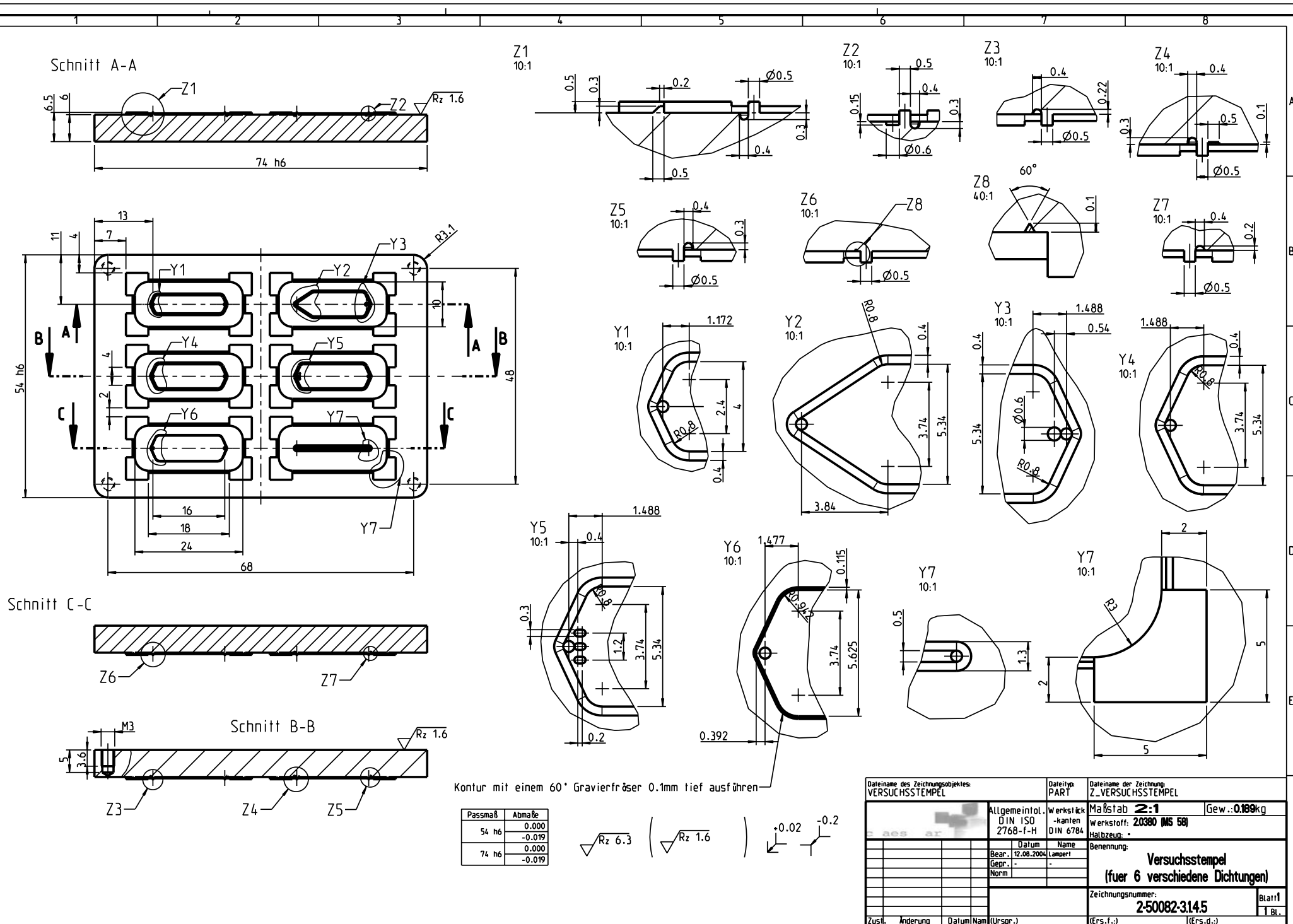

Passmaß	Abmaße
54 h6	0.000
	-0.019
74 h6	0.000
	-0.019

Dateiname des Zeichnungsobjektes: VERSUCHSSTEMPEL		Dateityp: PART	Dateiname der Zeichnung: Z_VERSUCHSSTEMPEL
	Allgemeintol. DIN ISO 2768-f-H	Werkstück -kanten DIN 6784	Maßstab 2:1 / Gew.: 0.189kg
			Werkstoff: 2.0380 (MS 58)
			Halbzeug: -
	Datum / Name		Benennung: Versuchsstempel (fuer 6 verschiedene Dichtungen)
	Bear. 12.08.2004 Lampert		
	Gepr. - -		
	Norm		
Zust. Änderung Datum Nam	(Ursp.)		Zeichnungsnummer: 2-50082-3.14.5 / Blatt 1 / 1 Bl.
			(Ers.f.:) (Ers.d.:)

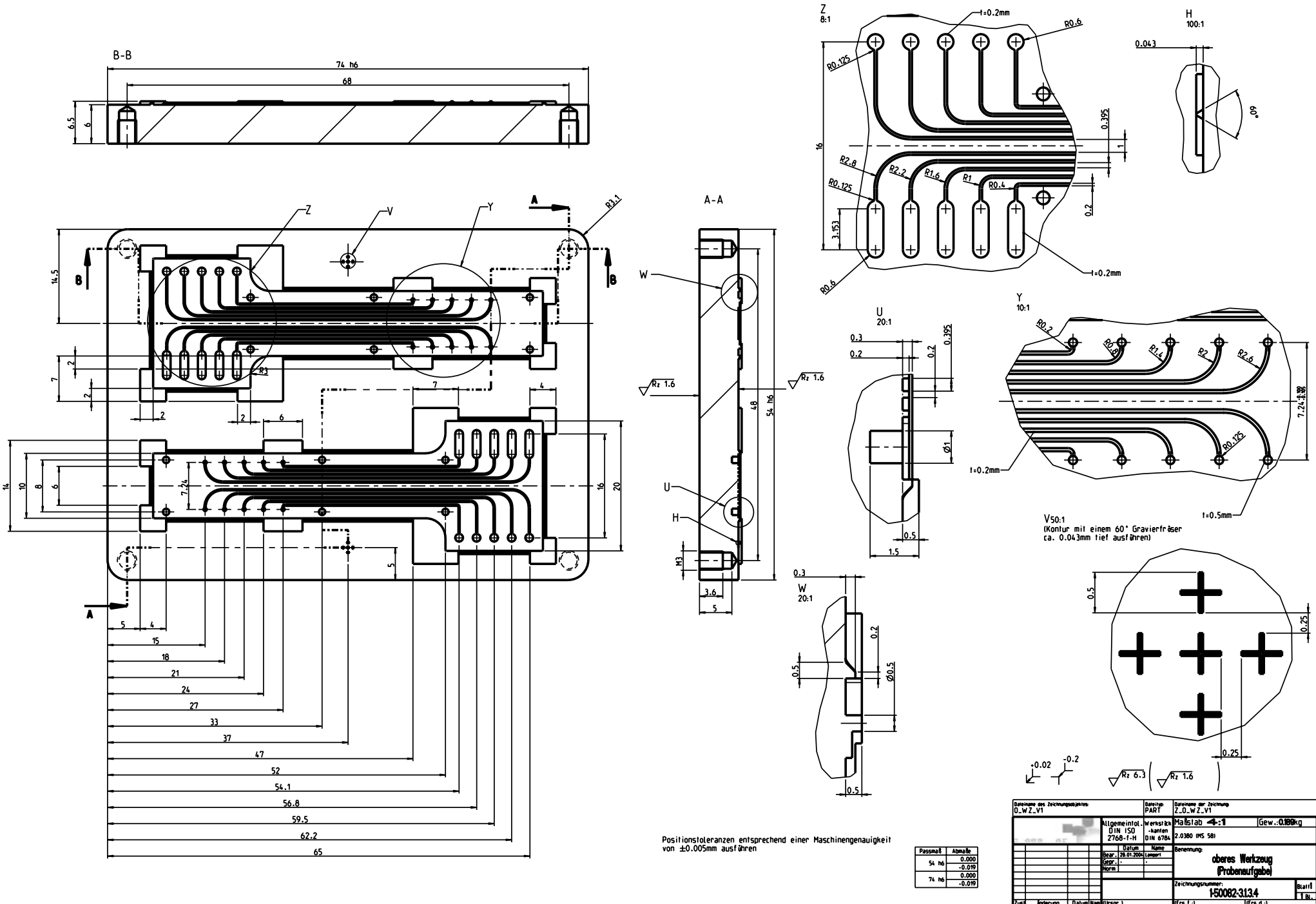
B-B
74 h6
68
6.5
6
A-A
Z
8:1
H
100:1
0.043
60°
R0.6
t=0.2mm
R0.125
0.395
16
1
R2.8
R2.2
R1.6
R1
R0.4
0.2
3.153
U
20:1
0.3
0.2
Ø1
0.5
1.5
Y
10:1
R0.2
R0.8
R1.4
R2
R2.6
7.24
t=0.5mm
V50:1
(Kontur mit einem 60° Gravierfräser
ca. 0.043mm tief ausführen)
W
20:1
Ø0.5
3.6
M3
48
54 h6
Rz 1.6
Rz 6.3
14.5
7
4
6
10
8
14
20
5
15
18
21
24
27
33
37
47
52
54.1
56.8
59.5
62.2
65
Positionstoleranzen entsprechend einer Maschinengenauigkeit
von ±0.005mm ausführen
Passmaß
Abmaße
54 h6
0.000
-0.019
74 h6
0.000
-0.019
Allgemeintol.
DIN ISO
2768-f-H
Werkstück
-kanten
DIN 6784
Maßstab 4:1
Gew.:0.188kg
2.0380 (MS 58)
Bear. 28.01.2004 Lenzert
Gepr. -
Norm
Benennung:
oberes Werkzeug
(Probenaufgabe)
Zeichnungsnummer:
I50082-3.1.3.4
Blatt 1
1 Bl.

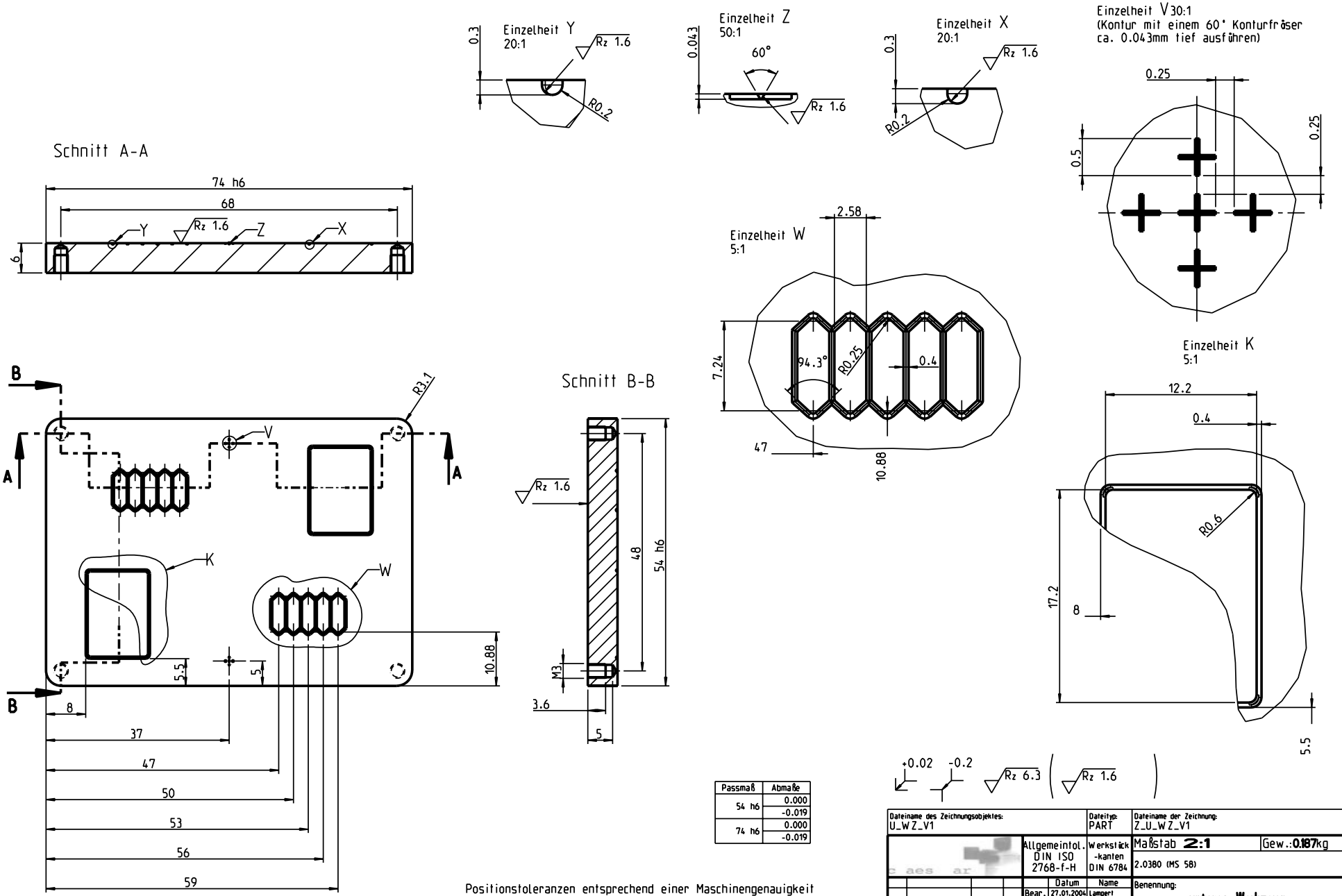
Einzelheit Y
20:1
Rz 1.6
R0.2
0.3
Einzelheit Z
50:1
60°
Rz 1.6
0.043
Einzelheit X
20:1
Rz 1.6
R0.2
0.3
Einzelheit V 30:1
(Kontur mit einem 60° Konturfräser
ca. 0.043mm tief ausführen)
0.25
0.25
0.5
Schnitt A-A
74 h6
68
Rz 1.6
Y
Z
X
6
Einzelheit W
5:1
2.58
94.3°
R0.25
0.4
7.24
47
10.88
Einzelheit K
5:1
12.2
0.4
R0.6
17.2
8
5.5
B
A
R3.1
V
K
W
5.5
5
10.88
8
37
47
50
53
56
59
Schnitt B-B
Rz 1.6
48
54 h6
M3
3.6
5
+0.02
-0.2
Rz 6.3
Rz 1.6
Passmaß
Abmaße
54 h6
0.000
-0.019
74 h6
0.000
-0.019
Positionstoleranzen entsprechend einer Maschinengenauigkeit
von ±0.005 mm ausführen.
Dateiname des Zeichnungsobjektes:
U_WZ_V1
Dateityp:
PART
Dateiname der Zeichnung:
Z_U_WZ_V1
Allgemeintol.
DIN ISO
2768-f-H
Werkstück
-kanten
DIN 6784
Maßstab 2:1
Gew.: 0.187kg
2.0380 (MS 58)
Datum
Name
Bear. 27.01.2004 Lampert
Gepr. -
Norm
Benennung:
unteres Werkzeug
(Probenaufgabe)
Zeichnungsnummer:
2-50082-3.14.3
Blatt 1
1 Bl.
Zust. Änderung Datum Nam
(Ursor.)
(Ers.f.:)
(Ers.d.:)

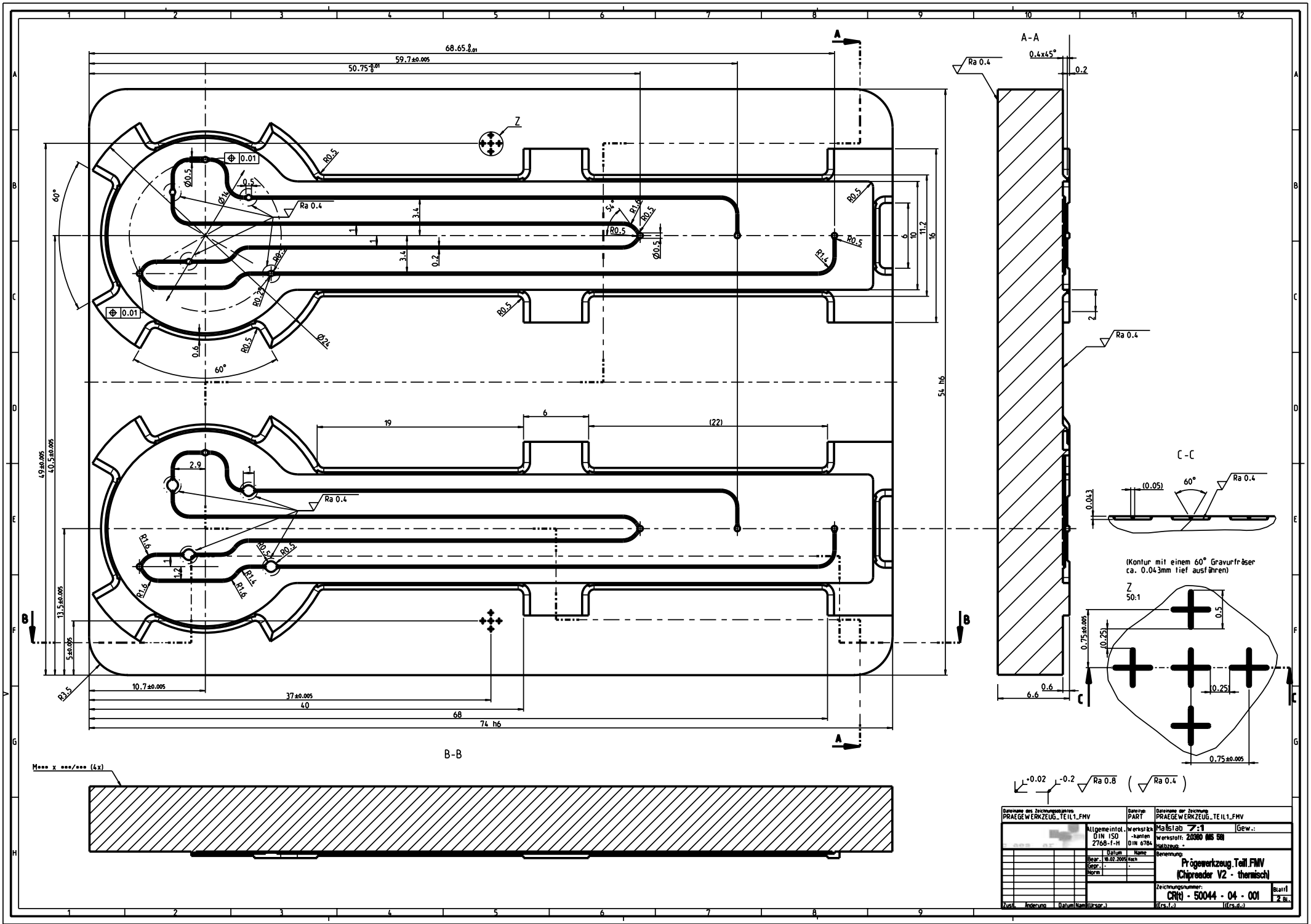
A-A
B-B
C-C
Ra 0.4
0.4x45°
0.2
68.65 0 -0.01
59.7±0.005
50.75 0 -0.01
54 h6
74 h6
68
40
37±0.005
10.7±0.005
R1.5
49±0.005
40.5±0.005
13.5±0.005
5±0.005
19
6
(22)
2.9
3.4
0.2
0.6
6.6
2
0.043
(0.05)
60°
(Kontur mit einem 60° Gravurfräser
ca. 0.043mm tief ausführen)
Z
50:1
0.5
(0.25)
0.75±0.005
Maße x ●●●/●●● (4x)
Allgemeintol.
DIN ISO
2768-f-H
Werkstückkanten
DIN 6784
Maßstab 2:1
Gew.:
Werkstoff: 20MnCr5
Halbzeug: -
Benennung:
Prägewerkzeug_Teil1_FMV
(Chipreader V2 - thermisch)
Zeichnungsnummer:
CR(t) - 50044 - 04 - 001
Blatt 1
2 Bl.
PRAEGEWERKZEUG_TEIL1_FMV
PART

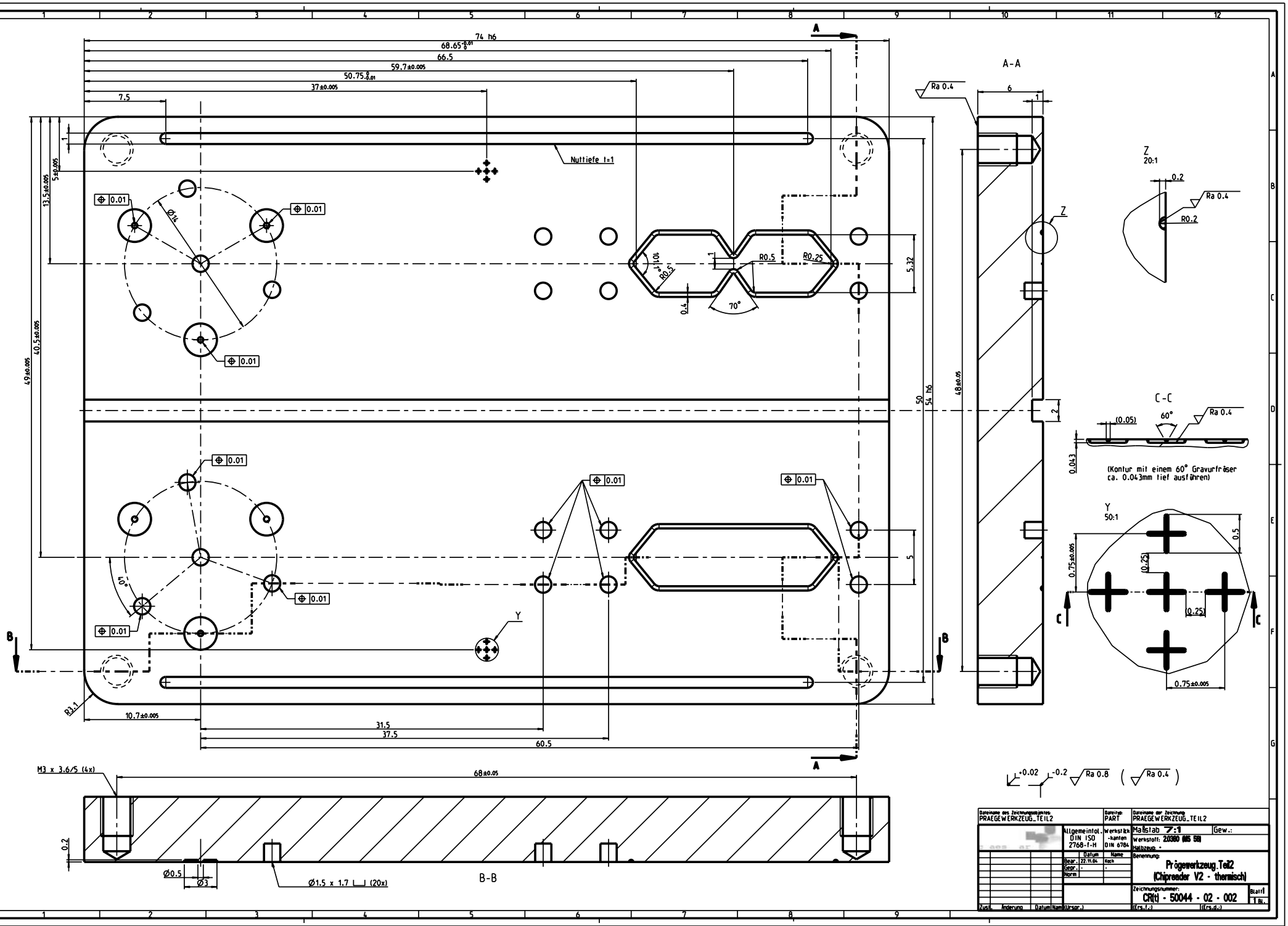
74 h6
68.65 -0.01 -0.01
66.5
59.7±0.005
50.75 -0.01 -0.01
37±0.005
7.5
Nuttiefe t=1
Ø14
R0.5
R0.25
70°
5.32
5
50
54 h6
49±0.005
40.5±0.005
13.5±0.005
5±0.005
10.7±0.005
31.5
37.5
60.5
R3.1
A-A
Ra 0.4
Z
20:1
R0.2
C-C
60°
(0.05)
0.043
(Kontur mit einem 60° Gravurfräser
ca. 0.043mm tief ausführen)
Y
50:1
0.5
0.25
0.75±0.005
M3 x 3.6/5 (4x)
68±0.05
Ø0.5
Ø3
Ø1.5 x 1.7 ⌴ (20x)
B-B
Ra 0.8
Datei-Name des Zeichnungsobjektes
PRAEGEWERKZEUG_TEIL2
Datei-typ
PART
Datei-name der Zeichnung
PRAEGEWERKZEUG_TEIL2
Allgemeintol.
DIN ISO
2768-f-H
Werkstück
-kanten
DIN 6784
Maßstab 2:1
Gew.:
Werkstoff: 20380 WS 58
Halbzeug: -
Benennung:
Prägewerkzeug Teil2
(Chipreader V2 - thermisch)
Datum
Name
Bear. 22.11.04
Kech
Gepr. -
-
Norm
Zeichnungsnummer:
CR(1) - 50044 - 02 - 002
Blatt 1
1 Bl.
Zust. Änderung Datum Name (Urspr.)
(Ers.f.:)
(Ers.d.:)

ACKNOWLEDGMENT

At first place, thank you very much to Prof. Dr. Volker Saile – for his time, for our discussions, for believing in me and for giving me the possibility to write this work. Thank you very much to PD Dr. Eckhard Quandt for his work as a second reviewer at Caesar, Bonn.
A very special thank to Dr. Markus Löhndorf – for the wonderful ideas and helpful discussions, for believing in me and supporting me all the time. Markus, it was my pleasure to work with you!
Thank you very much to Dr. Michael Tewes for the development of the bio-analytical system and for the interesting scientific discussions. He just always knew the answers of all difficult questions!
Thank you very much to:
Michael Koch and Zoltan Lampert for the technical drawings of the embossing molds, as well as to the fine mechanic workshops at Caesar and at University of Bonn for the molds fabrication.
Dr. Stefan Glass for the helpful discussions about the temperature dependence of the SAW sensors and fluid/solid interface effects.
Dr. Marc Schlensog and Dr. Antonio Malave for the fabrication of the SAW sensor chips.
Anne Kiwitz for the development of the software for the S-sens system.
Dr. Thomas Gronewold and Antje Baumgartner for the biochemical preparation of the sensors.
Dr. Dieter Pfeifle for the tests of the chemical resistance of the TPUs.
Dr. Christiane Zamponi, Dr. Corinna Bernsdorff, Dr. Ulrich Schlecht and Dr. Jan Bornemeier who I bothered with a number of software questiuons.
Thank you to the cleanroom team at Caesar: Angelika Sehrbrock, Peter Holik, Jörg Scheurer, Rene Borowski and Jacha van Hout, as well as Dr. Stefan Irsen and Günter Bermes for the fabrication of the epoxid resin molds for the silicone based devices.
Thank you very much to Prof. W.K. Schomburg, Dr. Zeno Rummler and Dr. Yue Cheng (IMT, Research center Karlsruhe) for our collaboration.
Special thanks to Prof. Hella-Christin Sheer and Mathias Wissen (University of Wuppertal, Germany) for our successful cooperation concerning the nanoimprinting technology.
Thank you very much to the companies:
Epurex Films GmbH, Walsrode, Germany – for the non-stop supply of thermoplastic materials.
Jenoptik Mikrotechnik GmbH, Jena, Germany for the HEX 03 embossing machine.
X-Lith, Ulm, Germany for the fabrication of the nanoimprinting stamp.
Rofin Baasel Lasertechnik GmbH, Starnberg, Germany for the tests for laser welding of polymers.